GEOLOGIC MAPPING AND $^{40}AR/^{39}AR$ GEOCHRONOLOGY IN THE NORTHERN NOGAL CANYON CALDERA, WITHIN AND ADJACENT TO THE SOUTHWEST CORNER OF THE BLUE MOUNTAIN QUADRANGLE, SAN MATEO MOUNTAINS, NEW MEXICO

by

Scott D. Lynch

Submitted in Partial Fulfillment
of the Requirements for the

Masters of Science in Geology

New Mexico Institute of Mining and Technology
Department of Earth and Environmental Science

Socorro, New Mexico

May, 2003

ABSTRACT

Geologic mapping and $^{40}Ar/^{39}Ar$ geochronology in the west-central San Mateo Mountains of southwestern New Mexico indicate that the Nogal Canyon Caldera (source of the 28.4 Ma Vicks Peak Tuff) is larger than previously proposed and was a topographic high until at least 27.4 Ma. Approximately 42 km^2 located north of the previously proposed caldera margin were mapped at 1:24,000 using the southwest quarter of the Blue Mountain Quadrangle and the three adjacent quadrangles as base maps. In this area, more than 690 m of Vicks Peak Tuff with no exposed base is overlain by 550 m of mineralogically similar rhyolite lavas. Several granite porphyries intrude the Vicks Peak Tuff and several rhyolite dikes intrude the rhyolite lavas. Overlying this sequence is the 24.4 Ma Turkey Springs Tuff (70 m - 110 m). Samples from each rock unit in this study area were collected for $^{40}Ar/^{39}Ar$ geochronological analysis. A total of 32 samples were analyzed using the single crystal laser fusion method on sanidine. Most samples yielded a tight, single population of sanidine crystals and a high precision age ($2\sigma < \pm$ 0.7%). The ages of the Vicks Peak Tuff, rhyolite lavas, and silicic intrusions overlap within 2σ error and show that they erupted and intruded during a brief (<0.42 Ma) episode of activity that occurred between 28.58 and 28.16 Ma.

Spatial and temporal relationships between the Vicks Peak Tuff, rhyolite lavas, and granite porphyries indicate that they came from a common magma system and that the rhyolite lavas and granite porphyries are associated with the development of the

Nogal Canyon Caldera. The thickness of the Vicks Peak Tuff and rhyolite lavas in this study area suggest that they are intracaldera facies, thereby suggesting that the northern margin of the Nogal Canyon Caldera is actually north of the field area. The estimated diameter of the caldera is 25 km and the estimated total volume of the Vicks Peak Tuff is 1816 km^3.

Notably missing from the stratigraphic sequence in this study area is the 27.4 Ma South Canyon Tuff, a 700 km^3 regional ignimbrite that erupted from a caldera less than 10 km to the north. This suggests that the Vicks Peak Tuff, rhyolite lava, and granite porphyry intrusions formed a topographic high during the 27.4 Ma eruption of the South Canyon Tuff such that the South Canyon Tuff was not emplaced or was completely eroded in less than 3 m.y. This high may be due to resurgent uplift of the caldera floor after caldera collapse.

ACKNOWLEDGEMENTS

I would like to thank committee members Bill McIntosh, Charles Ferguson, and Phil Kyle for setting up this project and providing assistance and support throughout its duration. Additional thanks go to my advisor, Bill McIntosh, a man of great kindness, generosity, and wisdom. He has provided tremendously helpful discussions, manuscript reviews, and insights into both field and laboratory problems. Charles Ferguson and Bob Osburn have been inspirational in the field, and I thank them for sharing their vast knowledge of field geology with me. A special thanks goes out to Tommy Abers and the folks at Aber's Ranch for their warm hospitality.

I truly cannot thank Lisa Peters and Rich Esser enough for their invaluable assistance, particularly with the collection, reduction, and presentation of geochronological data. They have been a genuine help and a great pleasure to work with. I also thankfully acknowledge Nelia Dunbar and Lynn Heizler for facilitating and assisting with electron microprobe analyses. Mark Mansell and Adam Read have provided much help with map compilation using ArcGIS.

This work would not have been possible without the support of the State of New Mexico and its residents. I gratefully acknowledge the New Mexico Bureau of Geology and Mineral Resources and the New Mexico Geochronology Research Laboratory for supporting this research with assistantships and geochronological analyses. They also provided maps, aerial photographs, literature, and field vehicles.

Finally, a heartfelt appreciation goes out to my family and friends. They have made all of my life's achievements possible, and I love them dearly. I especially thank Reyna Abeyta for her love and patience, and I thank her dog Hooch--who was my loyal, devoted, hard-working field assistant.

TABLE OF CONTENTS

LIST OF FIGURES

LIST OF TABLES

LIST OF PLATES

This thesis is accepted on behalf of the
Faculty of the Institute by the following committee:

William C McIntosh
Advisor

May 6, 2003
Date

I release this document to the New Mexico Institute of Mining and Technology.

Scott D Lynch
Student's Signature

6 May 03
Date

1. INTRODUCTION

The San Mateo Mountains are a 60 km x 24 km north-trending uplift within the mid-Tertiary Mogollon-Datil volcanic field of southwestern New Mexico (Fig. 1). They expose primarily middle-late Oligocene silicic volcanic rocks. The Nogal Canyon Caldera is located in the southern San Mateo Mountains (Fig. 1) and is the source caldera of the 28.3 Ma Vicks Peak Tuff (1816 km^3). The caldera is defined by an arc of small stocks along the southern margin and thick post-Vicks Peak rhyolite lavas along the western margin (Deal and Rhodes, 1976). Atwood (1982) recognized caldera related structures along the east margin and Hermann (1986) identified a strand of the southeastern structural margin. The northern margin of the Nogal Canyon Caldera is in the central San Mateo Mountains, and mapping is ongoing to constrain its location. Hermann (1986) mapped thick, intracaldera facies Vicks Peak Tuff in the vicinity of Deal and Rhodes' (1976) inferred northern caldera margin (Fig. 1), and he concluded that the actual caldera margin must be further to the north.

In this study, detailed mapping and $^{40}Ar/^{39}Ar$ geochronology were used to examine the geology north of the Nogal Canyon Caldera margin proposed by Deal and Rhodes (1976). The study area is located in the southwest 1/4 of the Blue Mountain 7.5 min. quadrangle and parts of the three adjacent quadrangles (Fig. 1). This report presents field and laboratory data and discusses their interpretation and geologic implications.

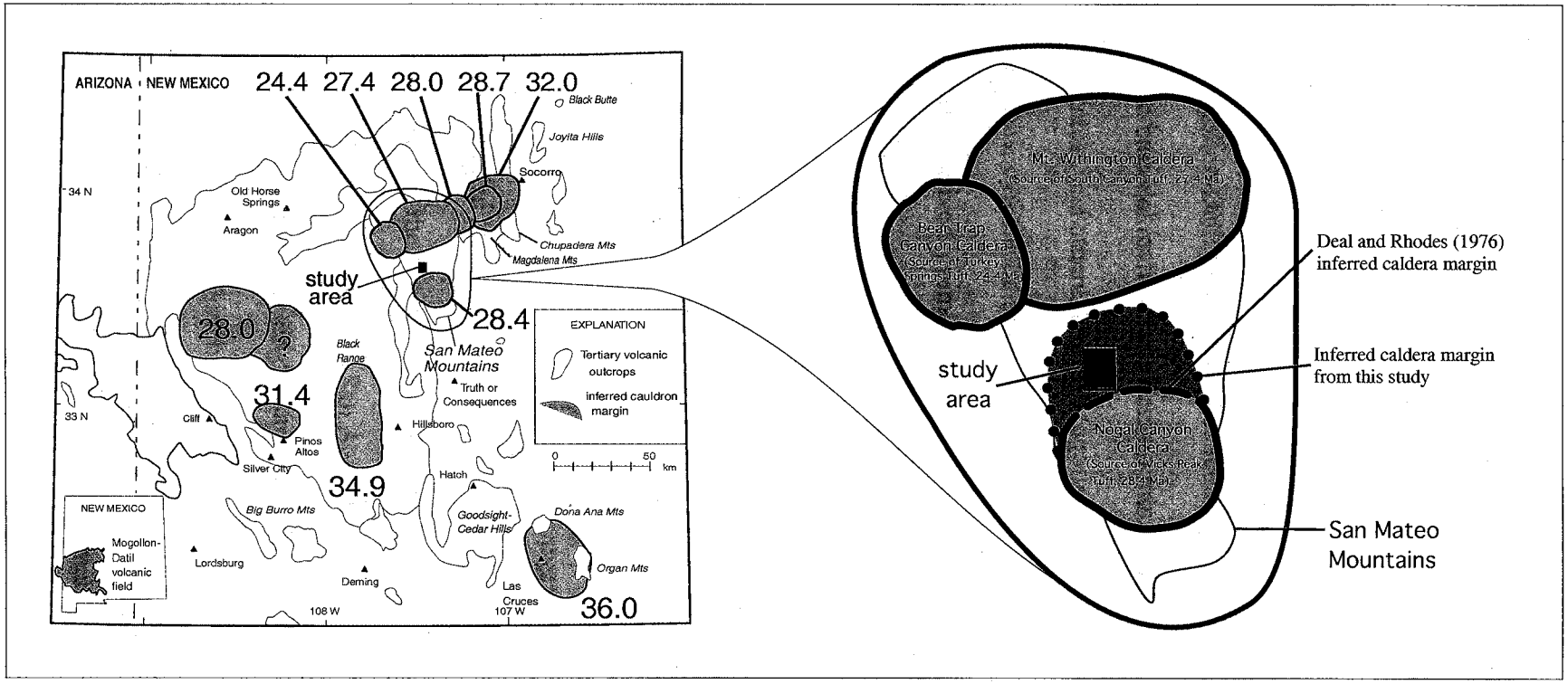

Figure 1. Map of the Mogollon-Datil volcanic field depicting inferred cauldrons, their ages, and generalized outcrop distribution of the late Eocene-Oligocene volcanic rocks. Blow-up of the San Mateo Mountains includes source cauldron information and the revised margin of the Nogal Canyon Cauldron. Modified from McIntosh and others, 1992.

1.1. Geologic Setting

The San Mateo Mountains are in the northeastern corner of the Mogollon-Datil volcanic field, which is part of a north-trending chain of silicic volcanic fields in southwestern North America (Fig. 2). This volcanism is thought to be the result of a brief episode of low-angle subduction of the Farallon plate (Lipman and others, 1972). Activity in the Mogollon-Datil field initiated at about 40 Ma with intermediate volcanism and progressed into bimodal mafic and caldera-forming silicic activity that lasted from 36 Ma to 24 Ma (McIntosh and others, 1992). Mogollon-Datil activity generated lava flows, lava domes, intrusions, pyroclastic flows, pyroclastic falls, and numerous calderas. Several of the caldera-derived ignimbrites extend over 200 km from source and are more than 1000 km^3 in volume (McIntosh and others, 1986). The generalized stratigraphic sequence of regional ignimbrites in the San Mateo Mountains is shown in Figure 3.

Late Cenozoic extensional tectonism associated with the development of the Basin and Range province and the Rio Grande Rift has broken the Mogollon-Datil volcanic field into fault-block mountain ranges that are separated by in-filled basins. The extension is variable, ranging from 0% to >100% (Chamberlin, 1983). The San Mateo Mountains are an east tilted fault block on the western edge of the Rio Grande Rift (Fig. 4). Adjacent structures are the Winston and Monticello grabens to the west and the Muligan graben to the east (Fig. 5). The San Augustin Plains are to the immediate north of the San Mateo Mountains and the Engle Basin is to the immediate south.

Predominant structures within the San Mateo Mountains are of two types: late Oligocene caldera collapse structures and north trending normal faults related to late Cenozoic extensional tectonism. In addition to the aforementioned Nogal Canyon

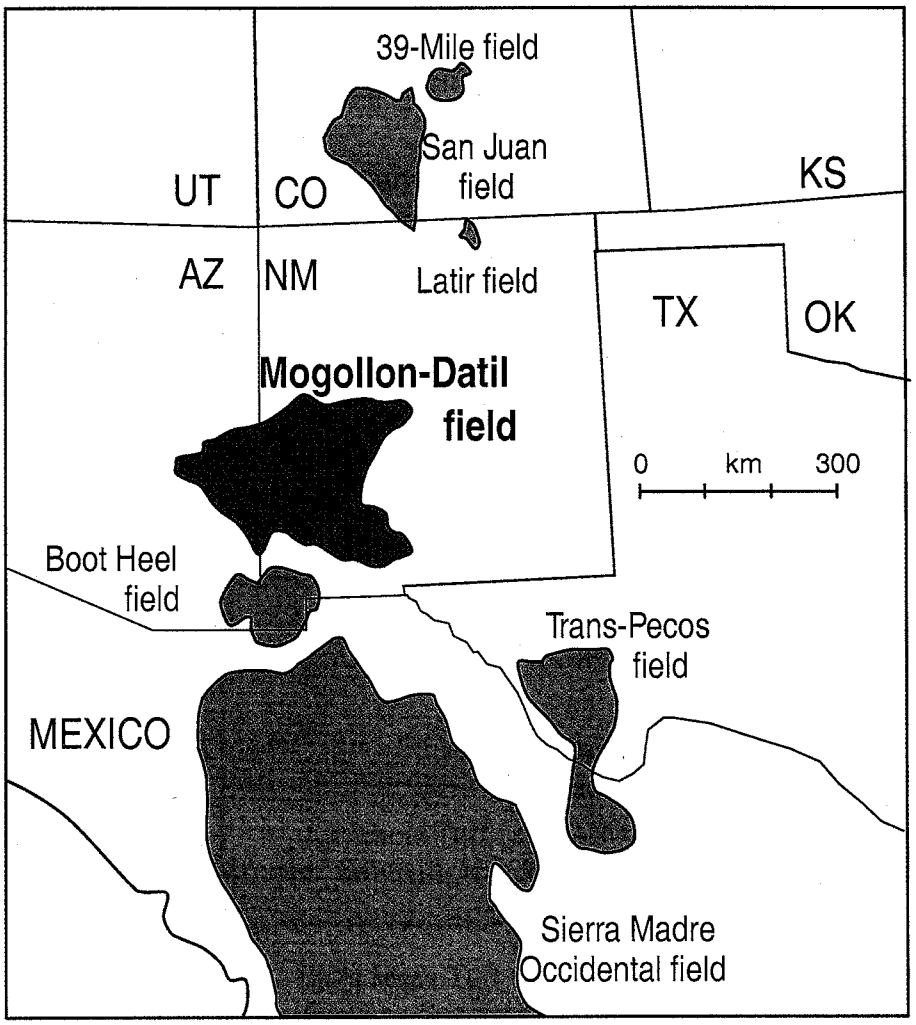

Figure 2. Present-day distribution of mid-Tertiary silicic volcanic fields of southwestern North America. Modified from McIntosh and others, 1992.

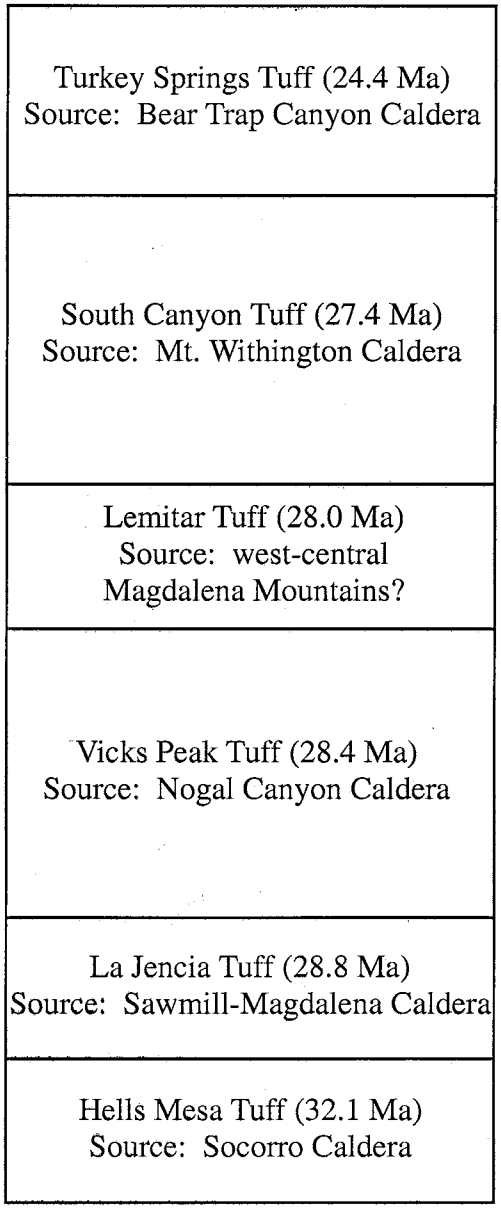

Figure 3. Generalized stratigraphic sequence of regional ignimbrites in the San Mateo Mountains. Age of Vicks Peak Tuff and Turkey Springs Tuff from this study, other ignimbrite ages from McIntosh and others (1992). Source caldera for the Turkey Springs Tuff from Osburn and others (1997). Other source calderas from Osburn and Chapin (1983b).

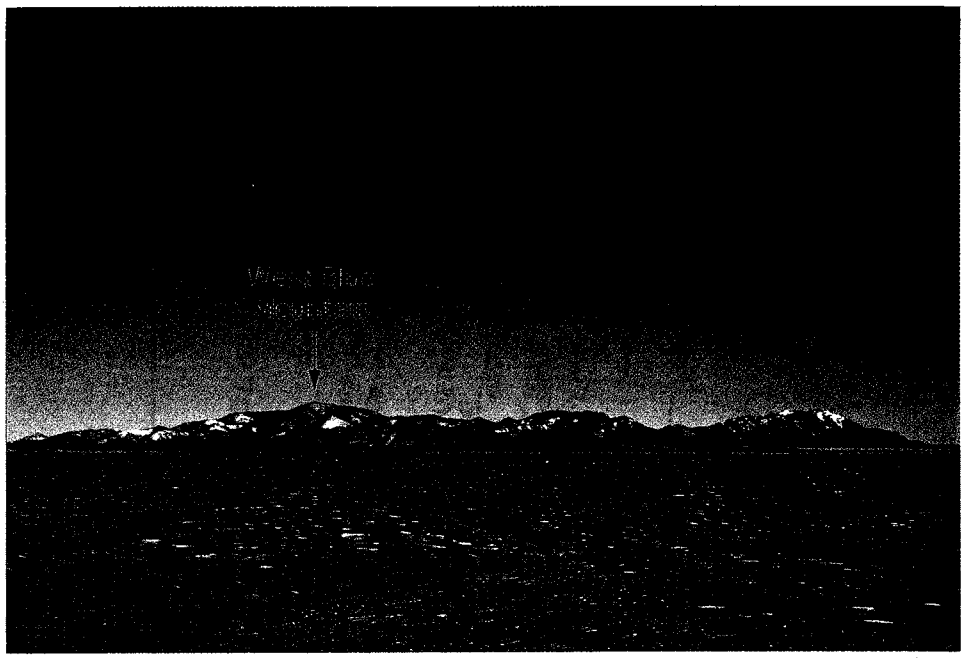

Figure 4. View looking southwest towards the southern 30 km of the San Mateo Mountains. West Blue Mountain is located in the east-central part of the study area. Camera location: UTM 13N 0225500(E), 3741300(N).

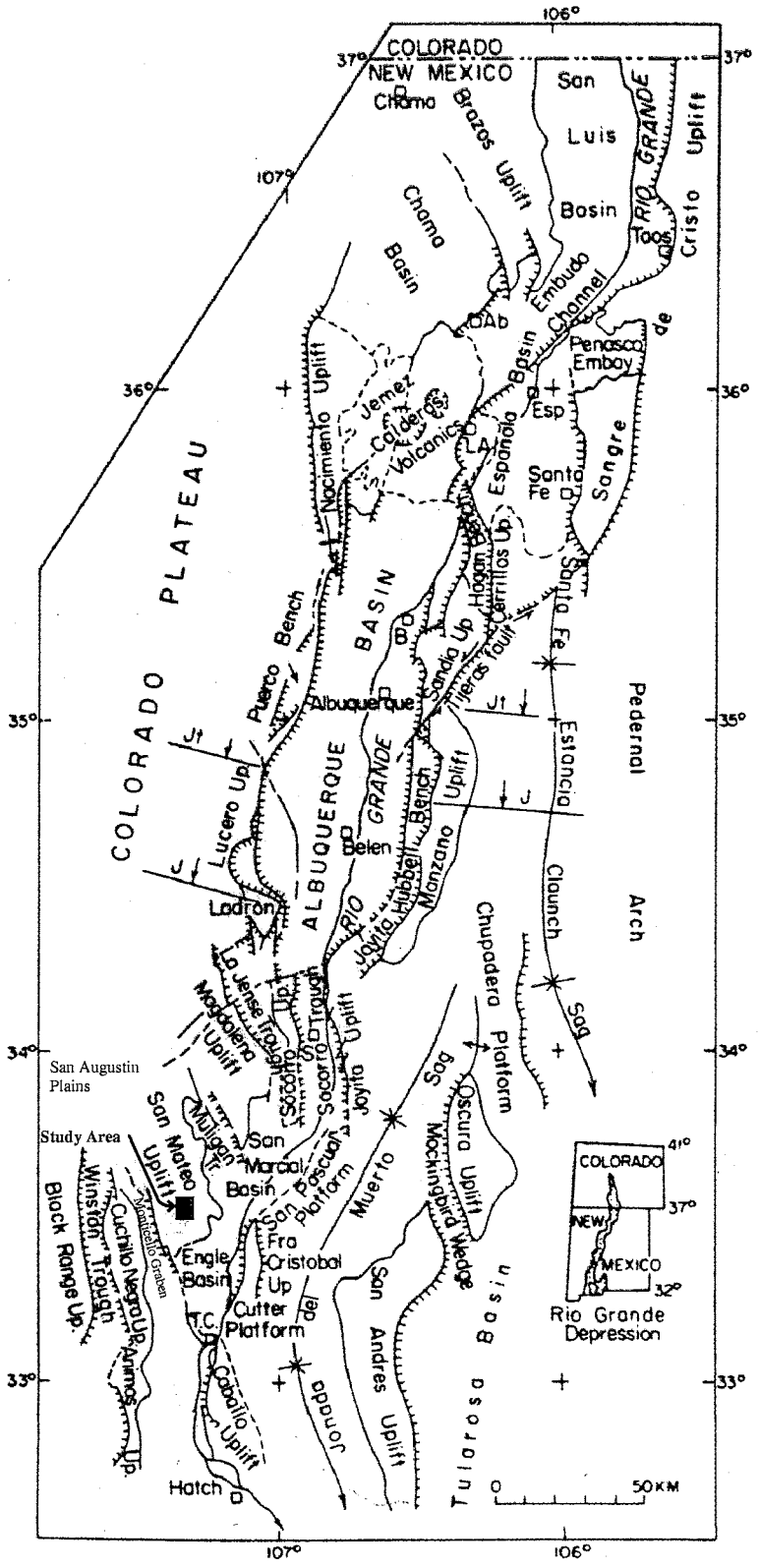

Figure 5. Generalized structures along the Rio Grande Rift (modified from Chapin and others, 1978). Study area shown with box in southern San Mateo uplift.

caldera, two other calderas have been identified in the San Mateo Mountains. The Mt. Withington caldera (Deal, 1973; Deal and Rhodes, 1976) occupies most of the northern San Mateo Mountains (Fig. 1) and is the source caldera of the 27.4 Ma South Canyon Tuff, a widespread 700 km^3 regional ignimbrite (McIntosh and others, 1992). The Bear Trap Canyon caldera (Osburn and others, 1997) is nested in the west end of the older Mt.Withington caldera (Fig. 1) and is the source caldera of the 24.4 Ma Turkey Springs Tuff.

The San Mateo Mountains are composed mostly of middle to late Oligocene silicic lavas, pyroclastic rocks, intrusions, and volcaniclastic sediment. Late Eocene through early Oligocene mafic and intermediate lavas and intrusions are also exposed, particularly in the southern part of the range (Hermann, 1986). Paleozoic sedimentary rocks crop out in the extreme south (Farkas, 1969), and a few exposures of Precambrian rocks have been mapped in the east-central (Atwood, 1982) and southeastern (Farkas, 1969) San Mateo Mountains.

Paleozoic rock overlain by Oligocene volcanic rock in the San Mateo Mountains and other nearby mountain ranges suggests that this area was a topographic high during the Eocene, because in adjacent areas the Paleozoic strata is overlain by thick deposits of early Tertiary sediments. Cather (1983) suggests that the area including the San Mateos is within the Laramide Sierra uplift (Eardley, 1962) and that adjacent areas are Laramide basins. Chapin and Cather (1981) proposed that north-northeastward translation of the Colorado Plateau in the early Eocene created compressive structures along its eastern margin including uplifts (such as the Sierra uplift) and basins (Fig. 6).

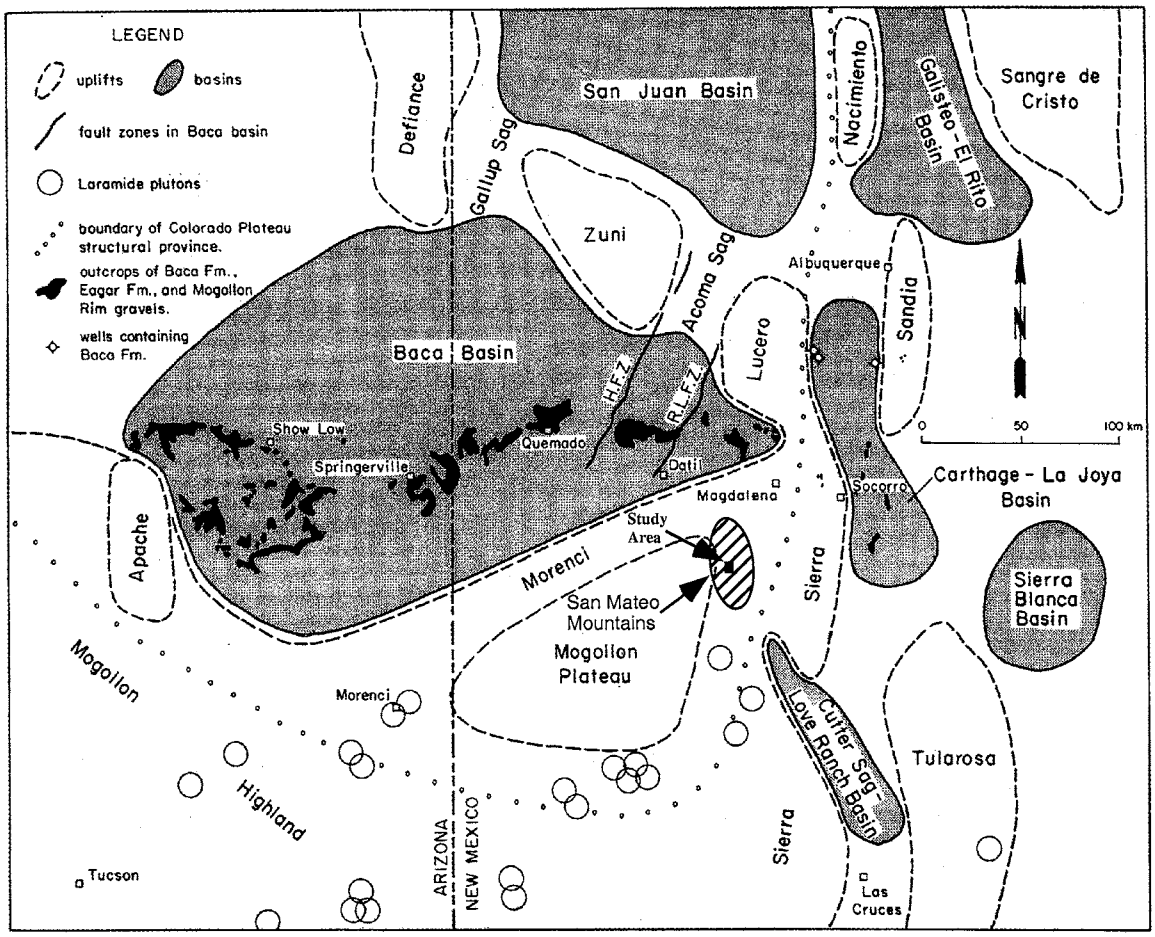

Figure 6. Distribution of Eocene uplifts and basins in western New Mexico and eastern Arizona (modified from Cather, 1983). Present day location of San Mateo Mountains added.

1.2. Purpose of Study

There are several purposes of this study: to examine the proposed margin of the Nogal Canyon Caldera, to investigate stratigraphic relationships in this study area and correlate them with adjacent areas, and to analyze the timing of events using high-precision geochronology. The southwest 1/4 of the Blue Mountain Quadrangle was chosen as the study area because of its proximity to the proposed margin of the Nogal Canyon Caldera.

1.3. Methods of Study

The geology of this study area was mapped at a scale of 1:24,000 onto U.S.G.S. 7.5' topographic quadrangles using standard geologic mapping techniques. In addition to the southwest 1/4 of the Blue Mountain Quadrangle, small parts of the adjacent Welty Hill, Montoya Butte, and Vicks Peak Quadrangles were mapped. 1:50,000 scale aerial photographs were used to supplement the topographic maps. Stratigraphic units were identified, characterized, and correlated using geochronology and the previously established stratigraphic framework of regional units (Osburn and Chapin, 1983; McIntosh and others, 1992) in the central San Mateo Mountains. Samples were collected in the field for petrographic analysis, geochemical analysis using electron microprobe, and geochronological analysis using the $^{40}Ar/^{39}Ar$ dating method. All sample locations were assigned GPS coordinates and are listed in Appendix A. All field data was compiled and integrated with laboratory data using ArcGIS 8.1.

1.4. Previous Work

Lasky (1932), Willard (1957), Dane and Bachman (1961), and Weber (1963) worked in the San Mateo Mountains using generalized stratigraphic units introduced by

Winchester (1920) and subdivided by Wilpolt and others (1946) and Tonking (1957). Furlow (1965) and Farkas (1969) documented a more complex volcanic stratigraphy in the southern San Mateo Mountains during reconnaissance mapping. Deal (1973) proposed the existence of the Mt. Withington Caldera and Deal and Rhodes (1976) proposed the Nogal Canyon Caldera and identified it as the source caldera of the Vicks Peak Tuff. Atwood (1982) mapped an area 7 km to the east of this study area revealing as much as 240 m of Vicks Peak Tuff overlain by rhyolite lava. He also recognized a structure related to the eastern margin of the Nogal Canyon Caldera. Cox (1985) investigated the geology of the San Jose mining district in the southern San Mateo Mountains and identified a thick section of Vicks Peak Tuff in that area. Detailed mapping by Ferguson (1985) in an area 7 km northeast of this study area reveals evidence for a south-side down fault that may be related to the development of the Nogal Canyon Caldera. Ferguson (1986) also identified the Tuff of Turkey Springs, which is the youngest ignimbrite in the northeast Mogollon-Datil volcanic field. Mapping by Hermann (1986) to the immediate south of this study area revealed Nogal Canyon Caldera related structures and over 1333 m of intracaldera facies Vicks Peak Tuff that is locally interlayered with caldera-collapse breccias.

More recently, Osburn and Ferguson (1986) and Ferguson (1988, 1990, 1991) redefined and scrutinized the Mt. Withington caldera. The Monica Saddle, Bay Buck Peaks, and Oak Peak Quadrangles were mapped in detail by Osburn and Ferguson (unpublished). Smith (1992) mapped 7 mi^2 in the southwestern San Mateo Mountains near the southwestern margin of the Nogal Canyon Caldera. Osburn and others (1997) identified the source caldera of the Turkey Springs Tuff in the northwestern San Mateo

Mountains and named it the Bear Trap Canyon Caldera. Currently Osburn and Ferguson (in progress) are mapping the Welty Hill Quadrangle, which is the adjacent quadrangle to the west of this study area. A location map of previous work areas is shown in Figure 7.

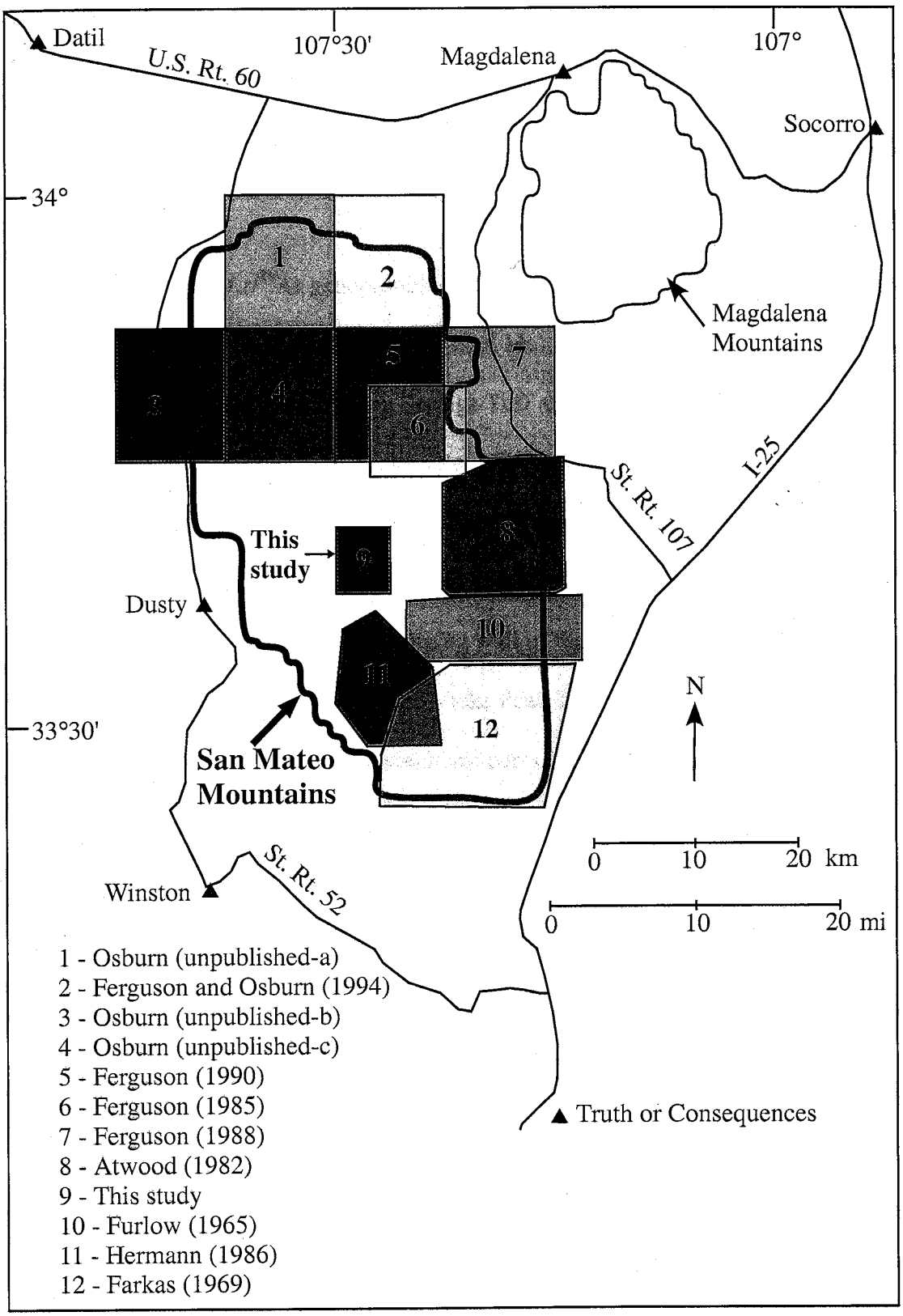

Figure 7. Location of this study area and previous study areas in the San Mateo Mountains.

2. STRATIGRAPHY

Mapping and $^{40}Ar/^{39}Ar$ geochronology in this study area has revealed a sequence of Vicks Peak Tuff (28.4 Ma), rhyolite lava (28.4 Ma), and volcaniclastic rocks (28.4 Ma - 27.9 Ma) overlain by 24.4 Ma Turkey Springs Tuff and volcaniclastic sedimentary rocks (Plate 1, Fig. 8). Intruding the Vicks Peak Tuff and lava are several 28.3 Ma felsic stocks and dikes. The complete stratigraphic section is not exposed in any of the single fault blocks in this study area. The upper part of the section is exposed mainly in the northwest part of the study area in the hanging wall of the Deep Canyon Fault (Plate 1). The footwall of this fault exposes only the Vicks Peak Tuff and rhyolite lava. The lowest parts of the section are exposed in the southeast part of the study area.

The stratigraphic sequence in this study area was correlated (Fig. 9) with the stratigraphy 7 km to the northeast (Ferguson, 1986) and to the immediate south (Hermann, 1986). The stratigraphic sequence to the south is similar, although much more section is exposed beneath the Vicks Peak Tuff in the south. In addition, the rhyolite lava overlying the Vicks Peak Tuff in this study area contains only 2% sanidine phenocrysts, whereas the lava to the south (Alamosa Creek rhyolite) contains 20% sanidine and quartz phenocrysts. The Vicks Peak Tuff and overlying lava thin northeast of this study area. Widely exposed to the northeast, but missing from the stratigraphy within the study area, are two regional ignimbrites between the Vicks Peak Tuff and Turkey Springs Tuff.

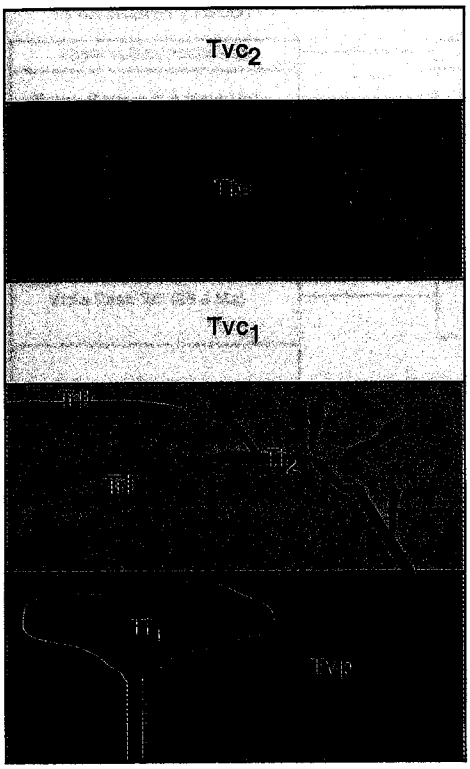

Volcaniclastic sediment (Tvc_2). Interbedded sandstone and conglomerate

Turkey Springs Tuff (Tts). Rhyolite ignimbrite. 24.4 Ma. 70-105 m thick. Sanidine (10%) and quartz (10%) bearing welded lapilli-tuff. Non-welded base and top. Source: Bear Trap Canyon Cauldron.

Volcaniclastic rocks. (Tvc_1). Sandstone to fine pebble conglomerate. 5-60 m thick.

Rhyolite lava (Trl). 28.4 Ma. 550 m thick max. Flow-banded with 1-3% sanidine phenocrysts. Contains 1-10 m thick, localized ignimbrite (Trlt). Intruded by 28.3 Ma rhyolite dikes (Ti_2) that are 5-60 m thick and contain sanidine (13%) and quartz (12%) phenocrysts.

Vicks Peak Tuff (Tvp). Rhyolite ignimbrite. 28.4 Ma. 690 m thick with no exposed base. Sanidine (1-10%) bearing densely welded lapilli-tuff. Source: Nogal Canyon Cauldron. Intruded by 28.3 Ma granite porphyry stocks (Ti_1) up to $1 km^2$.

Figure 8. Diagram of stratigraphic and intrusive units in this study area.

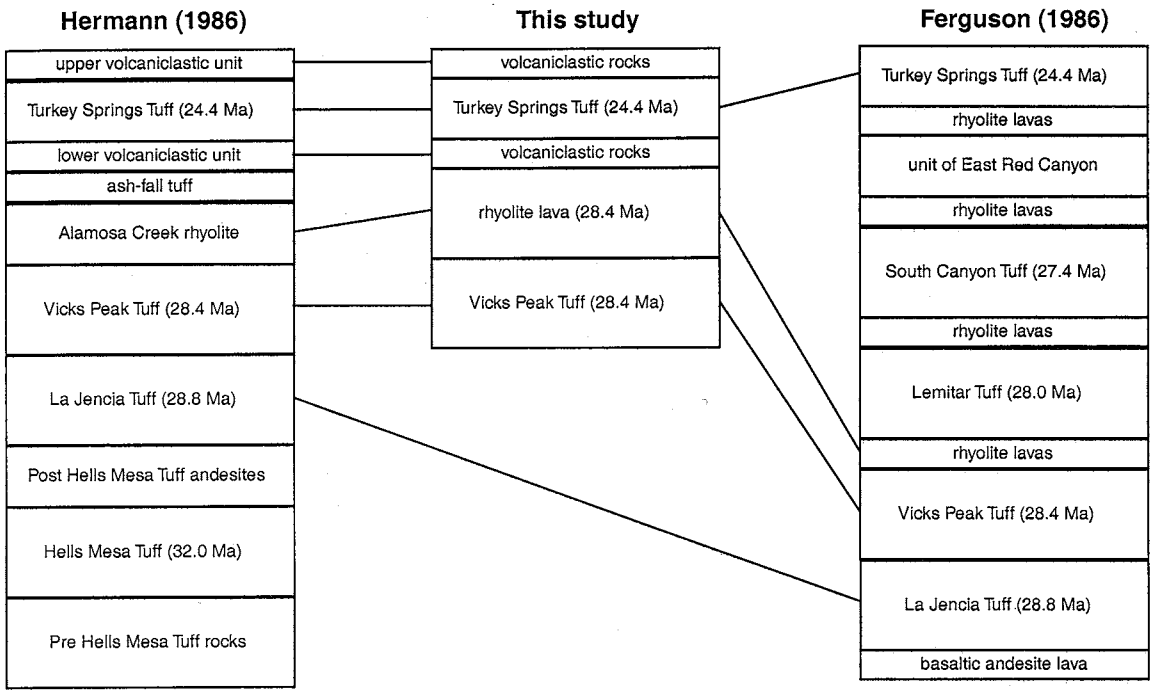

Figure 9. Stratigraphic correlation in the central and southern San Mateo Mountains. Hermann (1986) depicts stratigraphy in an area to the immediate south of this study area. Stratigraphic sequence of Ferguson (1986) from an area 7 km northeast of this study area. Unit ages are from this study and McIntosh and others (1992).

3. UNIT DESCRIPTIONS

3.1. Vicks Peak Tuff (Tvp)

The oldest rock unit in this study area is the 28.4 Ma Vicks Peak Tuff (Furlow, 1965). The thickest section of Vicks Peak Tuff occurs in an eastward dipping fault block bound on its west side by the Deep Canyon Fault. Over 690 m of the Vicks Peak Tuff is exposed beneath a conformable upper contact with rhyolite lava. The base of the Vicks Peak Tuff is not exposed in this study area, therefore total thicknesses are unknown. A composite stratigraphic section of the Vicks Peak Tuff was compiled and is shown in Figure 10.

The Vicks Peak Tuff is a densely welded, phenocryst-poor, sanidine bearing rhyolite ignimbrite containing 75% SiO_2 (Bornhorst, 1980). In outcrop it is pinkish grey and exhibits columnar jointing or, in its deepest exposures, intense jointing (Fig. 11 a, b). Phenocrysts throughout the unit are mostly tabular, euhedral, chatoyant sanidine (1-3 mm) set in a devitrified welded-ash-and-pumice matrix (Fig. 12 a, b). Phenocryst content in the Vicks Peak Tuff increases vertically from 1%-2% sanidine and trace biotite throughout much of the interior to 10%-11% sanidine and 0.5% biotite near the top. Pumice content also increases upsection from 4%-7% in the lowest exposures to 15% near the top. The upper 10 m of the Vicks Peak Tuff is moderately welded, less devitrified, and contains vapor-phase minerals. Vapor-phase minerals are lineated within each pumice fragment in the moderately welded top of the Vicks Peak Tuff. These

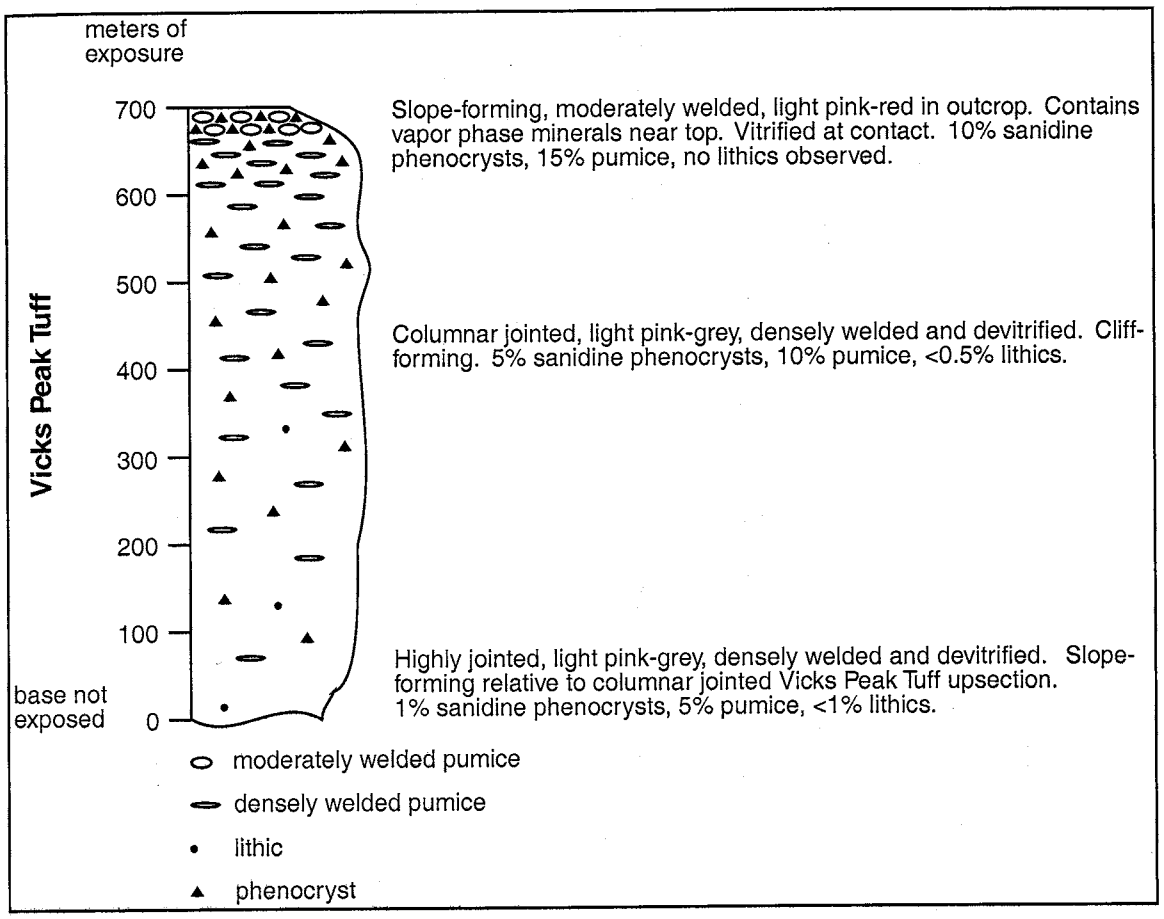

Figure 10. Composite columnar section of the Vicks Peak Tuff.

a)

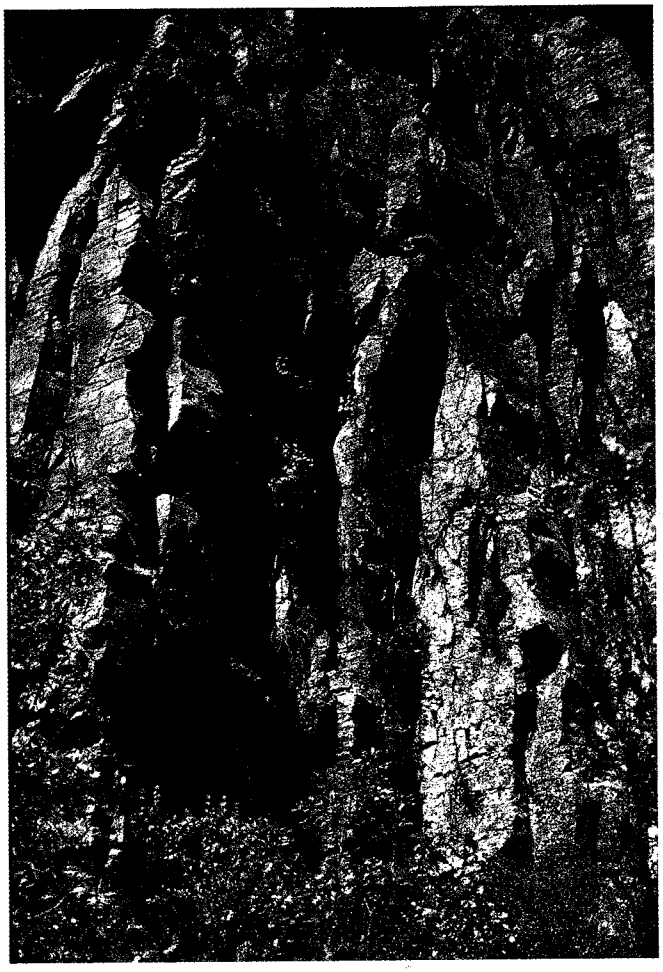

b)

Figure 11 a, b. Outcrop of Vicks Peak Tuff. **a.** Columnar jointing. Looking north from UTM 13N 0268672(E), 3724259(N). **b.** Welded texture at UTM 13N 0271971(E), 3728213(N).

a)

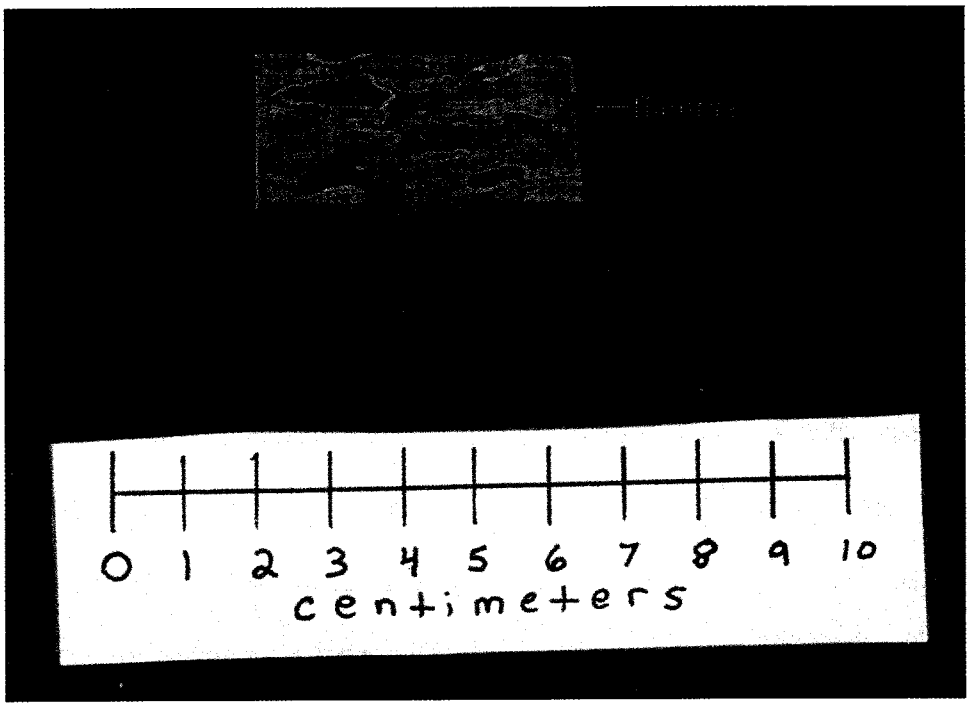

b)

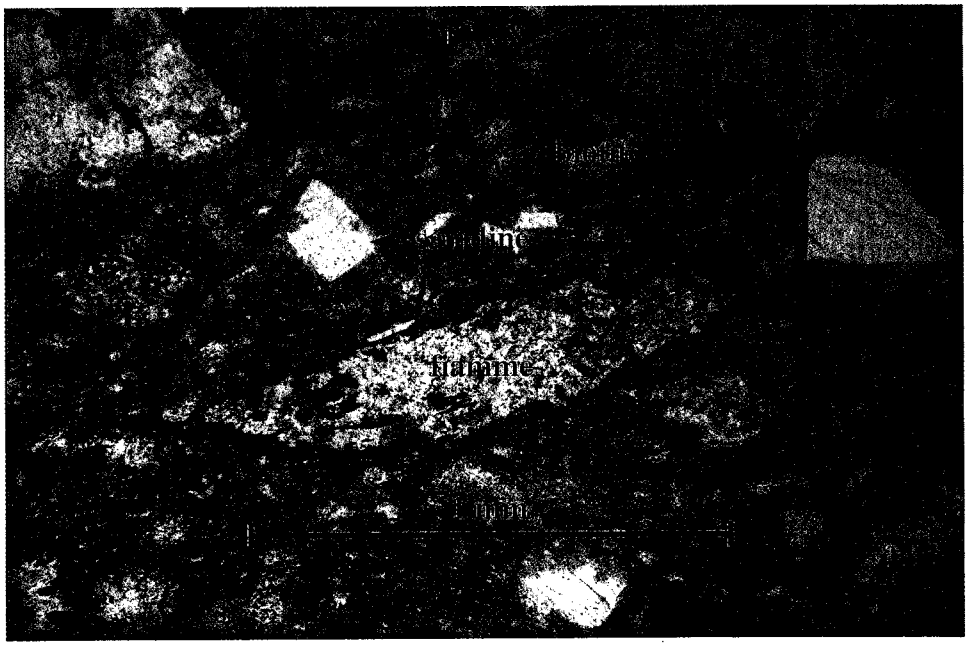

Figure 12 a, b. Vicks Peak Tuff sample S084. **a.** Hand sample cut perpendicular to eutaxitic foliation. **b.** Thin section in plane polarized light.

internally lineated pumice clasts are typically randomly oriented. Lithic fragments constitute trace amounts of the Vicks Peak Tuff in this study area.

3.2. Rhyolite Lavas (Trl)

A thick sequence of 28.4 Ma overlapping rhyolite lavas conformably overlies the Vicks Peak Tuff in this study area and is mapped as a single unit (Fig. 13). As much as to 550 m of this unit is exposed west of the Deep Canyon Fault. A 1-to-3 m thick basal vitrophere occurs in the lavas that are in contact with the underlying Vicks Peak Tuff. Thin vitropheres and/or brecciated margins are common at the contacts between individual lava flows. Thin, 1 m-10 m thick, moderately-welded ignimbrites (Trlt) with the same mineralogy as the lavas are interlayered with individual lava flows in some places and are mapped as a separate unit from the lavas.

In outcrop, the rhyolite lavas are typically pinkish grey and show knobby weathering and highly contorted flow bands (Fig. 14 a-c). They are phenocryst-poor with only 1%-3% euhedral, chatoyant sanidine (1 mm-5 mm) and less than 0.5% biotite (Fig. 15 a, b). The groundmass is composed of microcrystalline quartz and sanidine in the flow banded interior. Near flow margins the groundmass is glassy or partly crystallized to spherulitic quartz and sanidine (Fig. 16). A 3-7 m thick carapace breccia is locally preserved along the upper contacts of some lavas (Fig. 17). This clast-supported breccia is typically altered to a light green/yellow color and contains flow banded and vitric lava clasts ranging from <1 cm to 1 m in diameter.

3.3. Granite Porphyry Stocks (Ti1)

Several 28.3 Ma granite porphyry stocks intrude the Vicks Peak Tuff in the southern half of this study area. Surface exposures of these stocks range from 0.1 km^2 to

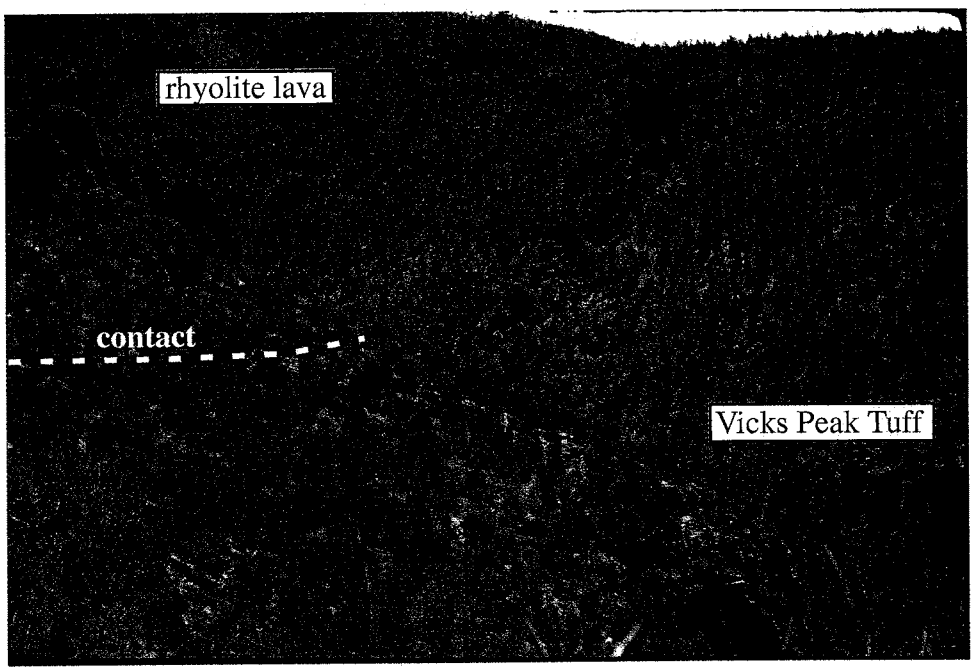

Figure 13. Vicks Peak Tuff conformably overlain by rhyolite lava. Looking east from UTM 13N 0268202(E), 3724309(N).

a)

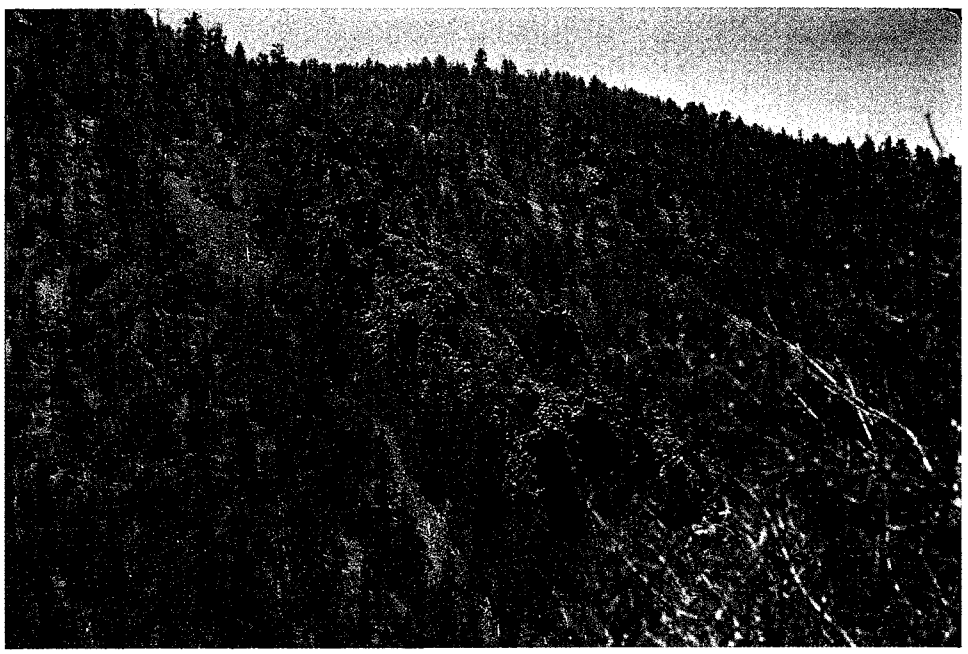

b)

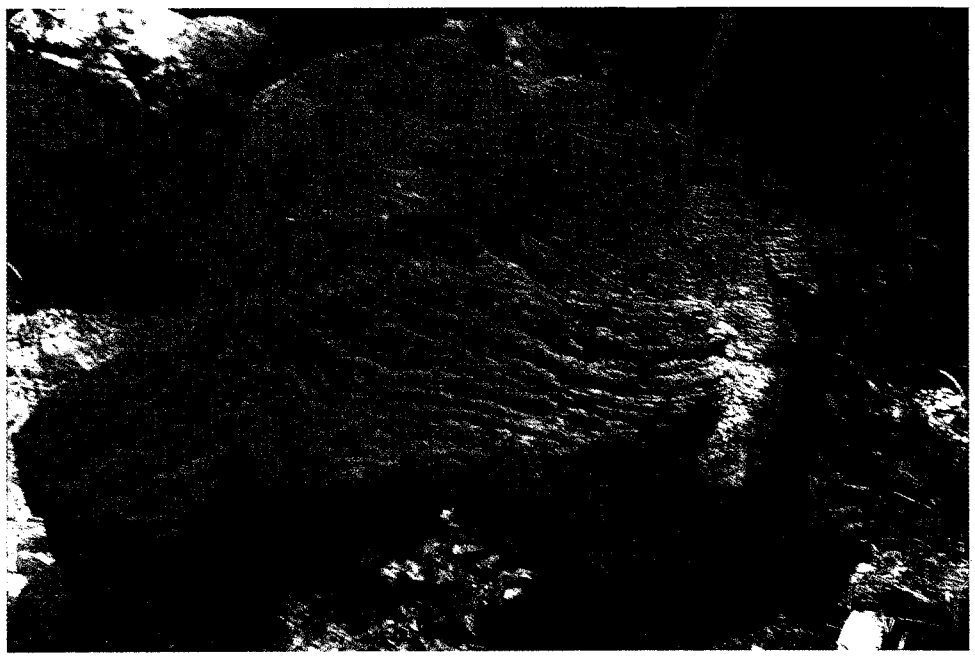

Figure 14 a-c. Outcrop of rhyolite lava. **a.** Knobby weathering pattern. Looking south from UTM 13N 0268301(E), 3724310(N). **b.** View perpendicular to flow foliation. Camera location: UTM 13N 0268427(E), 3725714(N). **c.** Viewing down a shallow, oblique angle to flow foliation. Camera location: UTM 13N 0267331(E), 3724884(N).

c)

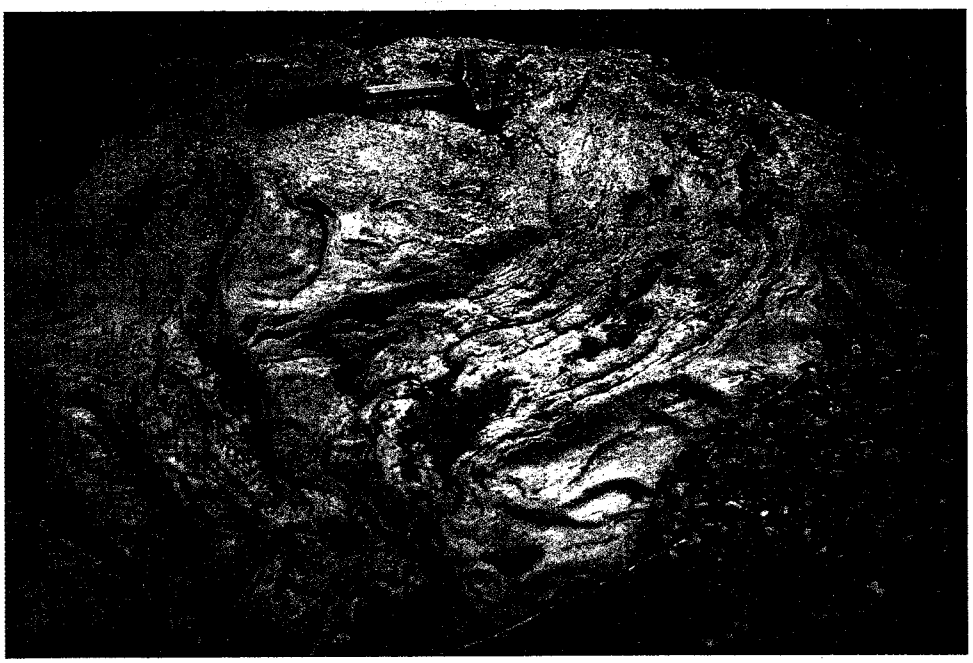

Figure 14 a-c (continued).

a)

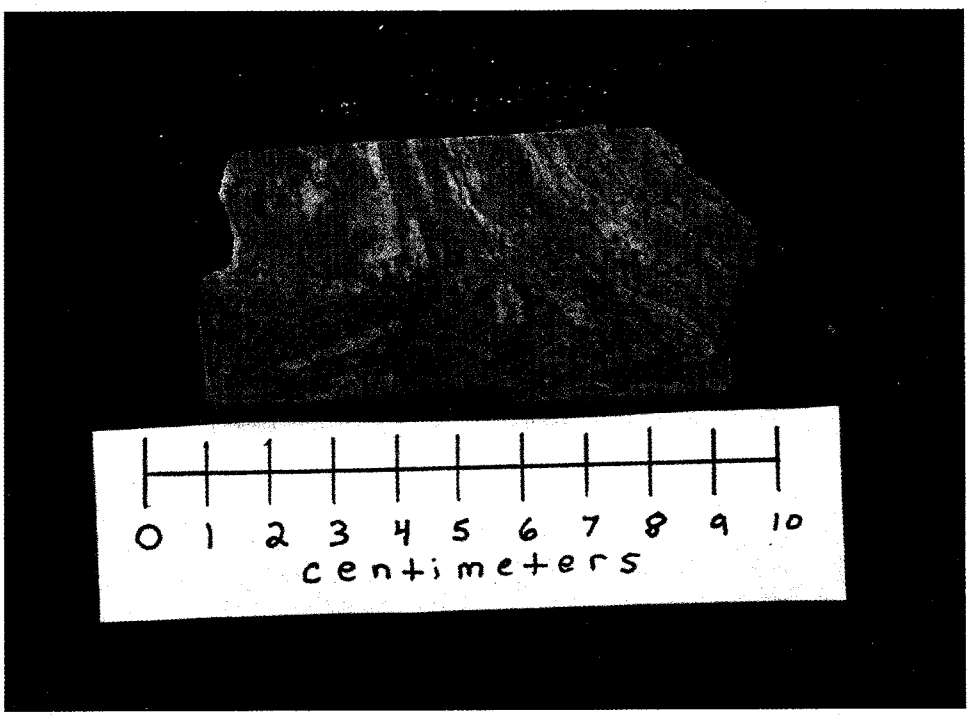

b)

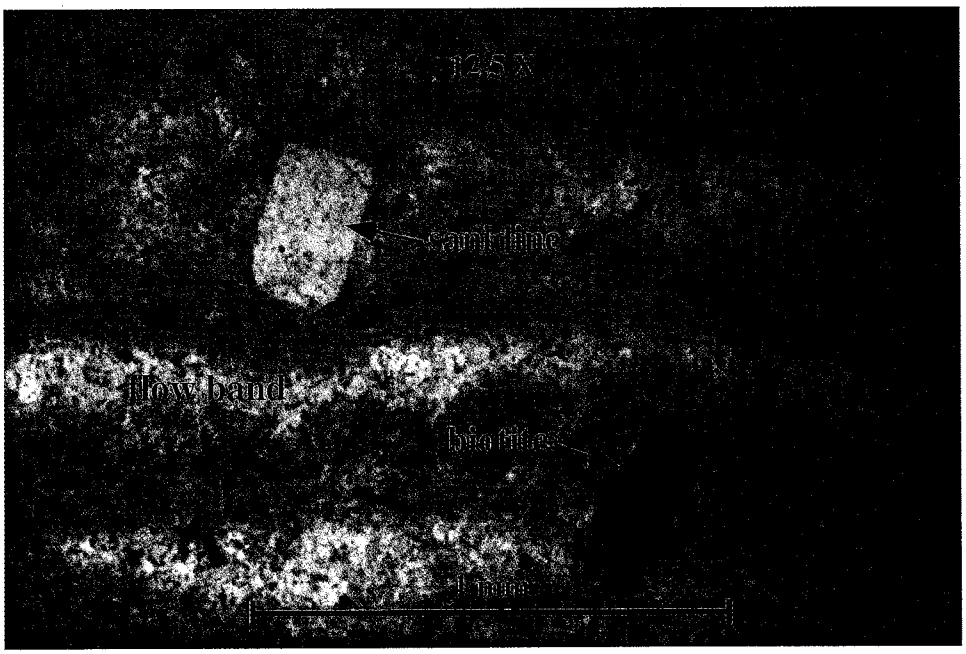

Figure 15 a, b. Rhyolite lava sample S079. **a.** Hand sample cut perpendicular to flow foliation. **b.** Thin section in plane polarized light.

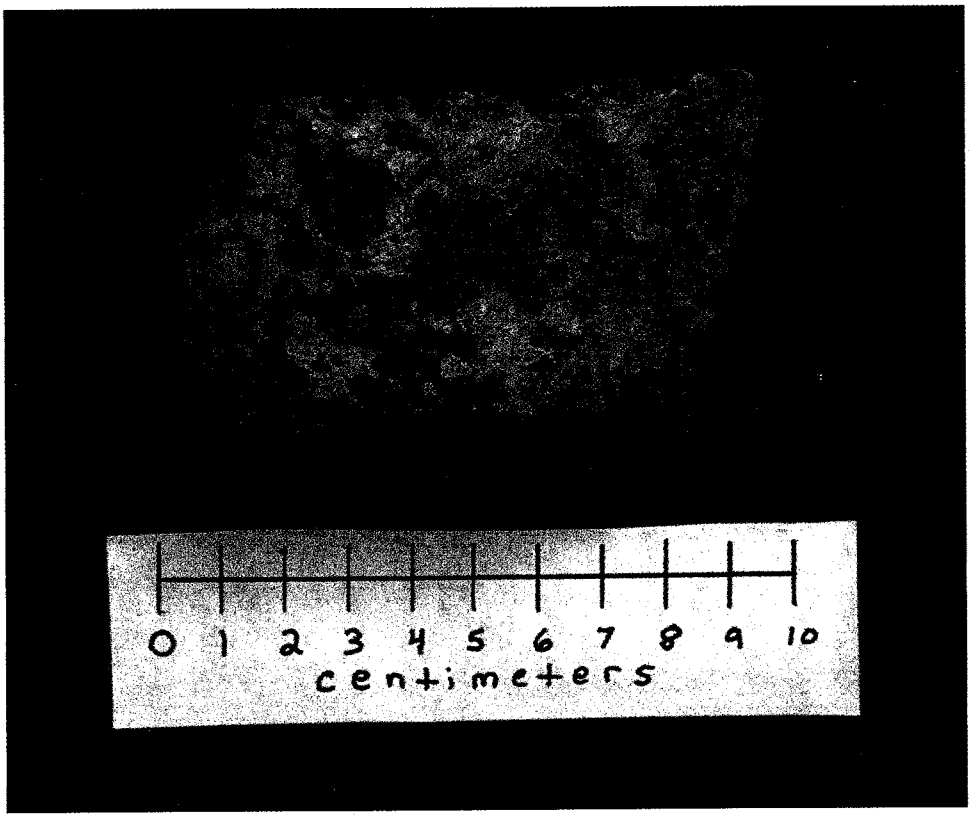

Figure 16. Sphereulitic texture of rhyolite lava. Sample from near lava flow margin.

Figure 17. Vitric carapace breccia of a rhyolite lava. Camera location: UTM 13N 0268683(E), 3726012(N).

1.1 km^2 and are sub-rounded, irregular, or elongate north-south. In outcrop they are pinkish grey and commonly weather spheroidally (Fig. 18). They are holocrystalline granite porphyries that consist of large (2 mm-15 mm) K-feldspar phenocrysts (35%) set in a microcrystalline groundmass (65%) of sanidine, quartz, and plagioclase (Fig. 19 a-c).

3.4. Rhyolite Dikes and Stocks (Ti2)

Several 28.3 Ma rhyolite dikes and small stocks intrude the rhyolite lavas in the northwest quarter of the study area. Dikes range from 5 m to 60 m thick, and stocks reach up to 300 m in diameter. Phenocrysts make up 25% of these rocks and consist of 13% euhedral sanidine (2 mm-6 mm), 12% rounded quartz (1 mm-4 mm), and trace biotite (Fig. 20 a, b). The groundmass (75%) is composed predominately of microcrystalline sanidine and quartz.

3.5. Lower Volcaniclastic Sediment (Tvc1)

A 5 m to 60 m thick sequence of volcaniclastic sedimentary rocks conformably overlies rhyolite lava west of the Deep Canyon Fault. The base of the unit is typically coarse-grained, moderately sorted, thin-bedded (4 cm-5 cm) or massive sandstone of variable thickness. In some places it grades upsection into a laminated or cross-bedded sandstone (Fig. 21). The upper contact of this sandstone is abrupt or gradational with overlying moderately sorted, thin-bedded, pebble conglomerate or very coarse sandstone. Clasts are sub-rounded to sub-angular and composed of potassium feldspar, quartz, and rhyolite with lesser amounts of pumice and biotite. Abruptly overlying this is a thin-bedded, poorly sorted, clast-supported pebble conglomerate composed of rhyolite lava clasts.

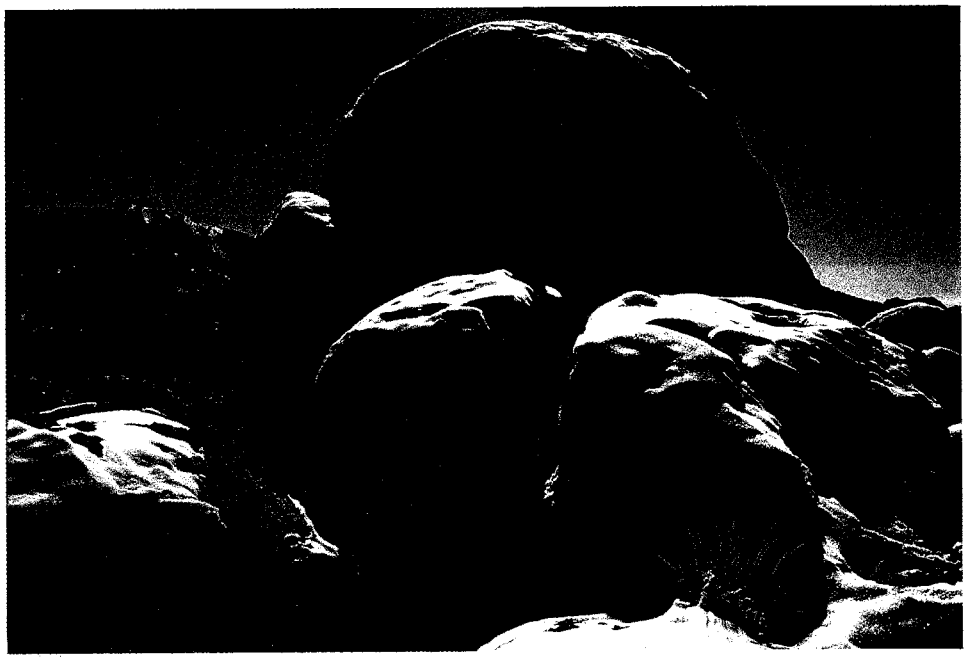

Figure 18. Spheroidal weathering of granite porphyry. Camera location: UTM 13N 0267310(E), 3724079(N).

a)

b)

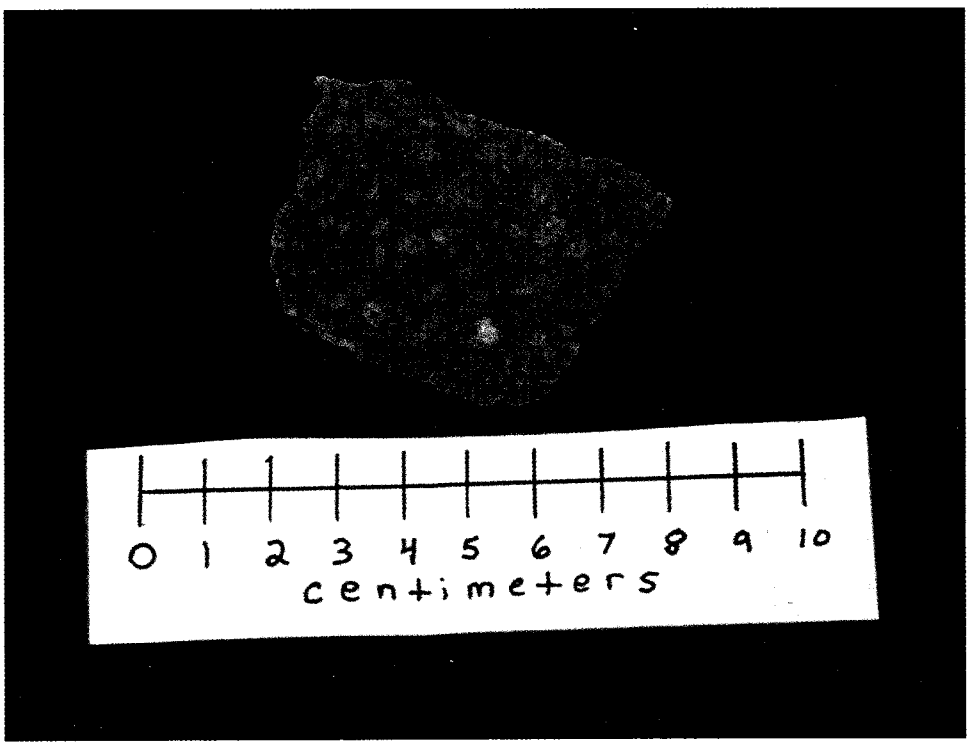

Figure 19 a-c. Granite porphyry. **a.** Outcrop located at UTM 13N 0271330(E), 3725612(N). **b.** Hand sample S047. **c.** Thin section of S047 under crossed polars.

c)

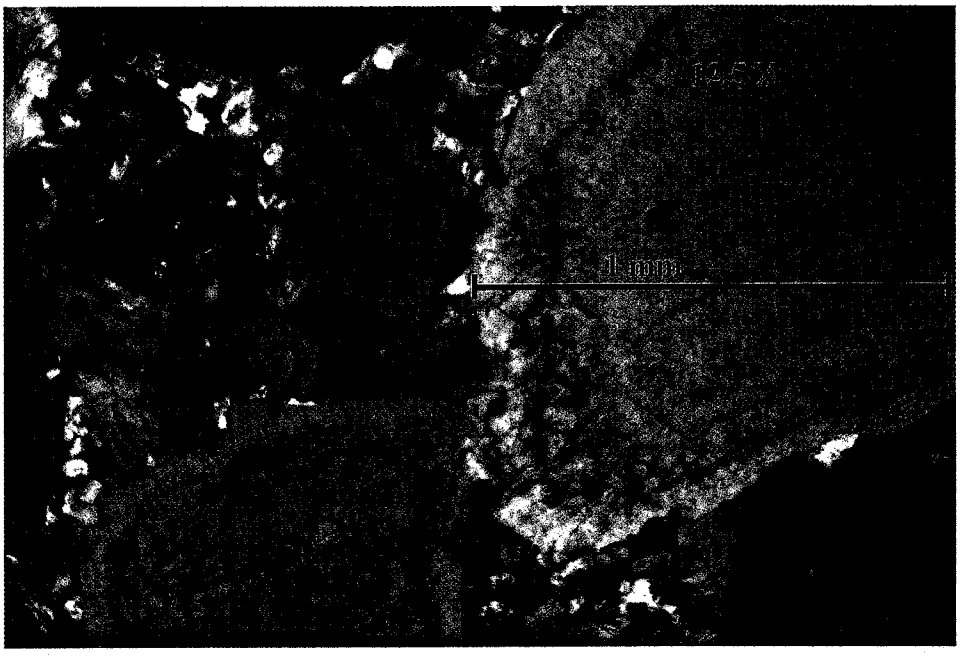

Figure 19 a-c (continued).

a)

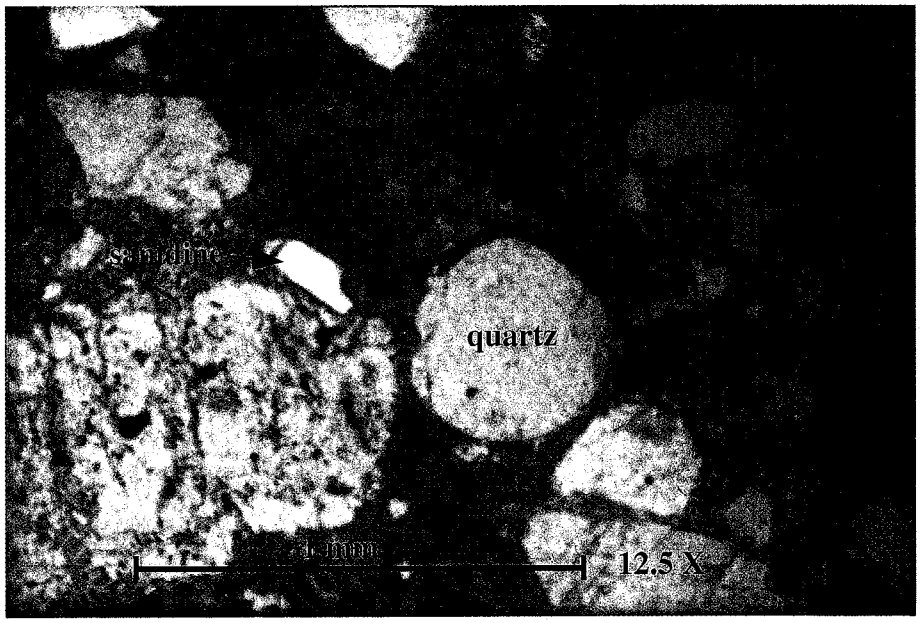

b)

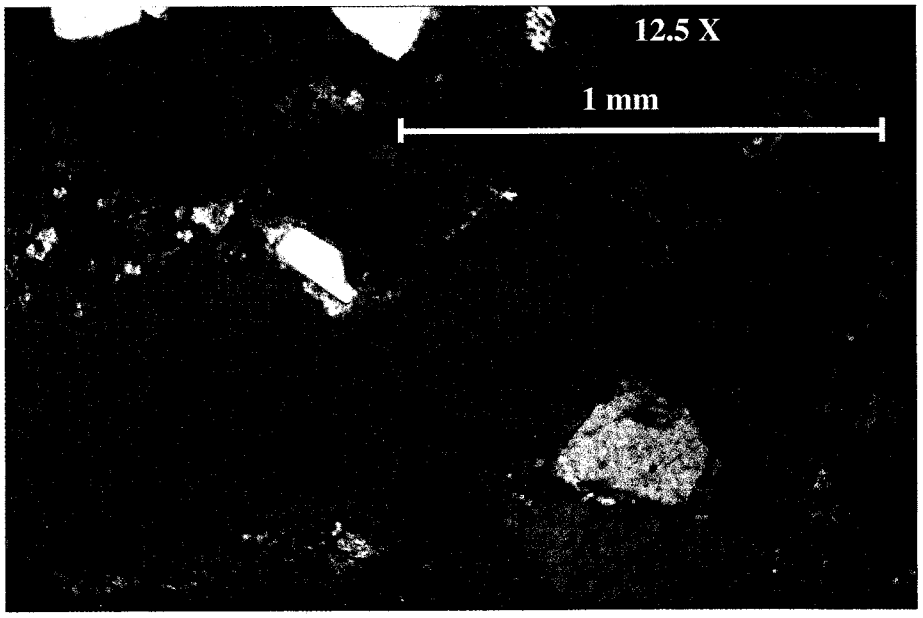

Figure 20 a, b. Photomicrographs of rhyolite intrusion sample S076. **a.** Plane polarized light. **b.** Crossed polars.

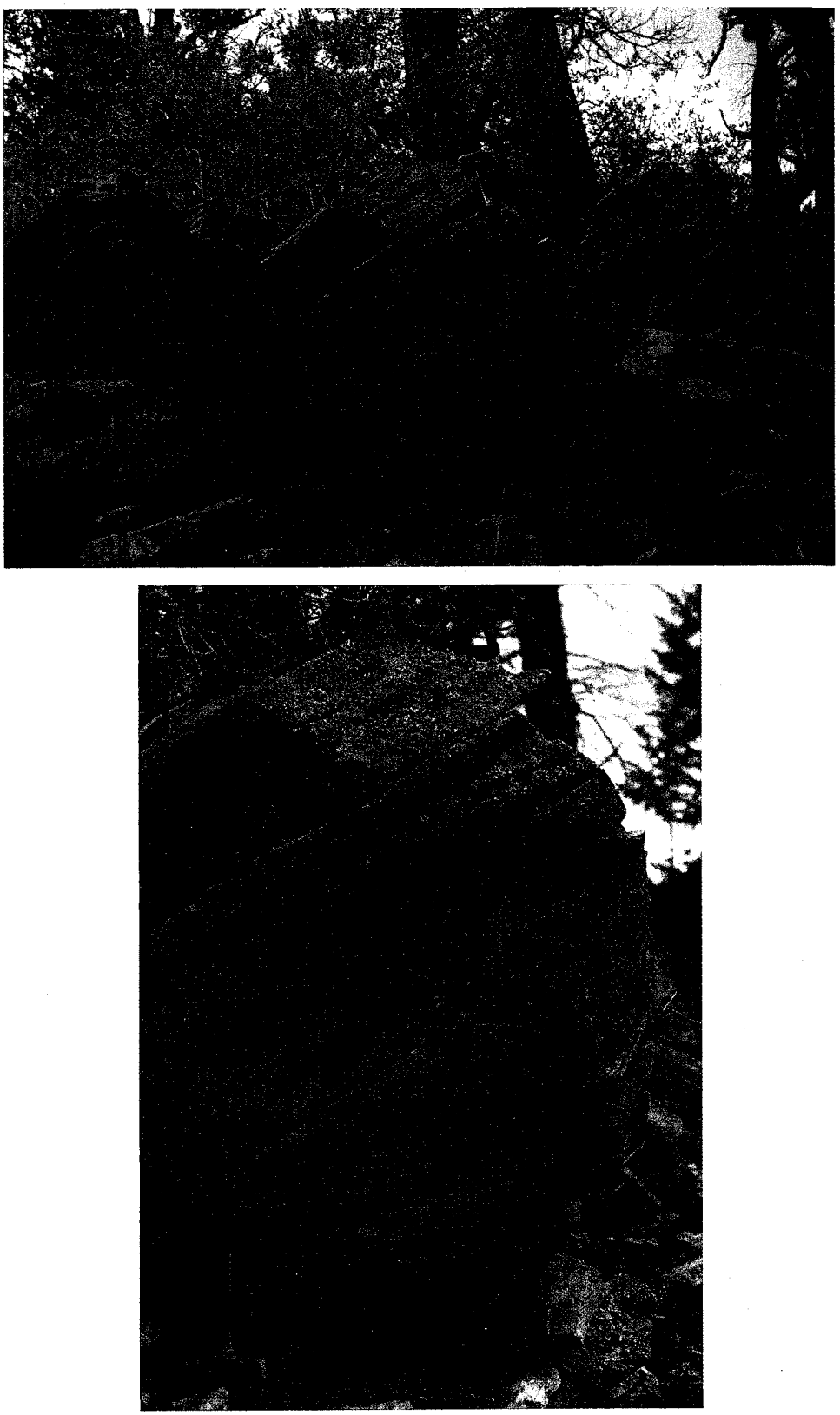

Figure 21. Sandstone beds in the lower volcaniclastic unit of this study area. Camera location: UTM 13N 269641(E), 3725839(N).

3.6. Turkey Springs Tuff (Tts)

The 24.3 Ma Turkey Springs Tuff is in between the upper and lower volcaniclastic units in this study area. It ranges from 70 m to 110 m in thickness and consists of a non-welded base (4 m-15 m, Fig. 22), welded interior (Fig. 23), and in some places a non-welded top (1 m-5 m). A 110 m section was measured at UTM 13N, 0270100(E), 3728400(N) (Fig. 24).

The Turkey Springs Tuff is a high-silica rhyolite ignimbrite containing of 77%-78% SiO_2 (Ferguson, 1986). Phenocrysts throughout the unit are mostly euhedral, chatoyant sanidine (1 mm-3 mm) and subhedral quartz (1 mm-2 mm) set in a partially devitrified groundmass of ash and pumice (Fig. 25 a, b). The unit also contains minor amounts of biotite and plagioclase. Phenocryst content increases from 3% sanidine and 1% quartz in the non-welded base to 10% sanidine and 10% quartz near the top. Pumice content and size increases from 3% pumice (0.2 cm-1 cm) in the base to 15% pumice (5 cm-10 cm) in the non-welded top. Fiamme in the welded interior have aspect ratios as large as 10:1. Lithic fragments of rhyolite lava constitute 10% of the non-welded base. Lithic content abruptly decreases upsection to less than 1%.

3.7. Upper Volcaniclastic Sediment (Tvc2)

Overlying the Turkey Springs Tuff is a sequence of volcaniclastic sedimentary rocks consisting of interbedded sandstone and conglomerate. As much as 18 m of this unit is exposed in the northern half of this study area, where it is in fault contact with older rhyolite lava. The sandstone beds are coarse-grained, moderately sorted, and 0.5 m to 5 m thick. Clast-supported, fine sandy matrix cobble and boulder conglomerate beds

a)

b)

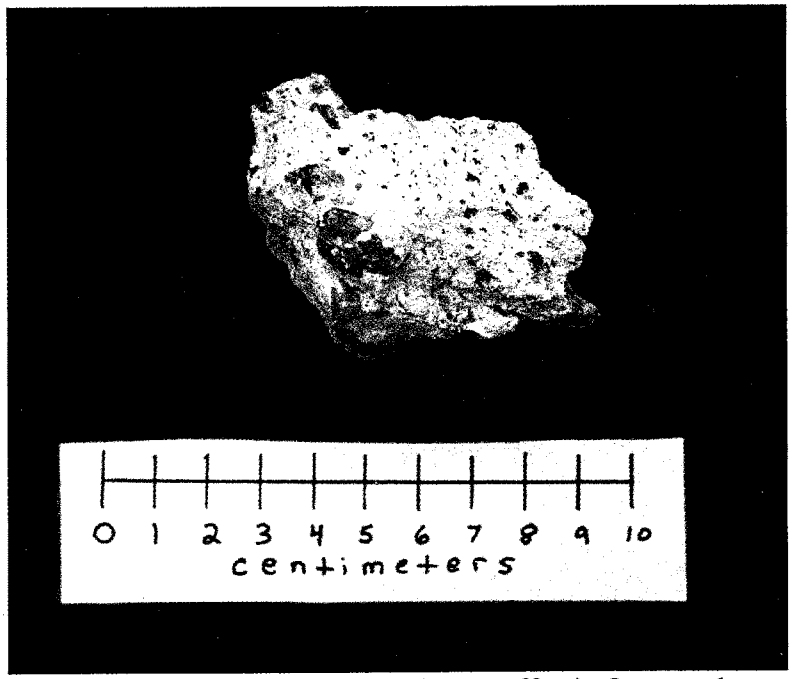

Figure 22 a, b. Non-welded basal Turkey Springs Tuff. a) Outcrop located at UTM 13N 0270117(E), 3728362(N). b) Hand sample.

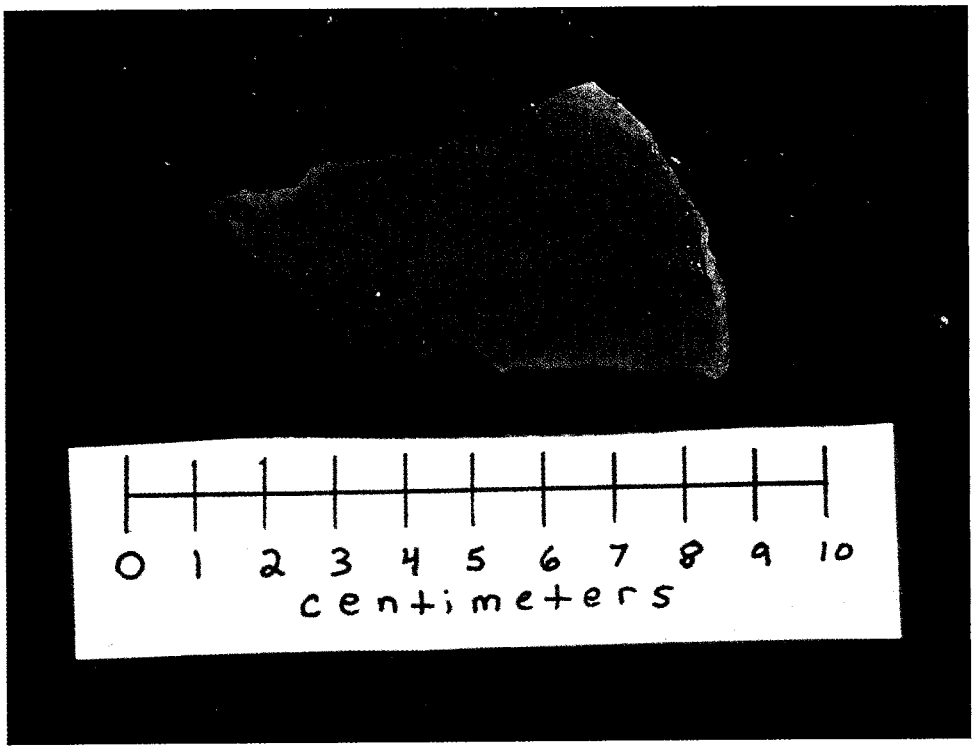

Figure 23. Hand specimen (S056) from welded interior of Turkey Springs Tuff.

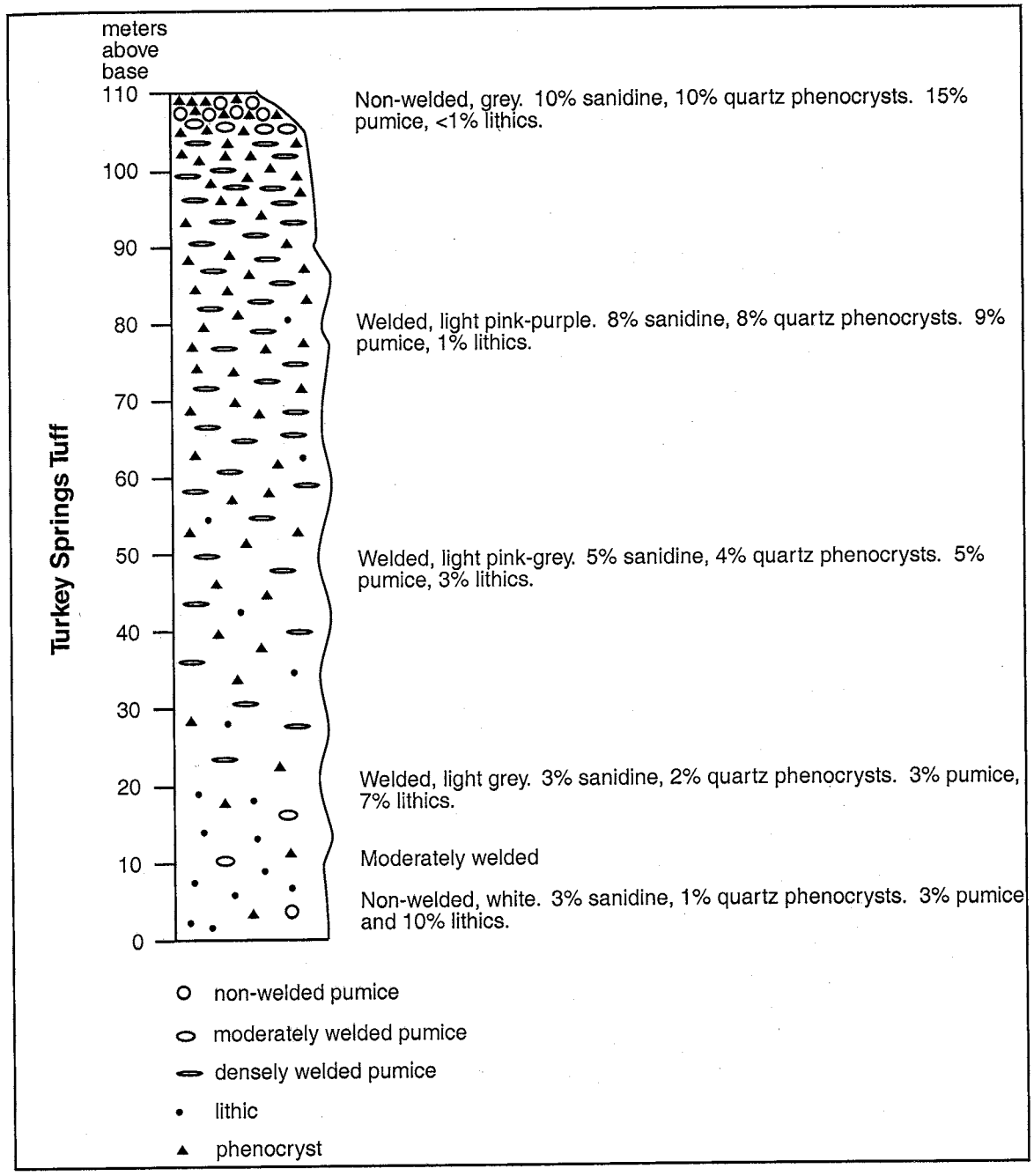

Figure 24. Stratigraphic section of the Turkey Springs Tuff. Base of measured section located at UTM 13N, 0270100(E), 3728400(N).

a)

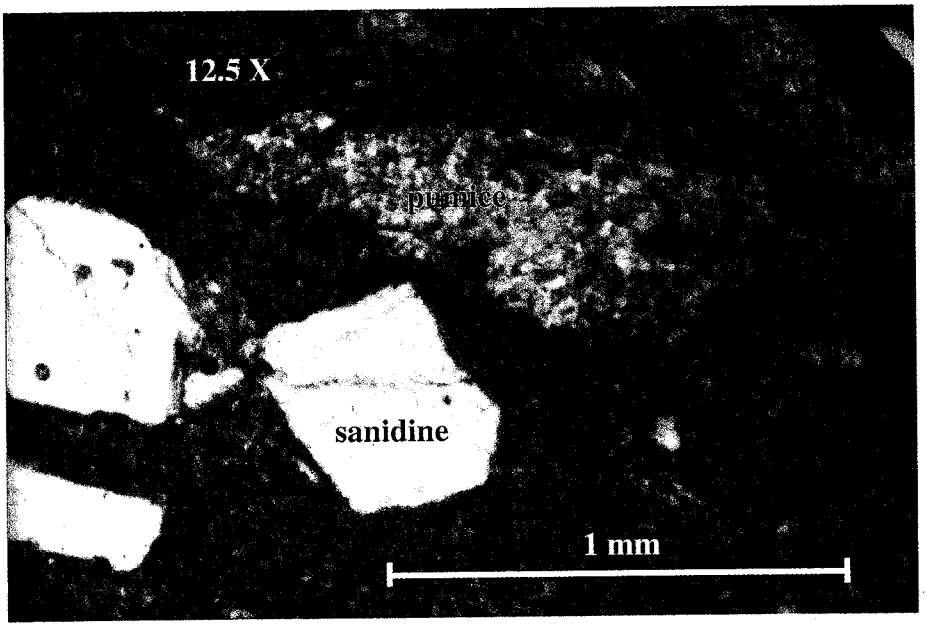

b)

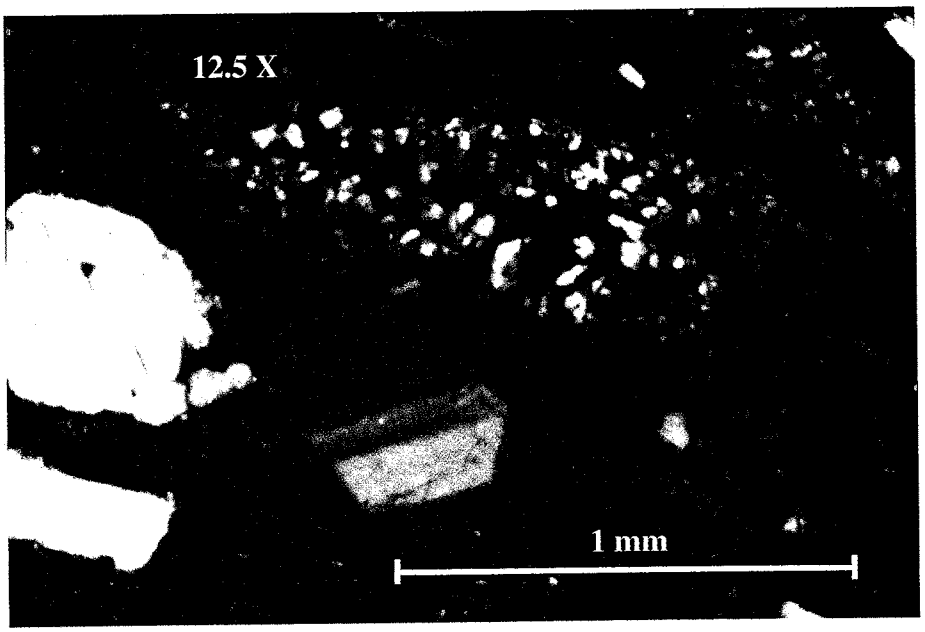

Figure 25 a, b. Photomicrographs of welded Turkey Springs Tuff (S025). **a.** Plane polarized light. **b.** Crossed polars.

are massive, poorly sorted, poorly indurated, and 0.5 m to 6 m thick. Clasts consist of sub-rounded rhyolite lava (0.5 cm-1 m) and sparse Turkey Springs Tuff.

4. STRUCTURE

Predominant structures within the San Mateo Mountains are of two types: late Oligocene caldera collapse structures and north-trending normal faults related to late Cenozoic extensional tectonism. This study area is within the oldest of these structures, which is the Nogal Canyon Caldera (28.4 Ma). It appears to be a resurgent caldera, although structures related to its development may be buried by thick sequences of post-caldera rhyolite lava in this study area. The Mt. Withington Caldera (27.4 Ma) in the northern San Mateo Mountains collapsed as a northwest-tilted trap door structure (Ferguson, 1991). Nested at the western end of the Mt. Withington Caldera is the 24.4 Ma Bear Trap Canyon Caldera, which is a symmetrical resurgent caldera with a central dome bisected by a north-trending apical graben (Osburn and others, 1997).

Extensional tectonism has tilted rocks in this part of the San Mateo Mountains gently to the east (11°-25°). The majority of the structures in this study area are north-south trending, down-to-the west normal faults (Fig. 26). Some east-west trending, small displacement normal faults are also present. A structure map of this study area is shown in Figure 27. The Deep Canyon Fault is a major normal fault that bisects this study area. In some places it has juxtaposed Vicks Peak Tuff and Turkey Springs Tuff, giving it an estimated stratigraphic displacement on the order of 1115 m. It continues to the north into an unmapped area. To the south its displacement increases to 1300 m and it cuts

Quaternary alluvial deposits (Hermann, 1986). Silicification occurs near the major faults in this study area as thin pervasive zones and quartz veinlets.

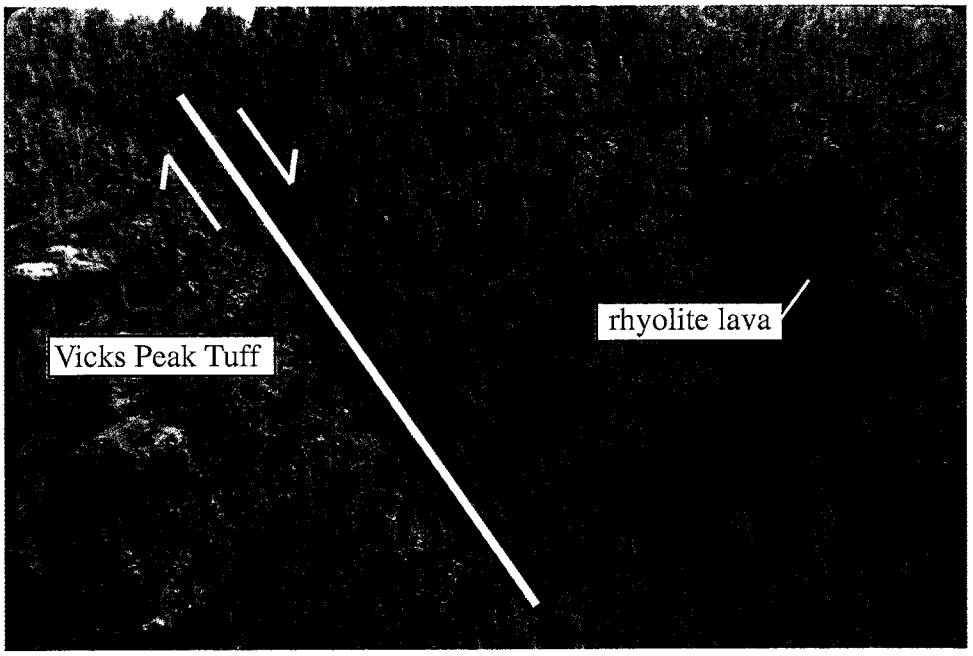

Figure 26. Rhyolite lava down-dropped against Vicks Peak Tuff along down-to-the-west normal fault. Looking south from UTM 13N 0268400(E), 3724321(N).

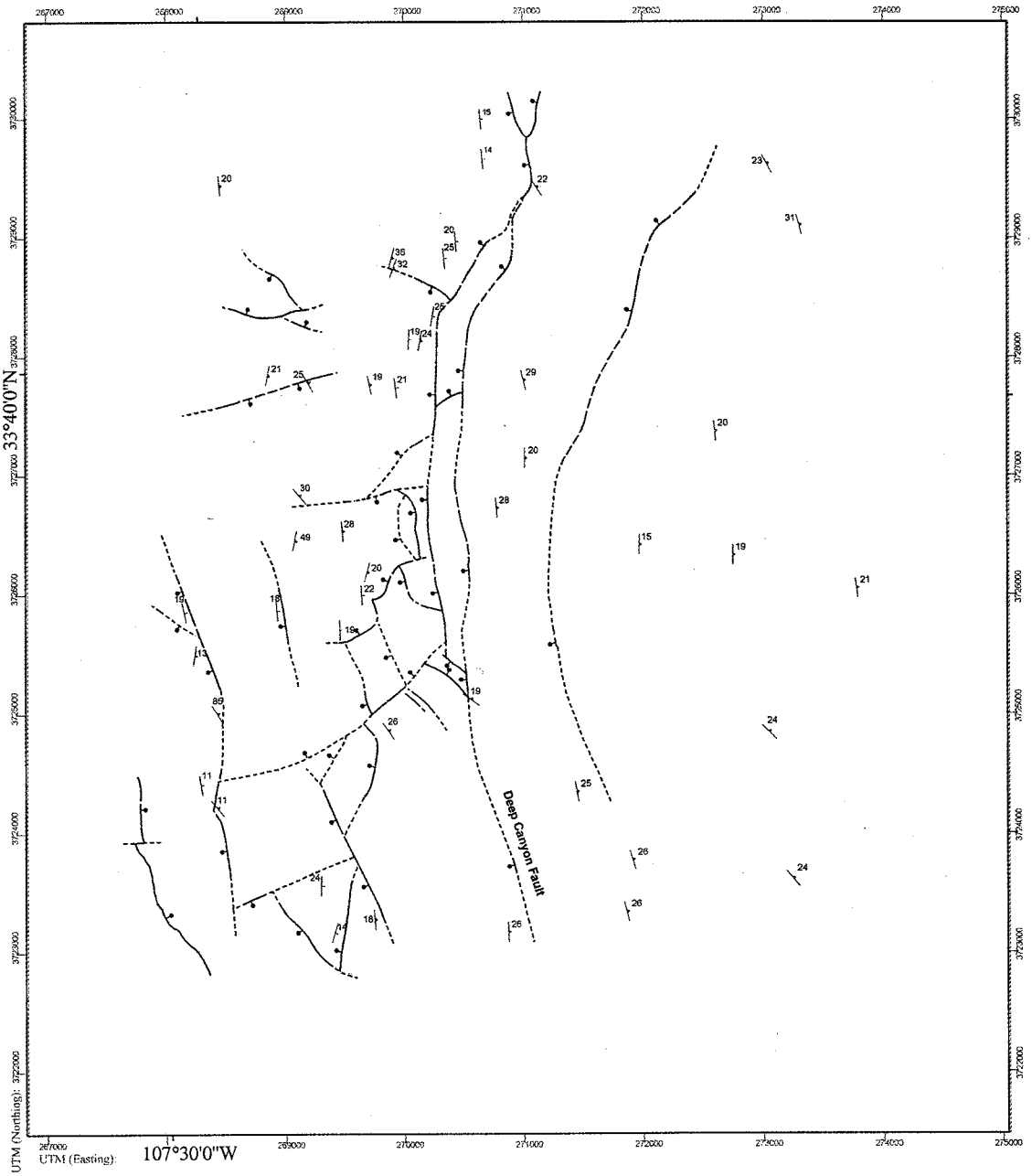

Figure 27. Structure map of this study area.

5. SANIDINE MINERALOGY

Sanidine mineralogy was studied in thin section by optical microscope and in polished grain mounts by electron microprobe. In thin section, sanidine appears euhedral or fragmental, tabular or blocky, and untwinned or Carlsbad twinned. They are mostly clear, homogeneous, and unaltered, although a few have minor kaolinite and/or sericite alteration along cleavages and fractures.

Three to nine grains from each of 14 samples were analyzed using the New Mexico Bureau of Geology CAMECA SX-100 electron microprobe with beam diameter set at 10 μm, beam current at 20 nA, and accelerating voltage at 15 kV. Back-scattered electron images show mostly unaltered crystals (Fig. 28 a-f). Some crystals from the granite porphyry stocks show significant chemical variation across the grain (Fig. 28 c), an indication of a more complex crystallization history.

The average SiO_2, Al_2O_3, K_2O and Na_2O compositions from 21 analyses of an orthoclase standard have 1σ errors of ±0.5%, ±0.7%, ±0.8% and ±2.1%, respectively (Appendix B). These averages agree within 0.1% - 0.2% of the established composition of the orthoclase standard (J. Donovan, personal communication). Quantitative analyses of crystal unknowns show that all are Na-rich sanidines that range in composition from $Or_{56}Ab_{43}$ to $Or_{39}Ab_{57}$ (Appendix C, Fig. 29). Ca contents range from $An_{7.3}$ to $An_{0.1}$. K/Ca ratios range from 7 to 498. The 28.4 Ma sequence of volcanic rocks in this study

a)

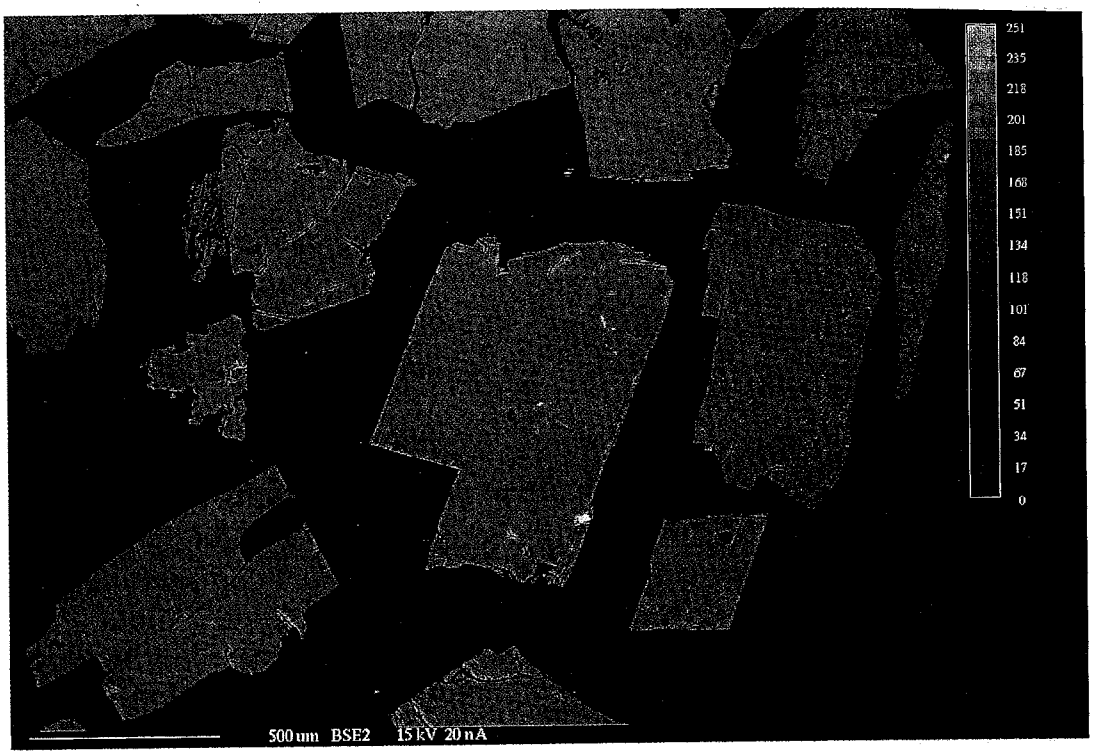

b)

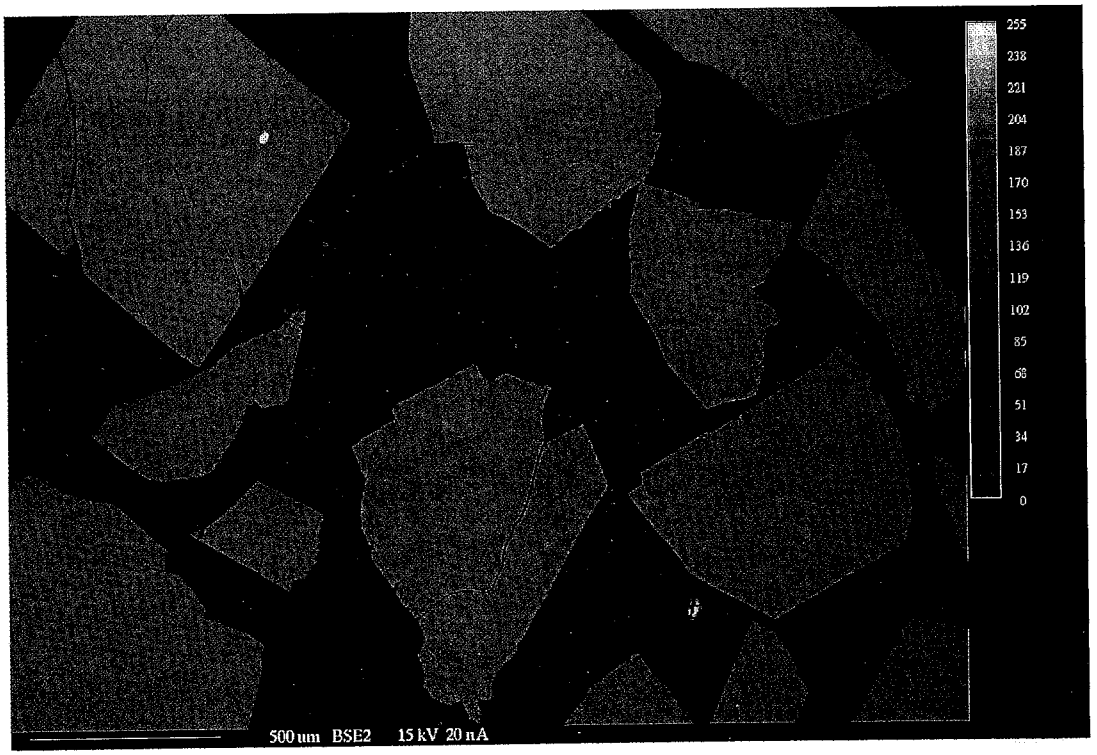

Figure 28 a-f. Representative back-scattered electron images of sanidine from each rock unit analyzed by electron microprobe. a) Vicks Peak Tuff (S085). b) Rhyolite lava (S069). c) Granite porphyry (S047). d) Rhyolite intrusion (S068). e) Rhyolite ignimbrite (S075). f) Turkey Springs Tuff (S071).

c)

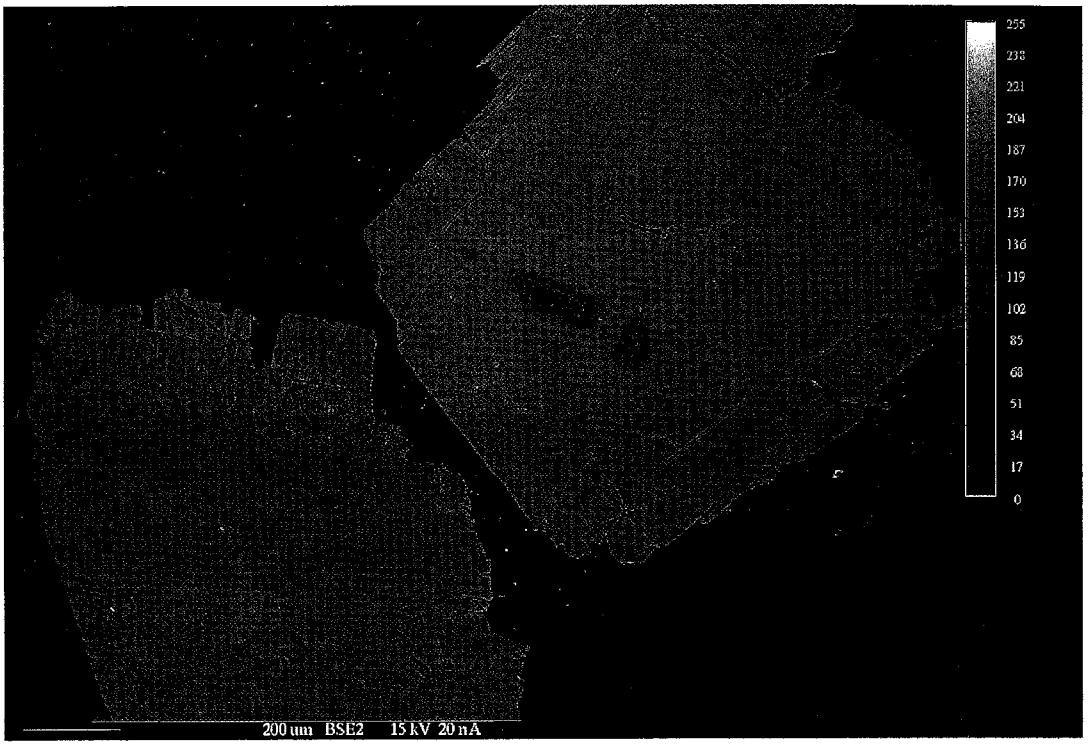

d)

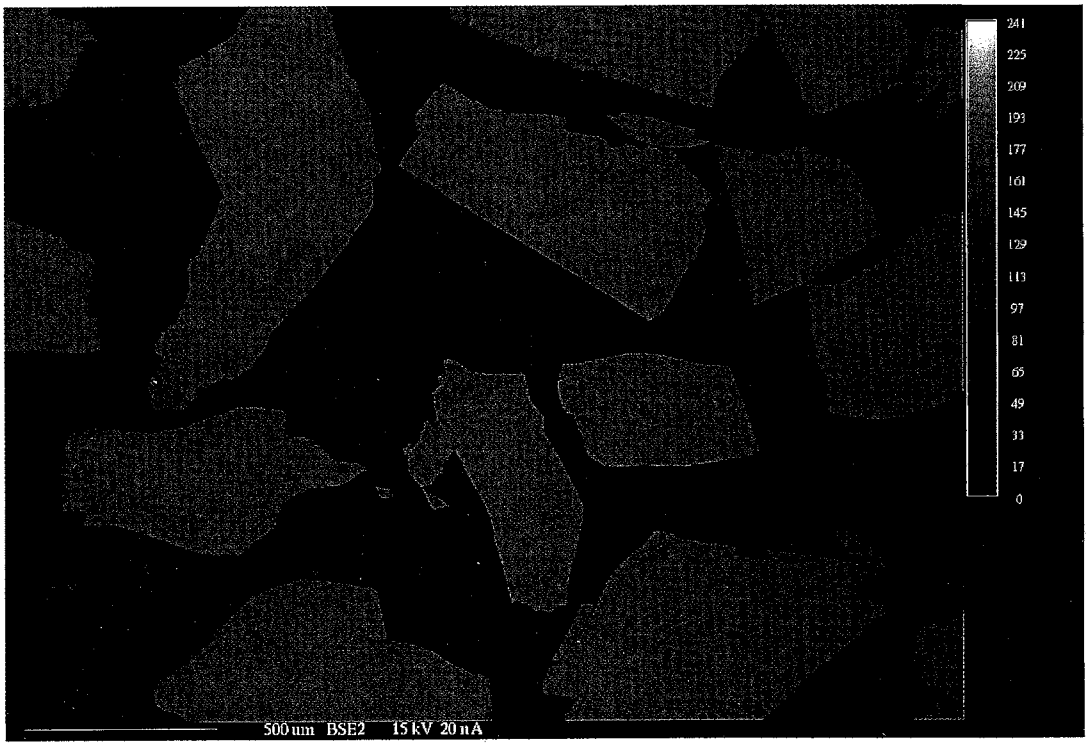

Figure 28 (continued).

e)

f)

Figure 28 (continued).

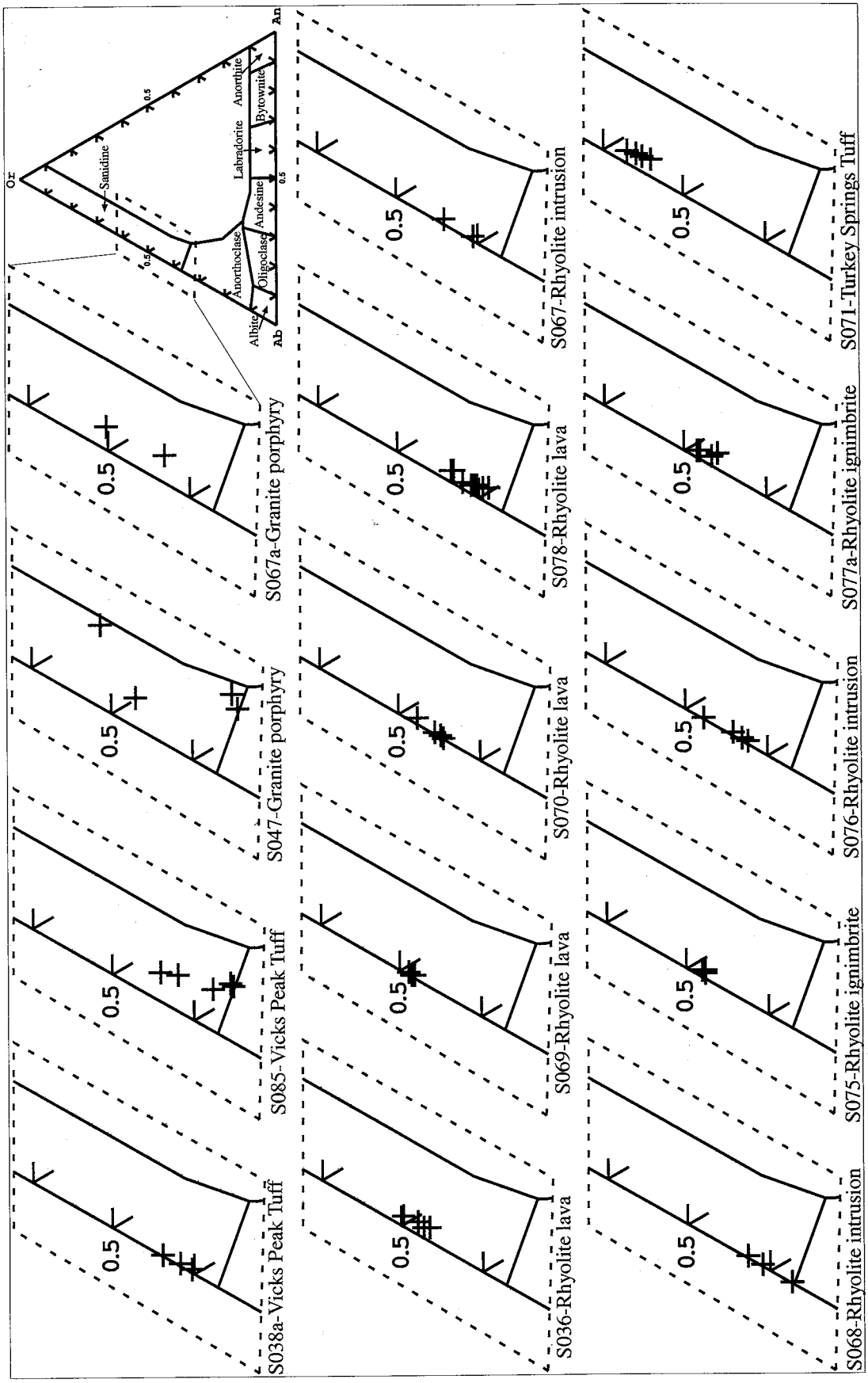

Figure 29. Feldspar classification diagrams of each sample analyzed in this study using electron microprobe.

area contain sanidine that cluster between $Or_{49}Ab_{51}$ and $Or_{39}Ab_{57}$, whereas the 24.4 Ma Turkey Springs Tuff sample averaged $Or_{56}Ab_{43}$ (Fig. 29). Although only a single sample of Turkey Springs Tuff was analyzed, this difference suggests some potential for using sanidine composition as a correlation tool.

6. $^{40}Ar/^{39}Ar$ GEOCHRONOLOGY

6.1. Methods

All of the rock units in this study area except for the upper volcaniclastic unit were sampled for geochronological studies. Samples were collected from fresh outcrops displaying no obvious alteration. The 32 samples collected were crushed and sieved, and sanidine crystals (0.4-1.2 mm in diameter) were separated using heavy liquid, magnetic, and hand picking techniques. Some separates were treated with 15% HF in an ultrasonic cleaner to remove glass from crystal surfaces.

Two separate packages of samples were each irradiated for 7 hours in the D-3 position of the Texas A&M reactor. Both irradiation packages contained several 16-hole Al discs, each hole loaded with approximately 50 sanidine crystals from a particular sample. Neutron fluxes were monitored with Fish Canyon Tuff sanidine with an assigned age of 27.84 Ma, equivalent to Mmhb-1 at 520.4 Ma (Samson and Alexander, 1987).

Irradiated samples were analyzed in the New Mexico Geochronology Research Laboratory at New Mexico Tech. 15-50 sanidines from each sample were individually

loaded into 221-hole copper sample trays and placed in a 3 3/8" diameter stainless steel conflat laser chamber with a ZnS window. Single sanidines were fused in a single increment using a Synrad CO_2 laser set to 1. 6 W for samples S025-S086 and 5 W for samples S103-S118. Gas evolved from the sanidine was expanded through a cold finger (-140° C) and into the extraction line where it was exposed to a tungsten filament (2000° C) and two SAES GP-50 getters (one at 450° C and the other at 20° C). After removal of reactive gases, argon was expanded into a MAP 215-50 mass spectrometer operated in static mode for analysis. Argon isotopes were measured on a Johnston electron multiplier with an average sensitivity of 1.89×10^{-16} moles/pA for samples S025-S086 and 8.82×10^{-17} moles/pA for samples S103-S118. Blanks were determined between every four analyses. Total system blank and background for samples S025-S086 averaged 108, 1.2, 0.2, 1.0, and 0.9×10^{-18} moles for ^{40}Ar, ^{39}Ar, ^{38}Ar, ^{37}Ar, and ^{36}Ar, respectively. The rest of the samples averaged 285, 2.9, 0.6, 1.4, and 1.5×10^{-18} moles for ^{40}Ar, ^{39}Ar, ^{38}Ar, ^{37}Ar, and ^{36}Ar, respectively. J-factors were determined to a precision of ±0.1% by CO_2 laser-fusion of 4 single crystals of Fish Canyon Tuff sanidine from each of 4 radial positions around the irradiation tray.

Weighted mean ages and standard error of the mean were calculated by weighting each age analysis by the inverse of the variance (Taylor, 1982). MSWD values were calculated for each sample. If the MSWD was outside the 95% confidence interval for n-1 degrees of freedom, then the error was multiplied by the square root of the MSWD. All errors are reported at $\pm 2\sigma$.

6.2. Results

All data collected from each crystal analyzed are detailed in Appendix D. The apparent age, K/Ca, radiogenic yield, and moles of ^{39}Ar from each crystal are plotted on age probability distribution diagrams for each sample (Fig. 30).

The radiogenic yields of most analyses were between 90% and 99.5%, and most sanidines released 10^{-16}-10^{-14} moles of ^{39}Ar. Average K/Ca ratios range from 3 to 94 for most samples. Samples from the rhyolite intrusions, however, have average K/Ca ratios between 95 and 257. Most K/Ca data from $^{40}Ar/^{39}Ar$ geochronology compares closely to K/Ca data of the same samples from electron microprobe (Appendix E). Apparent ages range from 24.28 Ma to 28.56 Ma, and their 2σ precisions range from ±0.21%-0.78% (±0.06-0.22 Ma). These errors are mostly reflective of the ^{36}Ar measurement and the ±0.1% uncertainty in the J-factor. A summary of $^{40}Ar/^{39}Ar$ results is presented in Table 1. The ages of all samples analyzed in this study are plotted on Figure 31, and they are plotted against K/Ca in Figure 32.

Analyses of the six Turkey Springs Tuff samples yielded relatively high precision results with an average within sample error of ±0.9 Ma (2σ). Only two of the 90 sanidines analyzed were excluded from the age calculations (due to low radiogenic yields, presumably from clay alteration). The other 88 sanidines generated relatively high radiogenic yields (ave.= 98.6%) and high signals (ave.= 2.78×10^{-15} moles of ^{39}Ar released). The K/Ca ratios among the different samples of Turkey Springs Tuff vary relatively little (between 27.7 and 39.5) and are typical values among sanidines from Mogollon-Datil ignimbrites. The six Turkey Springs Tuff samples have a weighted mean age of 24.38 Ma ± 0.03 Ma (2σ). McIntosh (1989) used an incremental heating method of

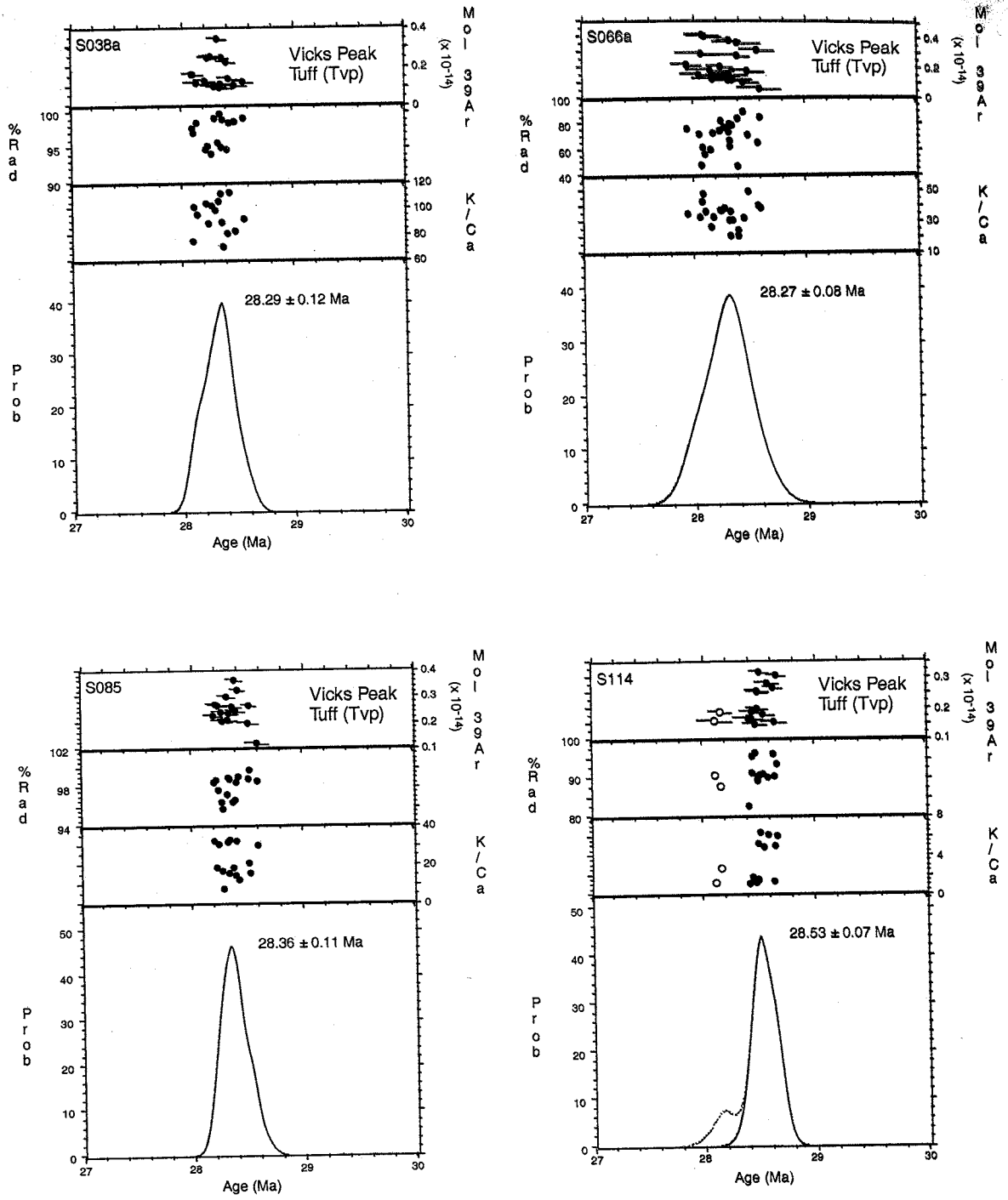

Figure 30. Age probability distribution diagrams of each sample dated in this study. All errors are 2σ.

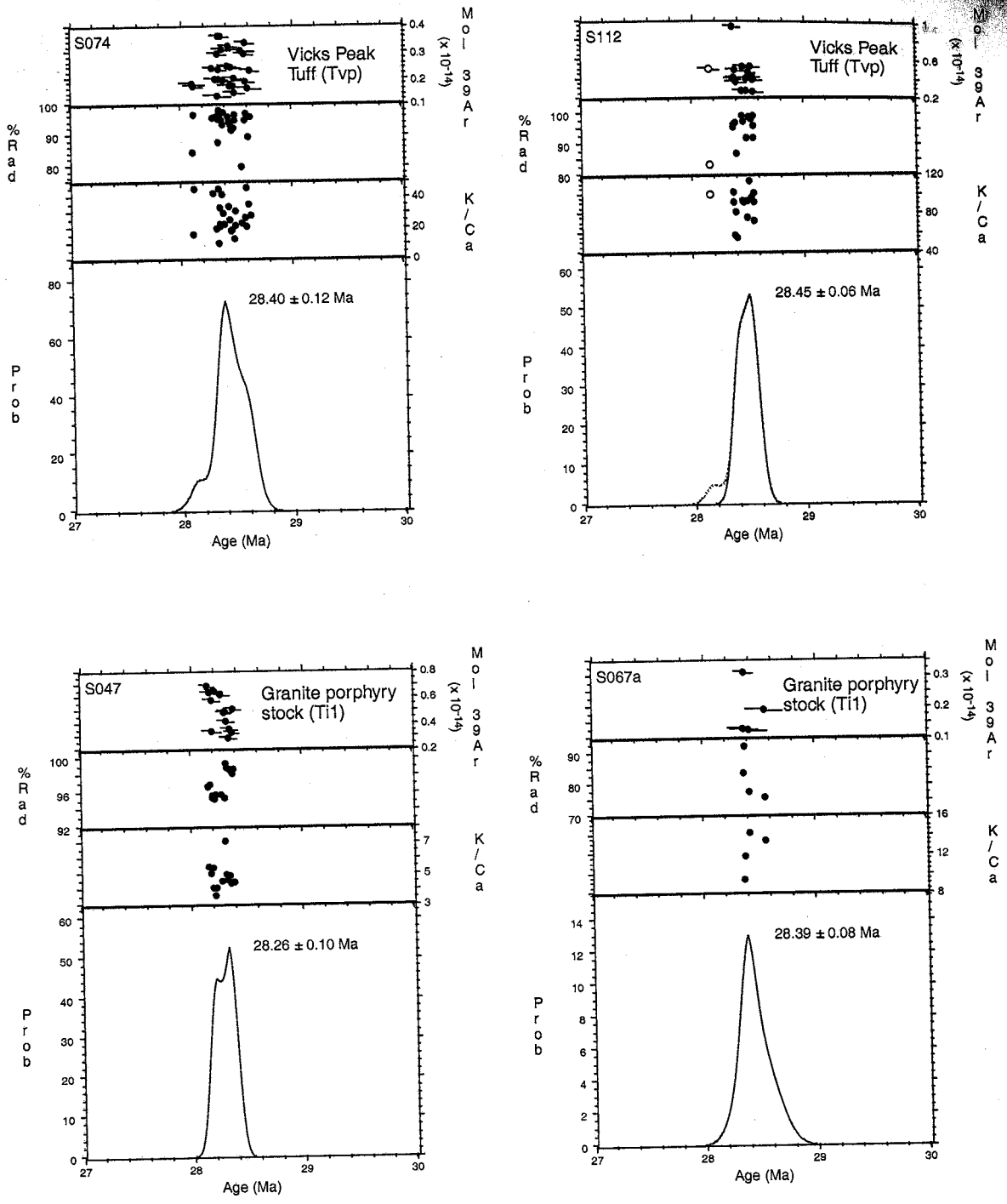

Figure 30 (continued).

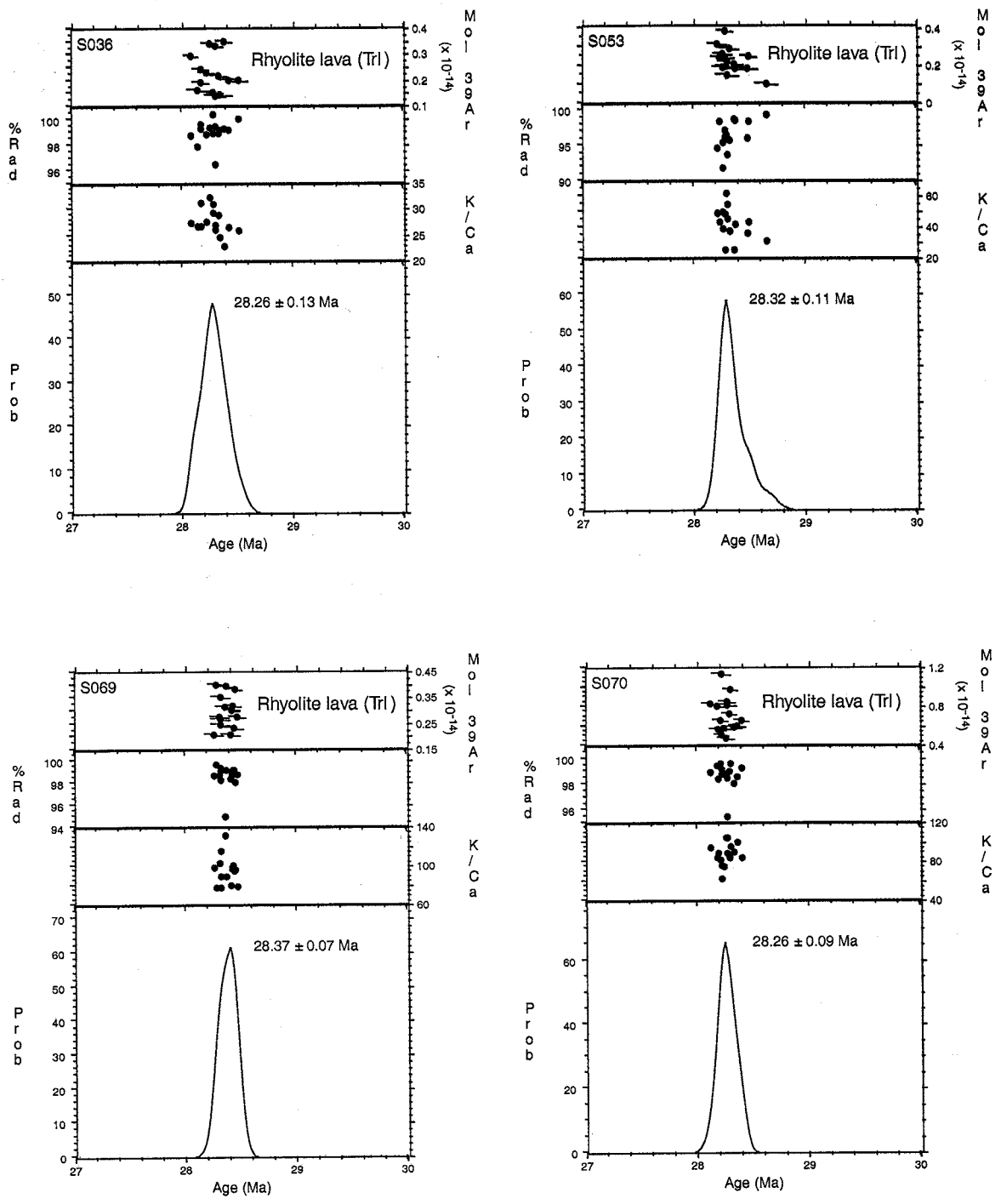

Figure 30 (continued).

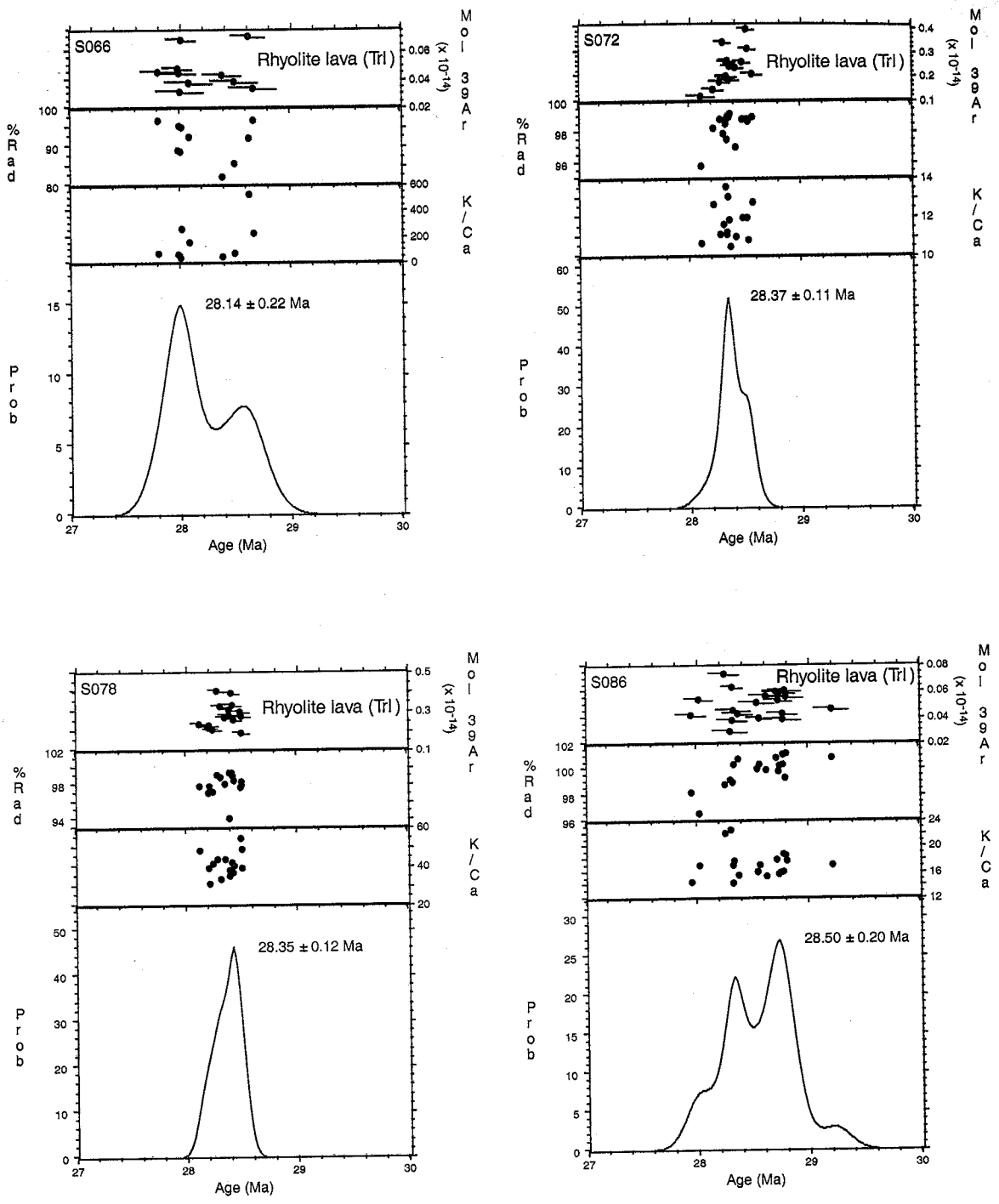

Figure 30 (continued).

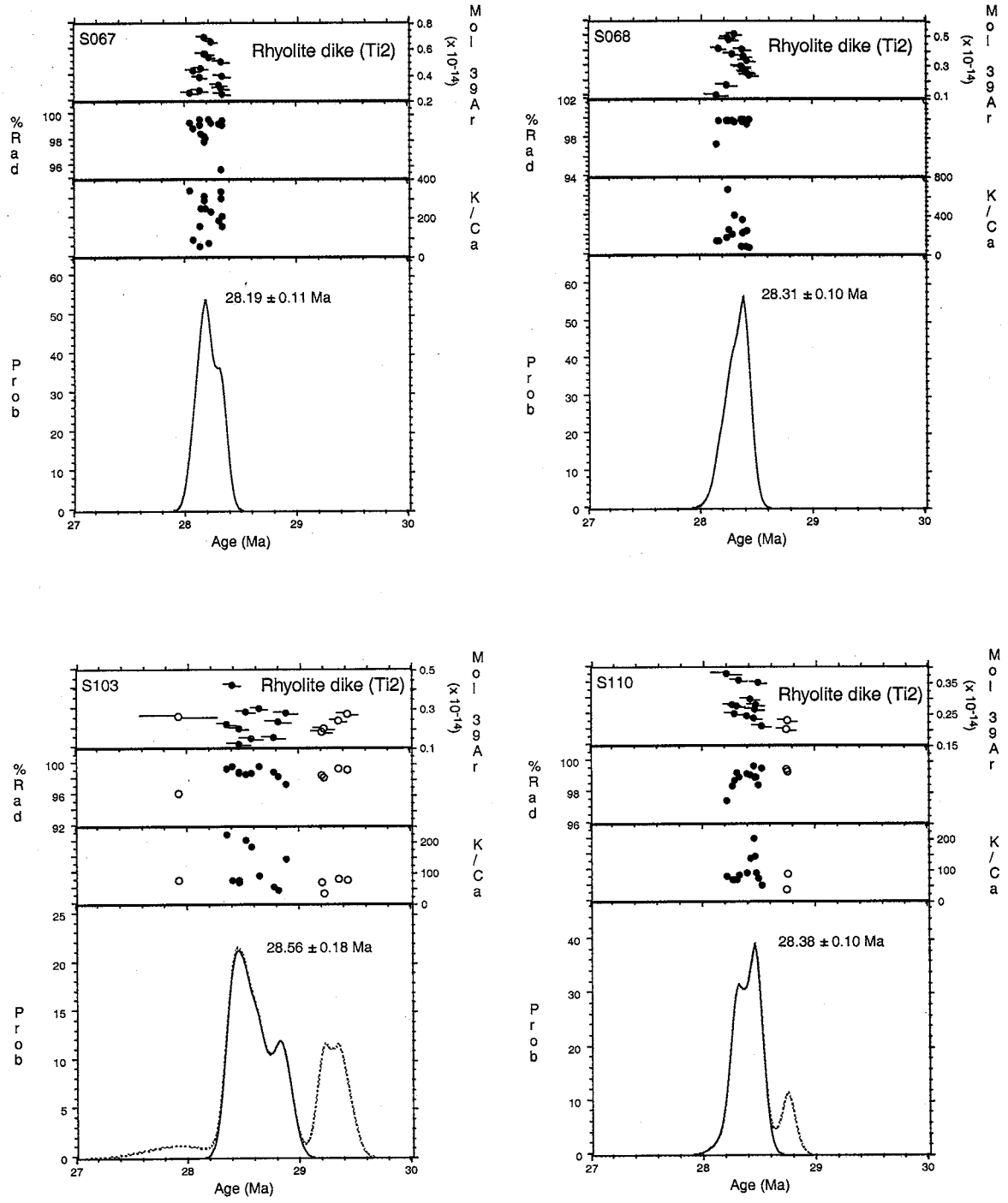

Figure 30 (continued).

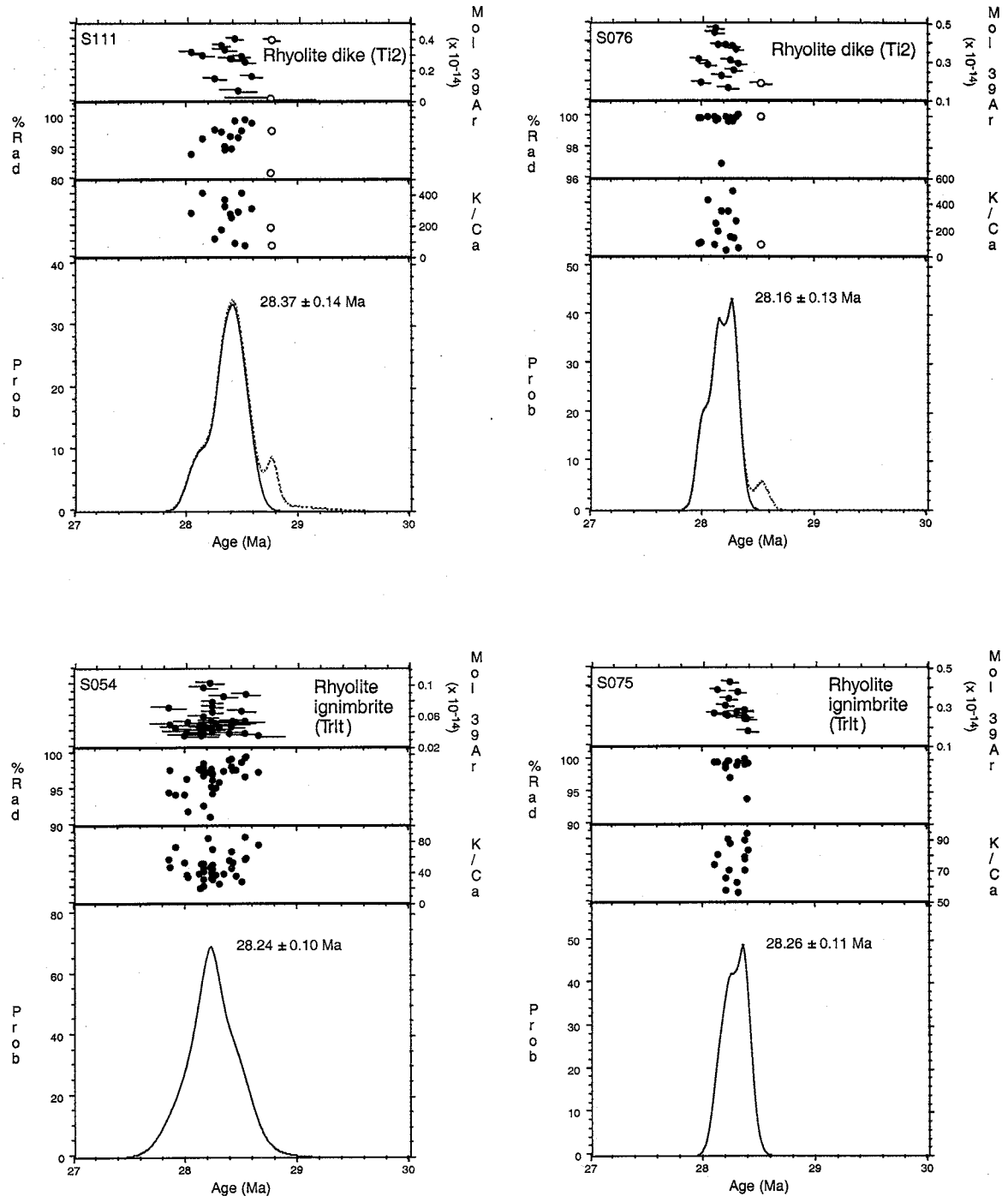

Figure 30 (continued).

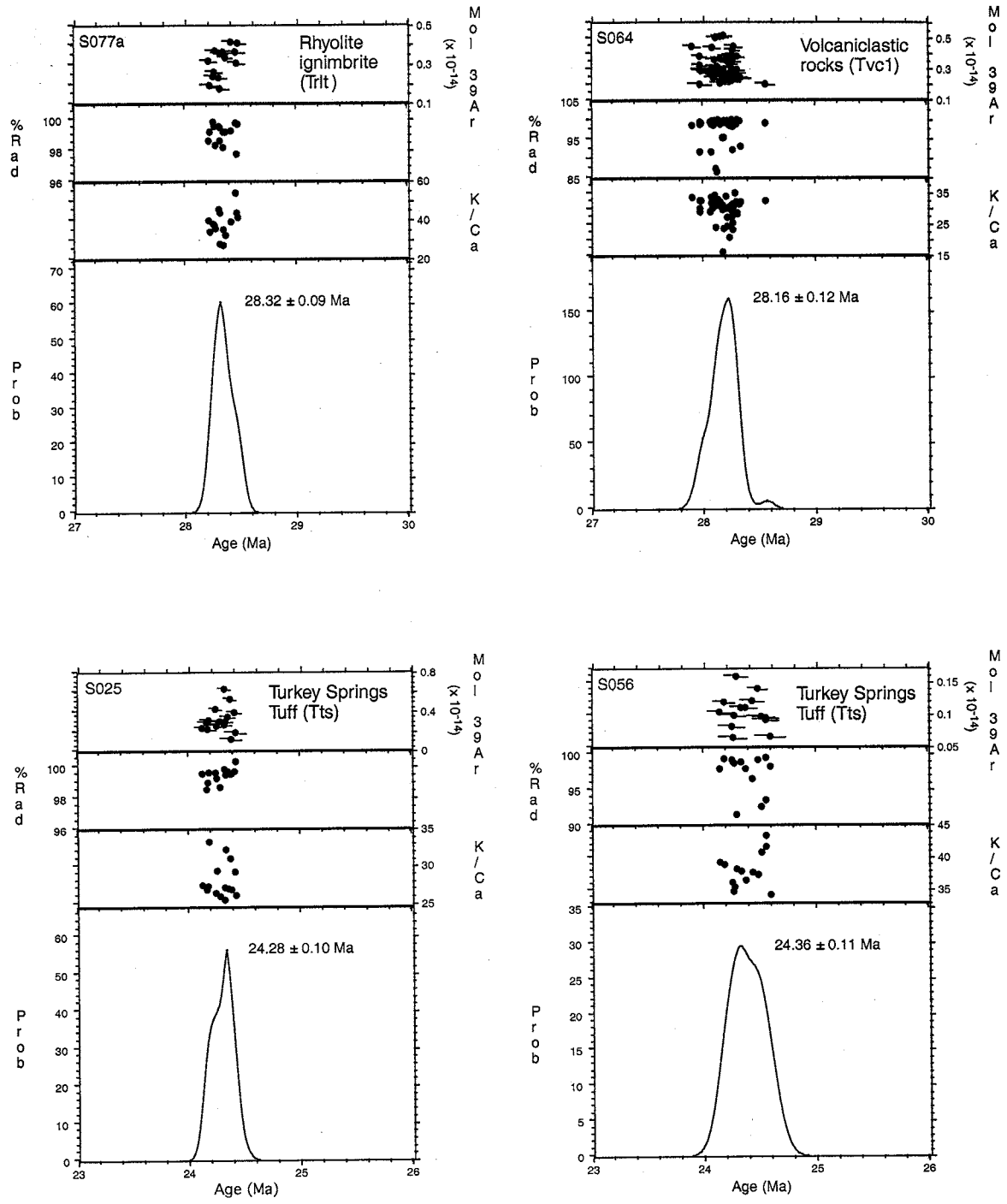

Figure 30 (continued).

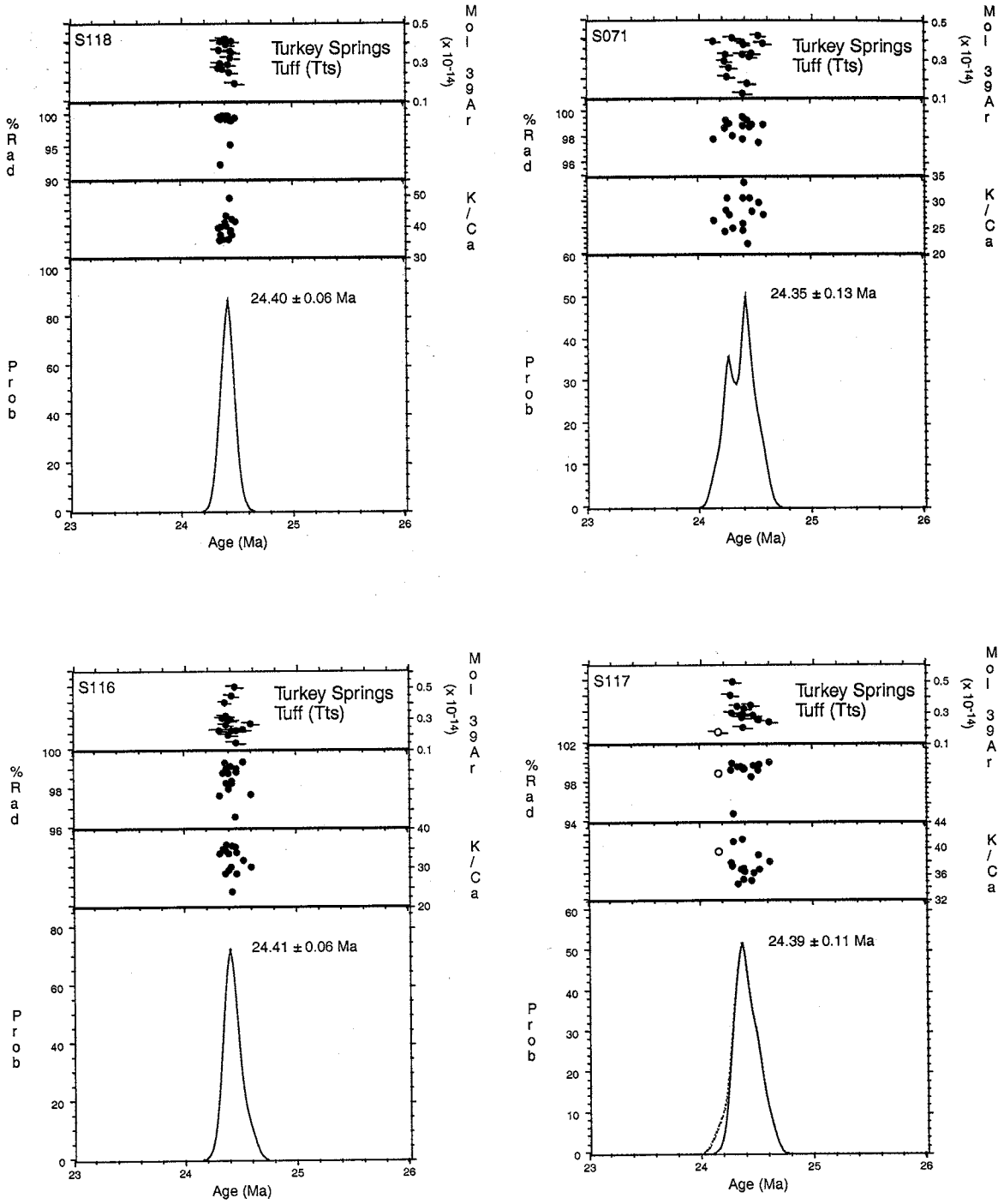

Figure 30 (continued).

Table 1. Summary of $^{40}Ar/^{39}Ar$ results.

Sample	Unit	Location (UTM): Zone (Easting, Northing)	n	K/Ca	±2σ	Age (Ma)	±2σ
S025	Turkey Springs Tuff (Tts)	13S (0270193, 3728384)	15	28.0	2.4	24.28	0.10
S056	Turkey Springs Tuff (Tts)	13S (0269645, 3726548)	14	37.9	2.6	24.36	0.11
S071	Turkey Springs Tuff (Tts)	13S (0270653, 3728959)	15	27.7	3.1	24.35	0.13
S116	Turkey Springs Tuff (Tts)	13S (0269452, 3722681)	15	31.8	3.5	24.41	0.06
S117	Turkey Springs Tuff (Tts)	13S (0269364, 3723250)	14	37.2	2.0	24.39	0.11
S118	Turkey Springs Tuff (Tts)	13S (0269354, 3723574)	15	39.5	3.5	24.40	0.06
		Weighted mean ± Taylor error (2σ)		MSWD=1.16		**24.38**	**0.03**
S064	Volcaniclastic sediment (Tvc_1)	13S (0269470, 3725750)	50	29.9	3.6	28.16	0.12
			Range = 27.89 ± 0.10 Ma - 28.55 ± 0.13 Ma				
S068	Rhyolite intrusion (Ti_2)	13S (0269492, 3728620)	15	230.6	152.2	28.31	0.10
S067	Rhyolite intrusion (Ti_2)	13S (0269550, 3728600)	15	212.2	94.5	28.19	0.11
S076	Rhyolite intrusion (Ti_2)	13S (0268518, 3728871)	14	213.3	143.7	28.16	0.13
S103	Rhyolite intrusion (Ti_2)	13S (0269923, 3728311)	10	115.2	66.5	28.56	0.18
S110	Rhyolite intrusion (Ti_2)	13S (0268525, 3729154)	12	95.2	43.2	28.38	0.10
S111	Rhyolite intrusion (Ti_2)	13S (0268466, 3729154)	13	257.2	113.4	28.37	0.14
		Weighted mean ± Taylor error (2σ)		MSWD=4.10*		**28.31**	**0.15***
S054	Rhyolitic ignimbrite (Trlt)	13S (0269585, 3726530)	35	46.3	16.6	28.24	0.10
S077a	Rhyolitic ignimbrite (Trlt)	13S (0274058, 3726865)	15	38.0	7.0	28.32	0.09
S075	Rhyolitic ignimbrite (Trlt)	13S (0268935, 3728460)	15	75.4	12.0	28.26	0.11
		Weighted mean ± Taylor error (2σ)		MSWD=0.78		**28.28**	**0.06**
S036	Rhyolite lava (Trl)	13S (0268700, 3724650)	15	27.5	2.6	28.26	0.13
S066	Rhyolite lava (Trl)	13S (0269568, 3728632)	10	148.8	153.0	28.14	0.22
S069	Rhyolite lava (Trl)	13S (0269427, 3728849)	15	94.5	14.7	28.37	0.07
S072	Rhyolite lava (Trl)	13S (0271410, 3728283)	15	11.7	0.9	28.37	0.11
S078	Rhyolite lava (Trl)	13S (0273280, 3727490)	15	40.7	6.2	28.35	0.12
S053	Rhyolite lava (Trl)	13S (0268820, 3726670)	15	41.8	10.1	28.32	0.11
S070	Rhyolite lava (Trl)	13S (0269750, 3728895)	15	86.9	11.5	28.26	0.09
S086	Rhyolite lava (Trl)	13S (0270912, 3727038)	19	17.1	2.2	28.50	0.20
S112	Rhyolite lava (Trl)	13S (0268452, 3729141)	14	86.6	16.7	28.45	0.06
		Weighted mean ± Taylor error (2σ)		MSWD=2.84*		**28.36**	**0.11***
S047	Granite porphyry (Ti_1)	13S (0267440, 3723794)	14	4.8	0.8	28.26	0.10
S067a	Granite porphyry (Ti_1)	13S (0271222, 3725620)	4	12.2	2.1	28.39	0.08
		Weighted mean ± Taylor error (2σ)		MSWD=4.12		**28.34**	**0.06**
S038a	Vicks Peak Tuff (Tvp)	13S (0268750, 3724370)	15	93.8	12.9	28.29	0.12
S066a	Vicks Peak Tuff (Tvp)	13S (0271220, 3725622)	21	34.7	7.6	28.27	0.08
S074	Vicks Peak Tuff (Tvp)	13S (0271219, 3728776)	25	27.4	10.5	28.40	0.12
S085	Vicks Peak Tuff (Tvp)	13S (0271898, 3727800)	15	21.8	8.7	28.36	0.11
S114	Vicks Peak Tuff (Tvp)	13S (0269680, 3723370)	13	3.3	2.2	28.53	0.07
		Weighted mean ± Taylor error (2σ)		MSWD=6.98*		**28.39**	**0.19***

* MSWD outside 95% confidence interval

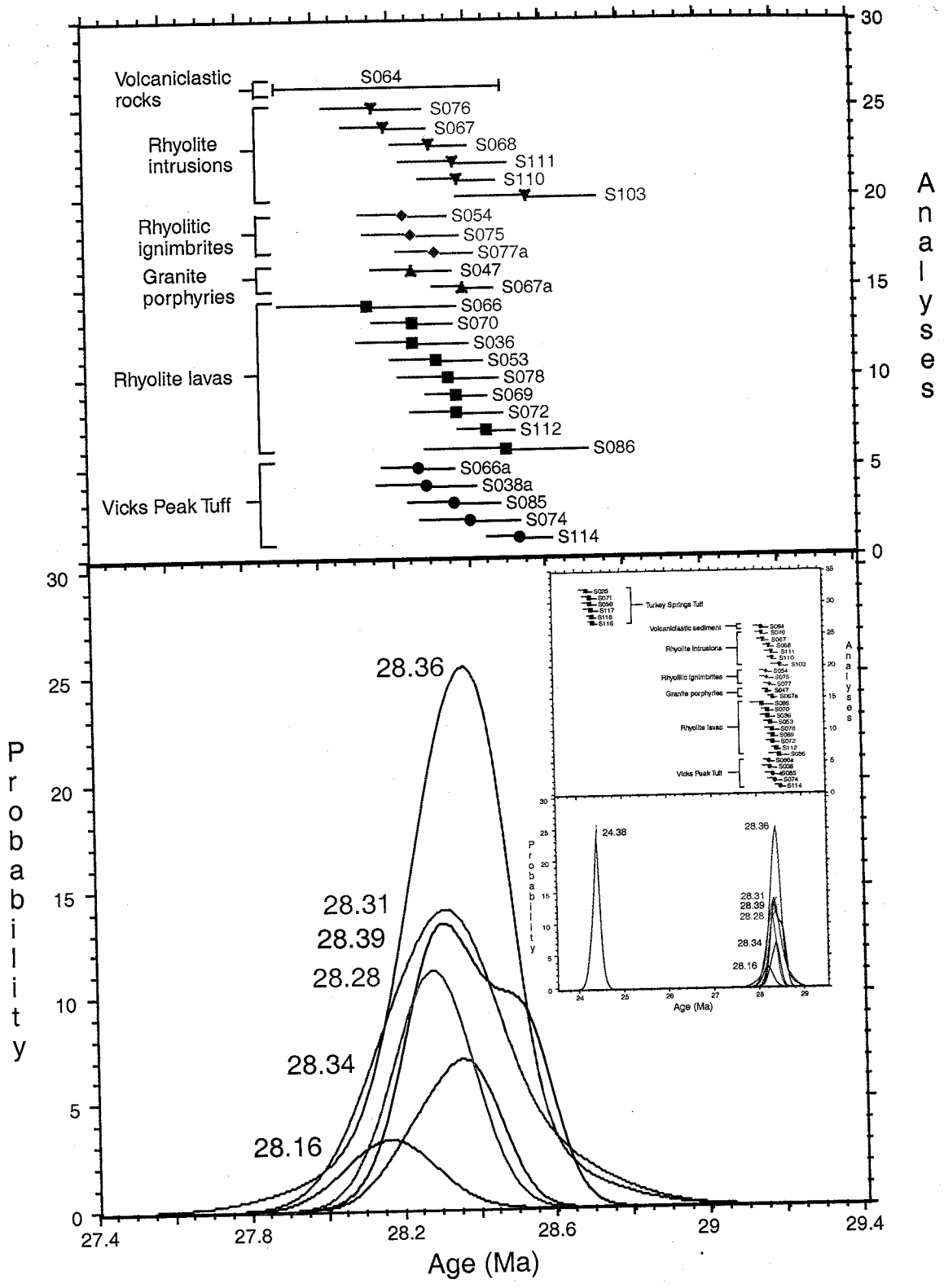

Figure 31. Age probability diagram comparing the ages of the 28 Ma samples analyzed in this study. Inset diagram includes the 24 Ma Turkey Springs Tuff.

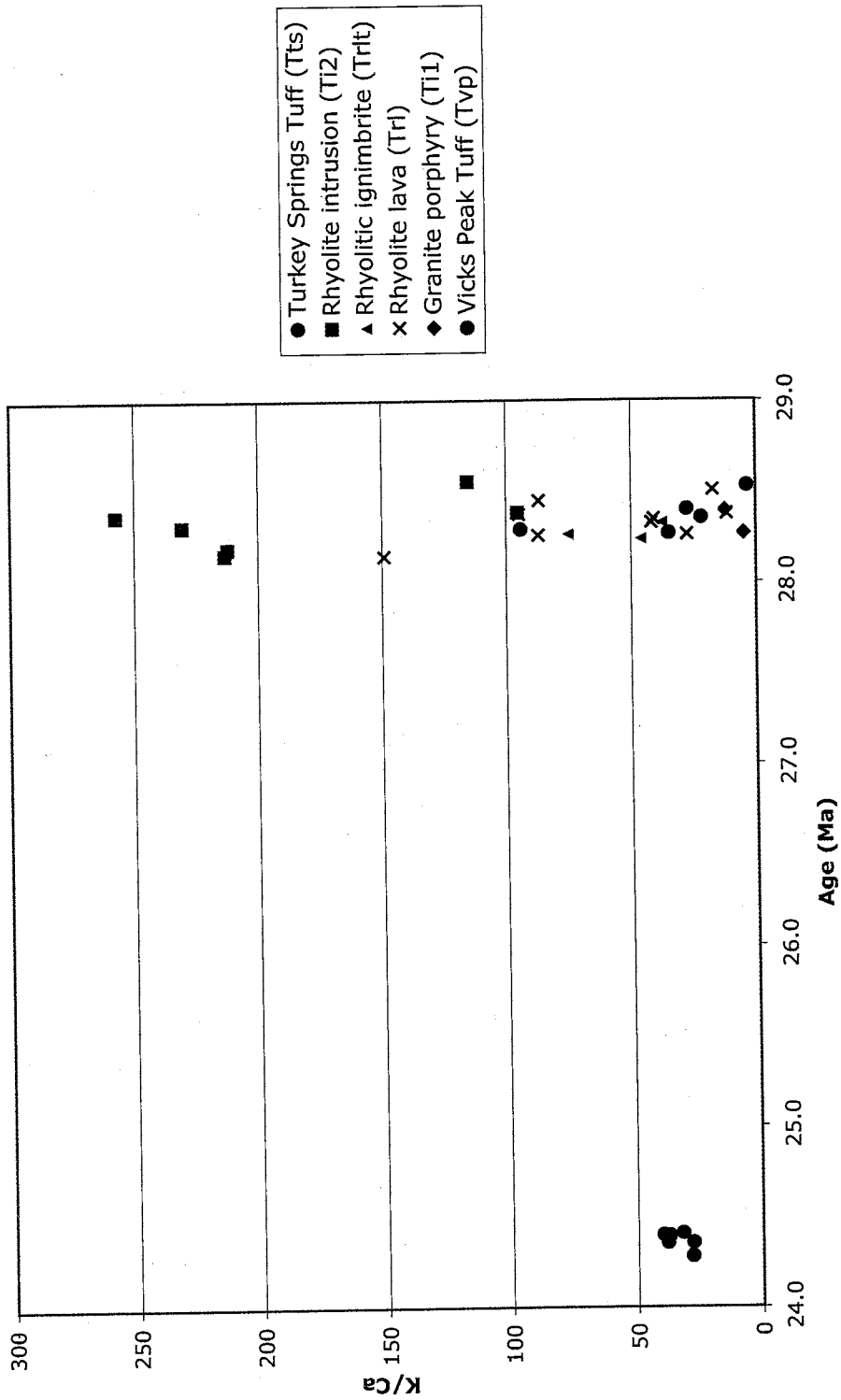

Figure 32. K/Ca vs. age diagram for each sample analyzed in this study.

multicrystal sanidine separates from two samples of Turkey Springs Tuff and obtained a mean age of 24.33 ± 0.06 Ma (2σ) and a mean K/Ca of 33.2, which agree within error with the data obtained in this study.

Seven of nine samples collected from the rhyolite lavas yielded high precision results (average 2σ error for individual sample = ±0.10 Ma). Of the 105 sanidines analyzed from these seven samples, only one low-yield crystal was excluded from the age calculations. The other 104 analyses produced relatively high radiogenic yields (ave.= 97.7%) and high signals (ave.= 3.42×10^{-15} moles of ^{39}Ar released). The two other rhyolite lava samples, S086 and S066, yielded apparent age errors of ±0.2 and ±0.22, respectively. The imprecision results from the relatively small crystal size (0.25-0.35 mm) of these mineral separates, which yielded low signals ranging from 0.09×10^{-15} to 0.73×10^{-15} moles of ^{39}Ar. Sample S066 was collected from an outcrop 50 m from a small intrusive stock and shows evidence of contact metamorphism in hand sample. Thirteen of the 23 sanidines analyzed from sample S066 were excluded from the age calculation because of signal sizes less than 0.275×10^{-15} moles ^{39}Ar. The K/Ca of S066 is relatively high at 148.8. The other rhyolite lava samples have K/Ca ratios ranging from 11.7 to 94.5. All of the sample ages overlap within 2σ error, and they have a weighted mean age of 28.36 ± 0.11 Ma (2σ).

The five samples of Vicks Peak Tuff yielded relatively high precision results with an average apparent age error of ±0.10 Ma (2σ) for all five samples. Of the 92 crystals analyzed, only one plagioclase crystal (from S066a) and two anomalously young crystals (from S114) were excluded from the age calculations. The remaining 89 crystals averaged 89.1% radiogenic yield and 2.17×10^{-15} moles of ^{39}Ar released. Excluding

sample S114, K/Ca ratios range from 21.8 to 93.8, which are typical values for a Mogollon-Datil ignimbrite. S114 has an especially low K/Ca (3.3) relative to other Mogollon-Datil ignimbrites and yielded the oldest apparent age. The five Vicks Peak samples have a weighted mean age of 28.39±0.19 Ma (2σ). Without S114, the weighted mean age is 28.32±0.05 Ma. McIntosh (1989) used an incremental heating method of multicrystal sanidine separates from three samples of Vicks Peak Tuff and obtained a mean age of 28.56 ± 0.08 Ma (2σ) and a K/Ca range from 43.2 to 80.3. The apparent age discrepancy between the McIntosh (1989) age and the age obtained in this study might be explained by the possibility of older, xenocrystic contaminants being included in the analysis of a multicrystal sanidine separate, although no xenocrysts were seen in this study.

Two samples (S054, S075) of the thin rhyolitic ignimbrite interlayered within the rhyolite lavas west of the Deep Canyon Fault and 200 m from the top of the rhyolite lavas yielded a weighted mean age of 28.25±0.07 Ma (2σ). All of the individual analyses were retained in the age calculation, and they averaged 97.4% radiogenic yield and 1.24×10^{-15} moles ^{39}Ar released. Sample S077a is of the thin rhyolitic ignimbrite east of the Deep Canyon Fault and 675 m from the base of the lavas. All 15 sanidines yielded high signals and radiogenic yields and a weighted mean age of 28.32±0.09 Ma (2σ).

Fifty sanidines from sample S064 were dated to collect provenance information about the volcaniclastic sediment overlying the rhyolite lavas. All 50 gave high yields and signals, and they range in age from 27.89±0.10 to 28.55±0.13 Ma and in K/Ca from 16.1 to 34.9.

Two of the granite porphyry stocks were sampled and analyzed in this study. Sample S047 yielded a mineral separate composed of large (0.85-1.2 mm), milky white, K-feldspar crystals. Only one of the analyses was excluded from the age calculation (due to low yield) and the remaining 14 crystals gave high radiogenic yields (>95%), large signals (>2.82×10^{-15} moles), and a precise weighted mean age of 28.26±0.10 Ma. K/Ca ratios range from 3.6 to 7.1 and are typical for plutonic K-feldspars. The other granite porphyry sample (S067a) yielded a smaller separate size (0.5-0.85 mm) of white feldspars. The separate contained low-yielding K-feldspar and also plagioclase, which were excluded from the age calculations. The four remaining K-feldspar crystals gave a weighted mean age of 28.39±0.08 Ma and K/Ca ratios ranging from 8.2 to 14.1.

The six samples of the rhyolite intrusions yielded weighted mean ages ranging from 28.16±0.13 to 28.56±0.18 Ma. In general, they produced high yields (>95%) and signals (>1.5×10^{-15} moles). Four of the six samples contained older xenocrysts which were excluded from the age calculation. The average K/Ca ratios for these samples range from 95.2 to 257.2, which are anomalously high values for this study area.

7. DISCUSSION

7.1. $^{40}Ar/^{39}Ar$ Geochronology

The $^{40}Ar/^{39}Ar$ ages of the Vicks Peak Tuff, rhyolite lavas, and silicic intrusions overlap within 2σ error indicating that they were produced during a brief (<0.42 Ma) episode of activity that occurred between 28.58 and 28.16 Ma. This was during the peak of volcanism in the Mogollon-Datil volcanic field, when more than 9 regional ignimbrites totaling more than 6000 km^3 were erupted between 29.1 Ma and 27.4 Ma (McIntosh and others, 1992). Volcaniclastic rocks overlying the rhyolite lavas contain sanidines ranging in age from 27.89±0.10 to 28.55±0.13 Ma. Most of the detrital sanidines were likely derived from the rhyolite lavas and Vicks Peak Tuff, although the younger ones may have been transported from some other volcanic source such as the 28.00 ± 0.08 Ma Lemitar Tuff, which is a regional ignimbrite present in the northern San Mateo Mountains. Overlying the volcaniclastic rocks is the Turkey Springs Tuff (24.4 Ma), the youngest regional ignimbrite in the Mogollon-Datil volcanic field (McIntosh, 1989).

7.2. Intracaldera Environment

The occurrence of thick rhyolite lavas and silicic intrusions with more than 690 meters of Vicks Peak Tuff argues that this study area lies within the Nogal Canyon Caldera. The rapid emplacement of these units, along with their similar petrology and K-feldspar chemistry, suggest that they were derived from a common magma system. The eruption of the Vicks Peak Tuff followed by rhyolite lava may represent progressive

degassing of this magma system. The rhyolite lavas and granite porphyries appear to be associated with the early development of the Nogal Canyon Caldera.

The northern margin of the Nogal Canyon Caldera is probably either very near the southern margin of the 27.4 Ma Mt. Withington Caldera or is concealed by its formation. A revision of the inferred caldera margin to include this study area increases its north-south diameter from 17 km to 25 km. Revised areal distribution and volume estimates for the Vicks Peak Tuff were calculated using a 25 km diameter cylinder to model the intracaldera fill and a 154 km diameter cone to approximate the outflow sheet (Fig. 33 a-c). An estimated thickness of the intracaldera facies Vicks Peak Tuff (1 km; Hermann, 1986) was used for cylinder height, and the inferred caldera margin from this and other studies was used to approximate the cylinder diameter (25 km). Typical thickness of near-caldera outflow facies Vicks Peak Tuff (0.2 km; Hermann, 1986) was used for cone height, and the areal extent of the Vicks Peak Tuff outflow (18645 km^2; McIntosh, 1992) was used to approximate the cone radius (77.0 km). The estimated total volume of the Vicks Peak Tuff is 1816 km^3.

7.3. Paleotopography of Nogal Canyon Caldera

Notably lacking from the stratigraphic sequence in this study area is the South Canyon Tuff, which erupted 27.4 Ma from a caldera less than 10 km to the north of this study area (Mt. Withington Caldera). The distal fringes of the outflow sheet extend 50 km to the southwest of this study area. The fact that it is missing from this study area suggests that the Vicks Peak Tuff and rhyolite lavas persisted as a topographic high in this area for over 1 million years after the formation of the Nogal Canyon Caldera. This topographic high may be due at least in part to resurgent uplift associated with magmatic

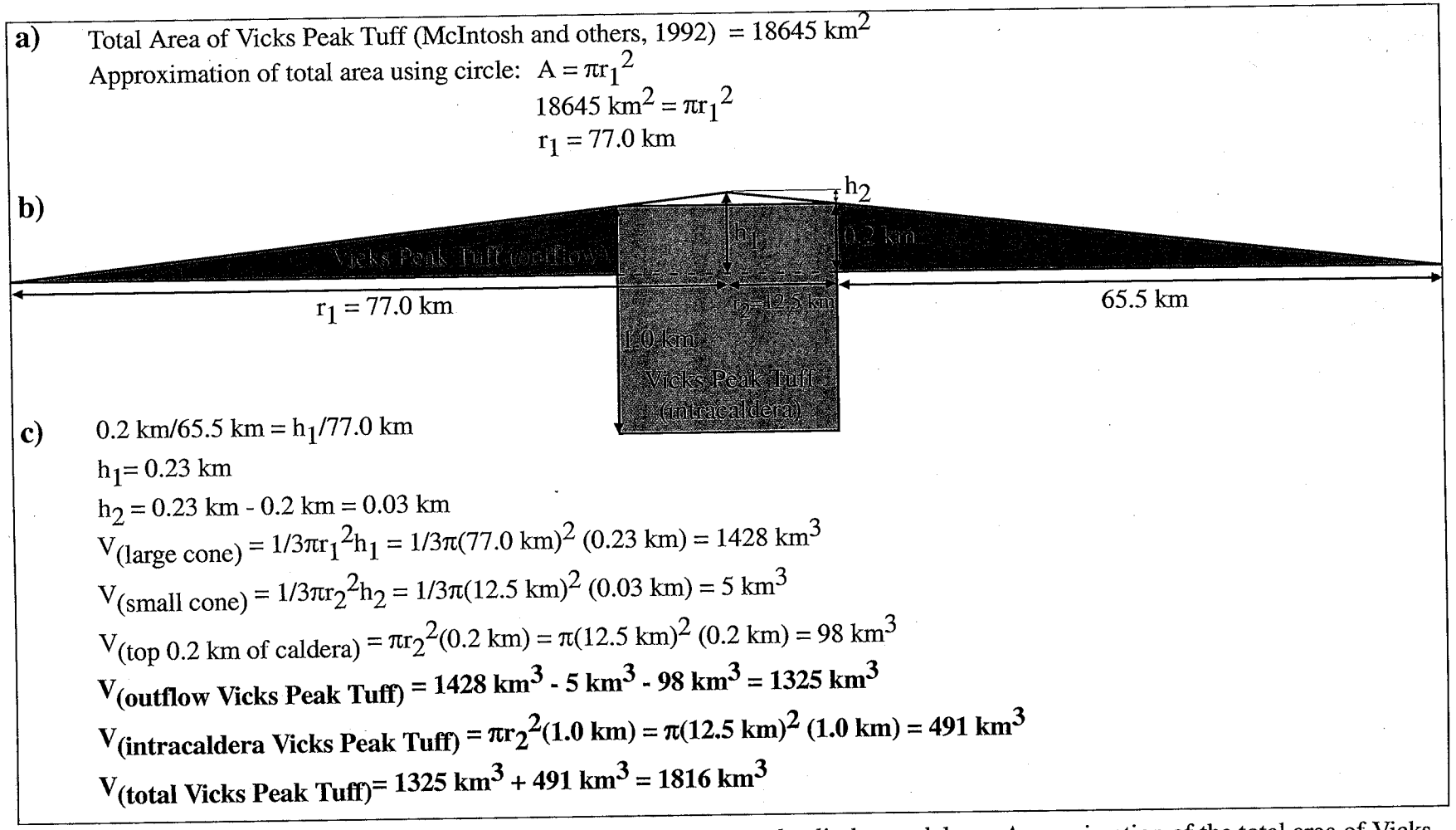

Figure 33 a-c. Volume calculation of Vicks Peak Tuff using a cone and cylinder model. **a.** Approximation of the total area of Vicks Peak Tuff using a circle. Radius (r_1) calculation uses an area approximated from a Vicks Peak Tuff extent map (McIntosh and others, 1992). **b.** Cross-section through center of cone and cylinder (not to scale). Typical outflow thickness near caldera (0.2 km) and an estimated intracaldera thickness (1 km) are used. Radius of caldera (r_2) approximated from this and other studies. **c.** Calculation of outflow facies volume, intracaldera facies volume, and total volume of Vicks Peak Tuff.

activity near 28.4 Ma. The accumulation of rhyolite lava may have also resulted in high topography. The presence of the 24.4 Ma Turkey Springs Tuff in this study area indicates that enough erosion and/or subsidence had occurred by that time to allow for its emplacement.

7.4. Development of Nogal Canyon Caldera

Furlow (1965) and Farkas (1969) mapped thick sections of Vicks Peak Tuff, thick post-Vicks Peak rhyolite lavas, and several porphyritic igneous stocks in the southern San Mateo Mountains (Fig. 34). Deal and Rhodes (1976) used this data along with reconnaissance traverses to propose the existence of the Nogal Canyon Caldera, and they inferred that the igneous stocks intruded along its southern structural margin and the rhyolite lavas (Springtime Canyon Formation) extruded from a source on the northwestern structural margin. Atwood (1982) recognized the Nogal Canyon fault (Farkas, 1969) as part of the eastern structural margin of the Nogal Canyon Caldera (Fig. 34). He mapped felsic dikes, plugs, and rhyolite lava domes along the Nogal Canyon fault. The fault places Pennsylvanian limestone against Vicks Peak Tuff, a minimum stratigraphic separation of 610 meters (Atwood, 1982). Detailed mapping by Ferguson (1985) in an area 7 km northeast of this study area reveals evidence for an east-west trending, south-side down fault that was active during the formation of the Nogal Canyon Caldera (Fig. 34). The eutaxitic foliation in the Vicks Peak Tuff is intensely folded in a zone where it thickens abruptly to the south across the fault (Ferguson, 1985). Hermann (1986) established that the Rock Spring fault (Fig. 34) is part of the southeastern structural margin of the Nogal Canyon Caldera. Felsic dikes and stocks intrude the Rock Spring fault, and the Vicks Peak Tuff thins abruptly across it from 1370 m to 650 m.

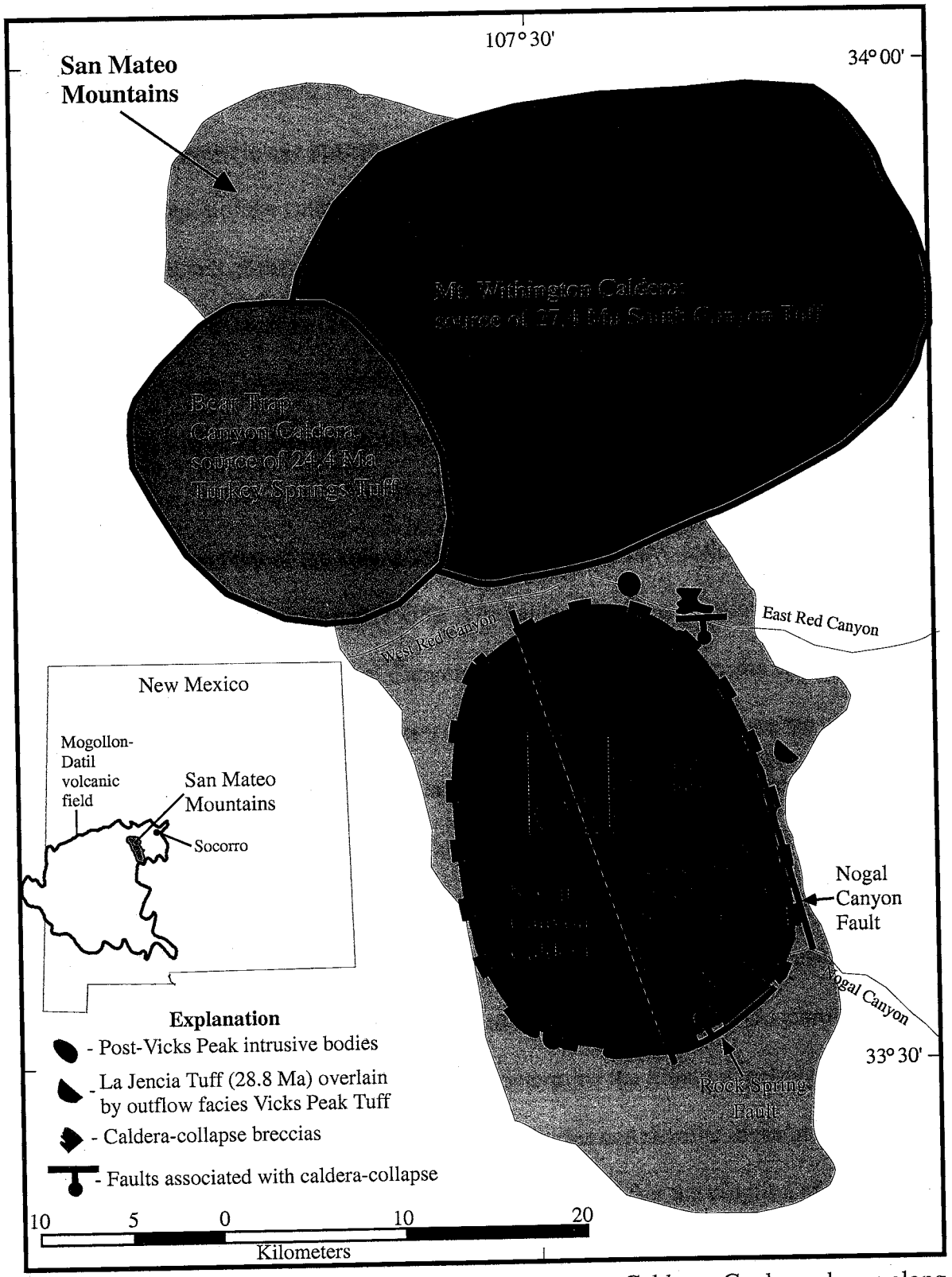

Figure 34. Inferred caldera marigin of the Nogal Canyon Caldera. Geology shown along its northeastern margin from Ferguson (1985), along its western margin from Atwood (1982), Furlow (1965), and Farkas (1969), and along its southern margin from Hermann (1986) and Farkas (1969).

Hermann (1986) also mapped caldera-collapse breccias within the intracaldera Vicks Peak Tuff that coarsen towards the Rock Spring fault and are absent across the fault. Breccia clasts increase in age upsection, suggesting that deposition was occurring during progressive collapse of the caldera.

The thickness of the Vicks Peak Tuff and rhyolite lava and the lack of structural evidence for a ring fracture in this study area strongly suggests that the northern margin of the Nogal Canyon Caldera is north of this study area (Fig. 34). Thus, the granite porphyry stocks have apparently intruded within the caldera, perhaps during a resurgent uplift event.

The development of the Nogal Canyon Caldera may have followed the resurgent caldera model of Smith and Bailey (1968). The caldera-forming eruptions continued during caldera collapse in the Nogal Canyon Caldera, as evidenced by the thick intracaldera facies and thin outflow facies Vicks Peak Tuff. Breccias from the caldera walls continued to develop during caldera-collapse, as evidenced by the breccias in the Vicks Peak Tuff (Hermann, 1986). At least 720 m of caldera subsidence is estimated from the difference in thickness between the intracaldera facies and outflow facies Vicks Peak Tuff across the Rock Spring fault (Hermann, 1986). Ring fracture intrusion and volcanism is evident along the Rock Spring and Nogal Canyon faults. Geochronological studies of these igneous rocks are necessary to determine the timing of activity along the ring fractures. Geochronology of the granite porphyries and rhyolite lavas in this study area show that they intruded and erupted within 0.42 m.y. after the eruption of the Vicks Peak Tuff. This post-collapse activity probably occurred before and/or during resurgent doming, if the Nogal Canyon Caldera's evolution is similar to other well-studied

resurgent calderas. Figure 35a-f illustrates a possible model for the development of the Nogal Canyon Caldera.

In the Valles Caldera, pre-resurgent volcanism and resurgent doming occurred in less than 90,000 years after caldera collapse (Phillips and others, 2003). Resurgence was accompanied with intrusion and effusion along fractures in the resurgent dome (Smith and Bailey, 1968). In the Long Valley Caldera, early post-collapse rhyolite volcanism was contemporaneous with resurgent doming which lasted 70,000 years after caldera collapse (Bailey and others, 1976). Intracaldera and ring fracture volcanism continued for approximately 600,000 years after caldera collapse. The Toba Caldera is a resurgent caldera that erupted 2500-3000 km^3 of pyroclastic material during its latest caldera-forming eruption (Rose and Chesner, 1987). Resurgent uplift occurred less than 74,000 years after this latest eruption (Chesner and others, 1991). Toba's resurgent dome contains an apical graben within which post-resurgent rhyolite lava erupted (Smith and Bailey, 1968). The 23.1 Ma Lake City Caldera in the San Juan volcanic field is a resurgent caldera where erosion has exposed the top of the resurgent intrusive body. Post-collapse intracaldera lava flows constrain the timing of resurgence to less than 300,000 years after the eruption of the caldera-forming Sunshine Peak Tuff (Reynolds and others, 1986).

The Mt.Withington Caldera and the Bear Trap Canyon Caldera are two other calderas that have been identified in the San Mateo Mountains. The Mt. Withington Caldera is a northeast-elongated elliptical caldera in the northern San Mateo Mountains (Osburn and Ferguson, 1986). It appears to have collapsed 27.4 Ma as a northwest-tilted trap door structure (Ferguson, 1991). The Beartrap Canyon Caldera (23.4 Ma) is a

resurgent caldera nested in the west end of the Mt. Withington Caldera. A central resurgent dome is bisected by a north-trending apical graben, and is "cut by several intrusions" (Osburn and others, 1997). A sequence of rhyolite domes erupted from the northern and western structural margin of the Bear Trap Canyon Caldera, and geochronology shows that they erupted less than 200,000 years after caldera collapse.

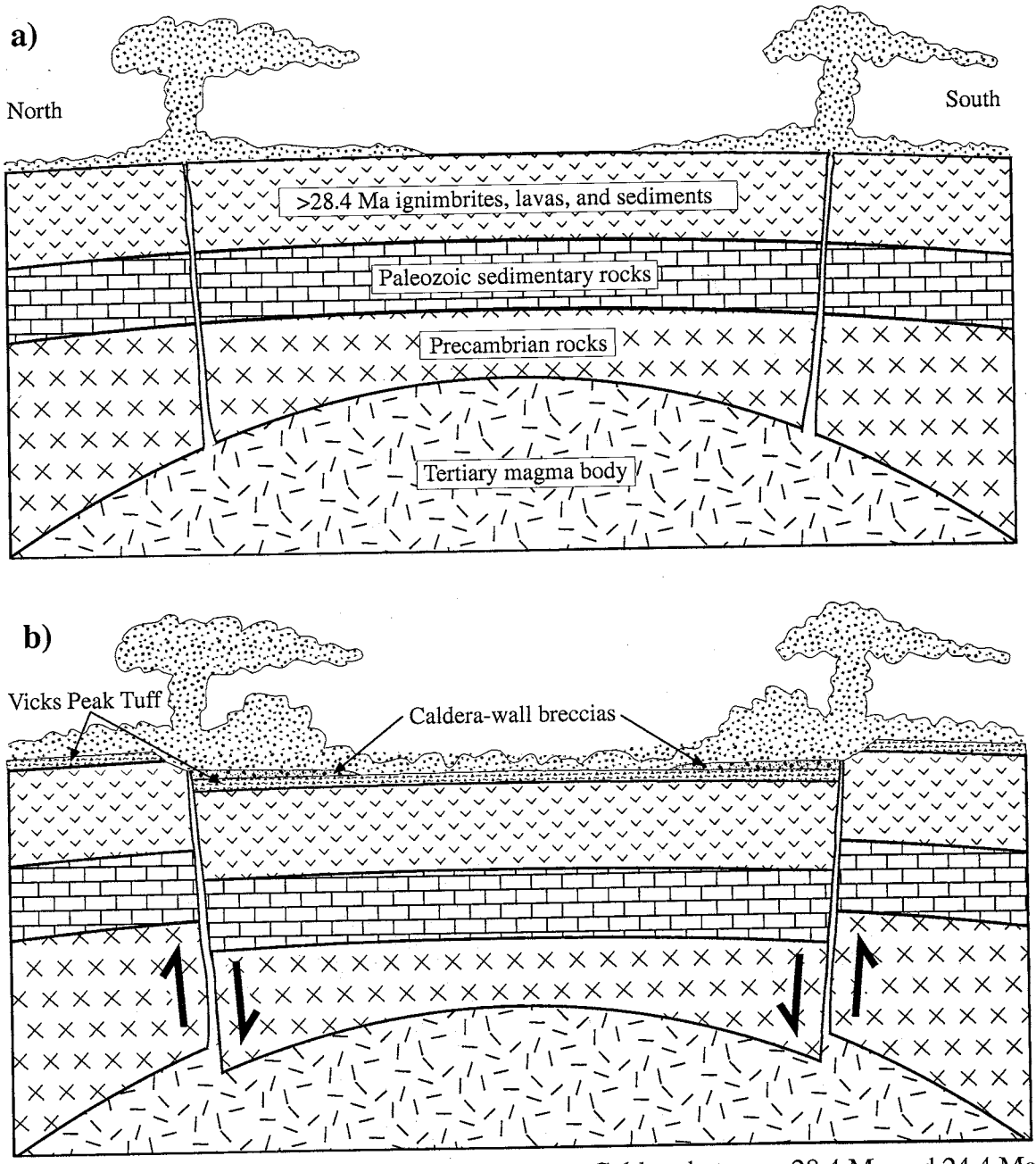

Figure 35 a-f. Development of the Nogal Canyon Caldera between 28.4 Ma and 24.4 Ma shown in a north-south cross-section through the caldera. Cross-section line shown in figure 31. **a)** Generation of ring fractures and the 28.4 Ma eruption of the Vicks Peak Tuff. **b)** Eruption continues during caldera collapse and breccias develop from the over-steepened caldera walls. **c)** Subsided caldera filled with up to1200 m. of intracaldera facies Vicks Peak Tuff. Outflow facies Vicks Peak Tuff approximately 200 m. **d)** Resurgent uplift and intrusion and volcanism in resurgent dome and ring fractures. Occurs within 400 ka after caldera collapse. **e)** 28.3 Ma - 27.4 Ma: emplacement of Lemitar Tuff, volcaniclastic sediments, and South Canyon Tuff. 27.4 Ma - 24.4 Ma: erosion of highlands and development of volcaniclastic sediment. 24.4 Ma: Eruption of Turkey Springs Tuff from the northern San Mateo Mountains. **f)** Approximate location of a north-south cross-section through this study area and the location of the Rock Spring Fault.

c)

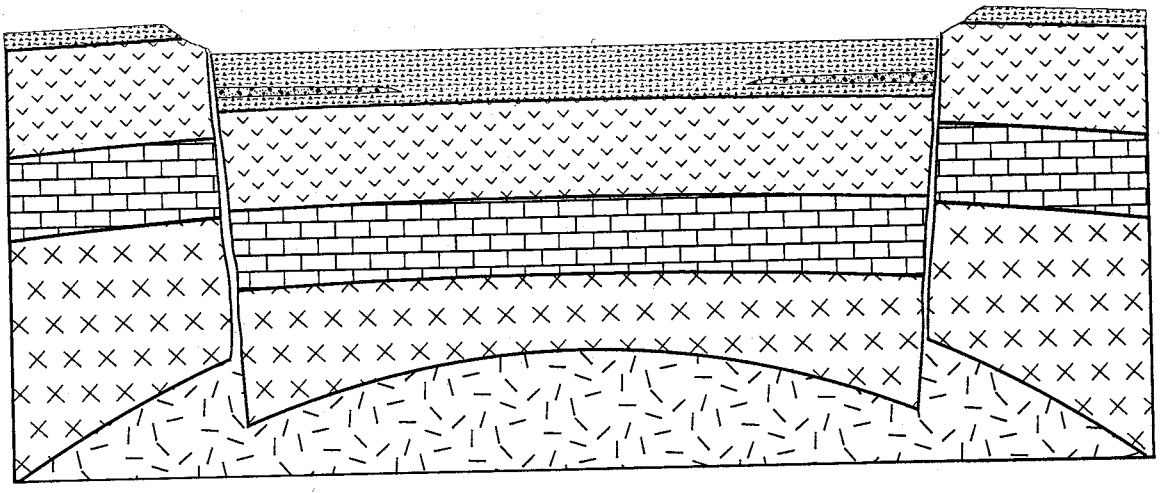

d)

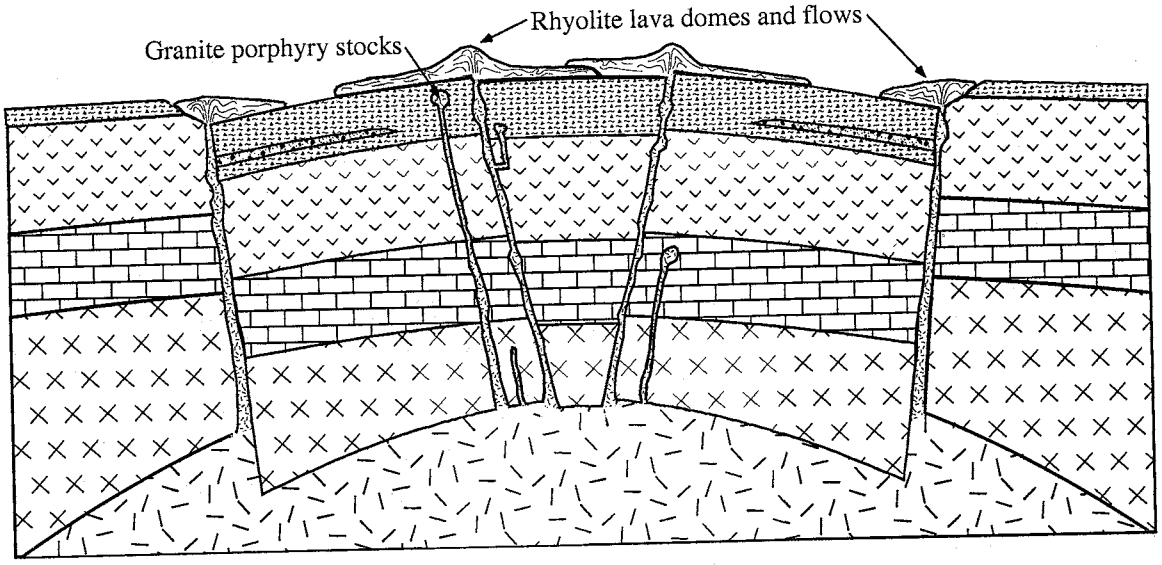

Figure 35 a-f (continued).

e)

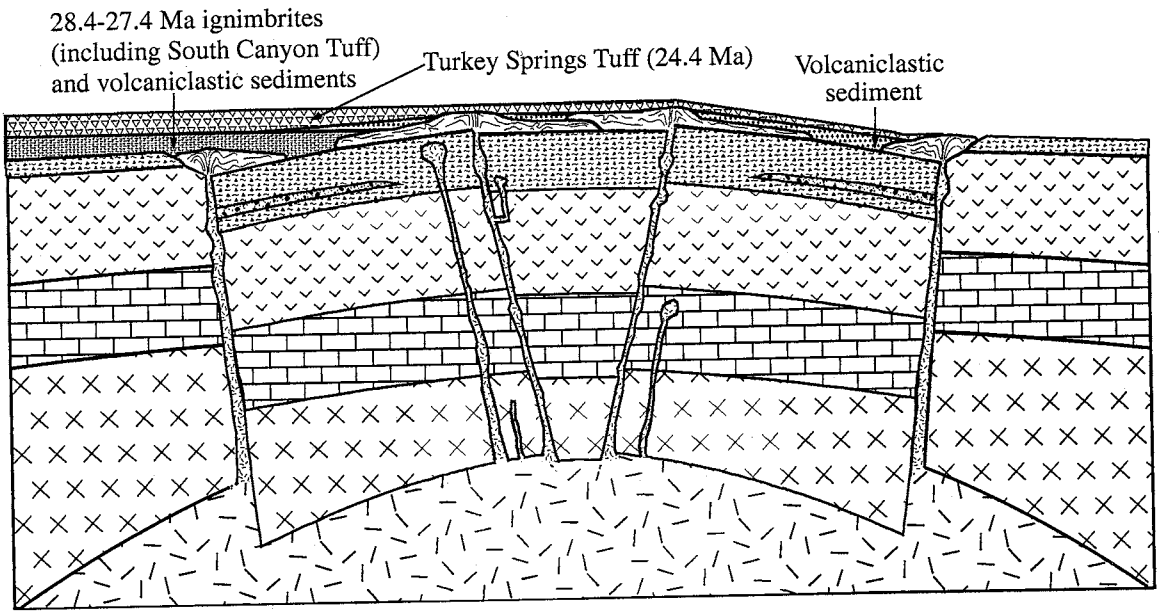

f)

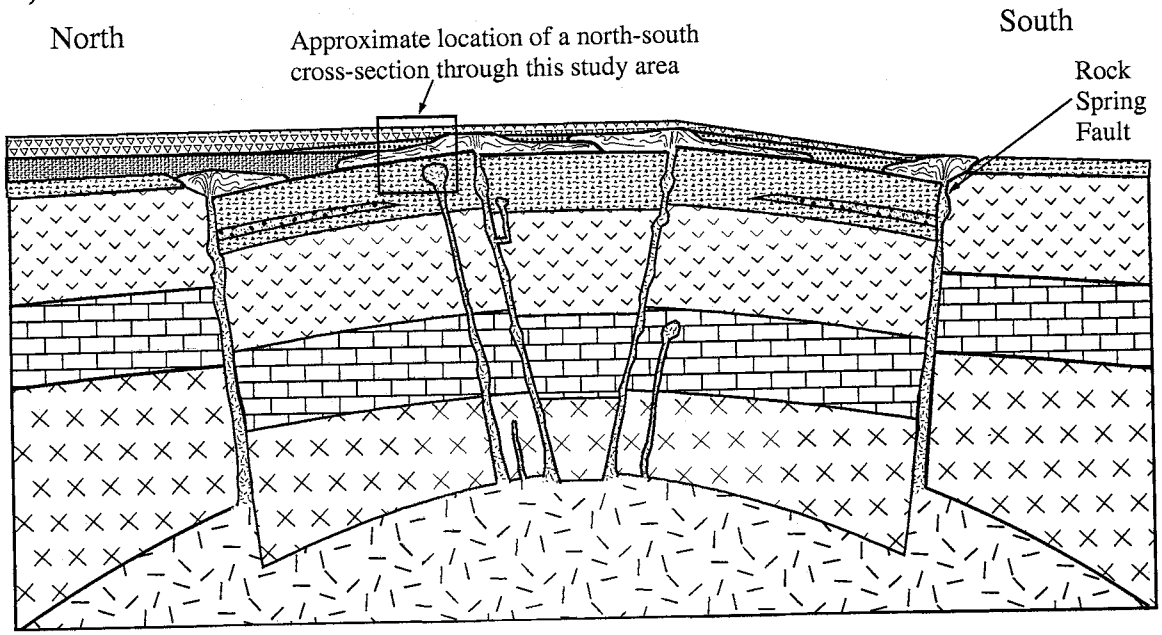

Figure 35 a-f (continued).

8. SUMMARY AND CONCLUSIONS

1) In this study area, more than 690 m of Vicks Peak Tuff with no exposed base is overlain by 550 m of mineralogically similar rhyolite lavas. Several chemically similar granite porphyries intrude the 28.4 Ma Vicks Peak Tuff and several petrologically distinct rhyolite dikes intrude the rhyolite lavas. Overlying this sequence is a thin volcaniclastic sedimentary sequence and the 24.4 Ma Turkey Springs Tuff.

2) Most of the rocks in this study area dip 11°-25° to the east. The majority of the structures in this study area are north-south trending down-to-the west normal faults associated with late Cenozoic extensional tectonism. The Deep Canyon Fault is a major Basin and Range normal fault that bisects this study area. In some places it has juxtaposed Vicks Peak Tuff and Turkey Springs Tuff, giving it an estimated stratigraphic displacement of 1115 m.

3) The ages of the Vicks Peak Tuff, rhyolite lavas, and silicic intrusions overlap within 2σ error and show that these units were produced during a brief (<0.42 Ma) episode of activity that occurred between 28.58 and 28.16 Ma.

4) The 28 Ma sequence of volcanic rocks in this study area contain sanidine crystals that cluster between $Or_{48.5}Ab_{51.1}$ and $Or_{38.8}Ab_{56.6}$, whereas sanidine crystals in the 24 Ma Turkey Springs Tuff averages $Or_{55.6}Ab_{42.9}$

5) Petrologic similarities between the Vicks Peak Tuff, rhyolite lavas, and granite porphyries, along with their spatial and temporal relationships, suggest that they came from a common magma system. The eruption of the Vicks Peak Tuff followed by the rhyolite lavas represents the progressive degassing of the system.

6) The rhyolite lavas and granite porphyries are associated with the development of the Nogal Canyon Caldera and were erupted and intruded < 0.42 my after its formation.

7) The thickness of the Vicks Peak Tuff and rhyolite lavas in this study area suggest that they are intracaldera facies, thereby suggesting that the northern margin of the Nogal Canyon Caldera is actually north of the field area by as much as 7 km.

8) The estimated diameter of the Nogal Canyon Caldera is 25 km and the total volume of the Vicks Peak Tuff is 1816 km^3.

9) Missing from the stratigraphic sequence in this study area is the 27.4 Ma South Canyon Tuff, a regional ignimbrite that erupted from a caldera less than 10 km to the north. This suggests that the study area was a topographic high during the 27.4 Ma eruption of the South Canyon Tuff. This high may be due to resurgent uplift of the caldera floor after caldera collapse.

9. REFERENCES

Atwood, G.W., 1982, Geology of the San Juan Peak area, San Mateo Mountains, Socorro County, New Mexico; with special reference to the geochemistry, mineralogy, and petrogenesis of an occurrence of riebeckite-bearing rhyolite [Master's thesis]: Albuquerque, NM, University of New Mexico.

Bailey, R.A., Dalrymple, G.B., and Lanphere, M.A., 1976, Volcanism, structure, and geochronology of Long Valley Caldera, Mono County, California: Journal of Geophysical Research, v. 81, p. 725-744.

Bornhorst, T.J., 1980, Major- and trace-element geochemistry and mineralogy of upper Eocene to Quaternary volcanic rocks of the Mogollon-Datil volcanic field, southwestern New Mexico [Doctoral thesis]: Albuquerque, NM, University of New Mexico.

Cather, S.M., 1983, Laramide Sierra uplift; evidence for major pre-rift uplift in central and southern New Mexico, New Mexico Geological Society thirty-fourth annual field conference; Socorro region II, Volume 34: Chapin, Charles E., New Mexico Geological Society, p. 99-101.

Chamberlin, R.M., 1983, Cenozoic domino-style crustal extension in the Lemitar Mountains, New Mexico; a summary, New Mexico Geological Society thirty-fourth annual field conference; Socorro region II, Volume 34: Chapin, Charles E., New Mexico Geological Society, p. 111-118.

Chapin, C.E., and Cather, S.M., 1981, Eocene tectonics and sedimentation in the Colorado Plateau - Rocky Mountain area, Relations of tectonics to ore deposits in the southern Cordillera, Volume 14: Dickinson, William R. Payne, William D., Arizona Geological Society, p. 173-198.

Chapin, C.E., and Seager, W.R., 1975, Evolution of the Rio Grande Rift in the Socorro and Las Cruces area: Guidebook - New Mexico Geological Society, p. 297-321.

Chesner, C.A., Rose, W.I., Deino, A., Drake, R., and Westgate, J.A., 1991, Eruptive history of Earth's largest Quaternary caldera (Toba, Indonesia) clarified: Geology, v. 19, p. 200-203.

Cox, E.W., 1985, Geology and gold-silver deposits in the San Jose mining district, southern San Mateo Mountains, Socorro County, NM [Master's thesis]: Socorro, NM, New Mexico Institute of Mining and Technology.

Dane, C.H., and Bachman, G.O., 1961, Preliminary geologic map of the southwestern part of New Mexico: Reston, VA, U. S. Geological Survey.

Deal, E.G., 1973, Geology of the northern part of the San Mateo Mountains, Socorro County, New Mexico: A study of a rhyolite ash-flow tuff cauldron and the role of laminar flow in ash-flow tuffs [Ph.D. thesis]: Albuquerque, University of New Mexico.

Deal, E.G., and Rhodes, R.C., 1976, Volcano-tectonic structures in the San Mateo Mountains, Socorro County, New Mexico: Special Publication - New Mexico Geological Society, v. 5, p. 51-56.

Deino, A.L., and Potts, R., 1990, Single-crystal $^{40}Ar/^{39}Ar$ dating of the Olorgesailie Formation, southern Kenya Rift: Journal of Geophysical Research, B, Solid Earth and Planets, v. 95, p. 8453-8470.

Eardley, A.J., 1962, Structural geology of North America (2d edition), 743 p.

Farkas, S.E., 1969, Geology of the southern San Mateo mountains, Socorro and Sierra counties, New Mexico [Doctoral thesis]: Albuquerque, NM, University of New Mexico.

Ferguson, C.A., 1990, Geology of the Grassy Lookout 7.5' Quadrangle, Socorro County, New Mexico: Socorro, NM, Calgary, AB, New Mexico Bureau of Mines and Mineral Resources.

Ferguson, C.A., 1985, Geology of the east-central San Mateo Mountains, Socorro County, New Mexico [Master's thesis]: Socorro, NM, New Mexico Institute of Mining and Technology.

—, 1986, Geology of the east central San Mateo Mountains, Socorro County, New Mexico, New Mexico Bureau of Mines and Mineral Resources Open-File Report 252, 135p.

—, 1988, Geology of the Tenmile Hill 7.5' Quadrangle, Socorro County, New Mexico: Socorro, NM, New Mexico Bureau of Mines and Mineral Resources Open-File Report 283, 23p.

—, 1991, Stratigraphic and structural studies in the Mt. Withington Caldera, Grassy Lookout Quadrangle, Socorro County, New Mexico: New Mexico Geology, v. 13, p. 50-54.

Ferguson, C.A., and Osburn, G.R., 1986, Structure of Mt. Withington Cauldron, Mogollon-Datil volcanic field, New Mexico, Geological Society of America, 99th annual meeting, Volume 18, Geological Society of America (GSA), p. 600.

Ferguson, C.A., and Osburn, G.R., 1994, Geologic map of the Mt. Withington 7.5-minute quadrangle, Socorro County, New Mexico, New Mexico Bureau of Mines and Mineral Resources Open-File Report 403.

Foruria, J., 1984, Geology, alteration and precious metal reconnaissance of the Nogal Canyon area, San Mateo Mountains, NM [Master's thesis]: Fort Collins, CO, Colorado State University.

Furlow, J.W., 1965, Geology of the San Mateo Peak area, Socorro County, New Mexico [Master's thesis]: Albuquerque, NM, University of New Mexico.

Hermann, M., 1986, Geology of the southwestern San Mateo Mountains, Socorro County, N.M [Master's thesis]: Socorro, NM, New Mexico Institute of Mining and Technology.

Lasky, S.G., 1932, The ore deposits of Socorro County, New Mexico: Socorro, NM, New Mexico Bureau of Mines and Mineral Resources, 139 p.

Lipman, P.W., Prostka, H.J., and Christiansen, R.L., 1972, Cenozoic volcanism and plate-tectonic evolution of the western United States; I, Early and middle Cenozoic, A discussion on volcanism and the the structure of the Earth, Volume 271, Royal Society of London, p. 217-248.

McIntosh, W.C., 1989, Ages and distribution of ignimbrites in the Mogollon-Datil volcanic field, Southwest New Mexico; a stratigraphic framework using $^{40}Ar/^{39}Ar$ dating and paleomagnetism [Doctoral thesis]: Socorro, NM, New Mexico Institute of Mining and Technology.

McIntosh, W.C., Chapin, C.E., Ratte, J.C., and Sutter, J.F., 1992, Time-stratigraphic framework for the Eocene-Oligocene Mogollon-Datil volcanic field, Southwest New Mexico: Geological Society of America Bulletin, v. 104, p. 851-871.

McIntosh, W.C., Sutter, J.F., Chapin, C.E., and Kedzie, L.L., 1990, High-precision $^{40}Ar/^{39}Ar$ sanidine geochronology of ignimbrites in the Mogollon-Datil volcanic field, southwestern New Mexico: Bulletin of Volcanology, v. 52, p. 584-601.

McIntosh, W.C., Sutter, J.F., Chapin, C.E., Osburn, G.R., and Ratte, J.C., 1986, A stratigraphic framework for the eastern Mogollon-Datil volcanic field based on paleomagnetism and high-precision $^{40}Ar/^{39}Ar$ dating of ignimbrites; a progress report, New Mexico Geological Society thirty-seventh annual field conference, Volume 37: Clemons, Russell E. King, William E. Mack, Greg H., New Mexico

Geological Society, p. 183-195.

Osburn, G.R., and Ferguson, C.A., 1986, Redefinition of the Mt. Withington Cauldron, San Mateo Mountains, Socorro County, New Mexico, New Mexico Geological Society, annual spring meeting, Volume 8: Anonymous, New Mexico Bureau of Mines and Mineral Resources, p. 98.

Osburn, G.R., Ferguson, C.A., and McIntosh, W.C., 1997, Young undeformed source cauldron for the tuff of Turkey Springs, northern San Mateo Mountains, Socorro County, New Mexico, New Mexico Geological Society annual spring meeting, Volume 19: Anonymous, New Mexico Bureau of Mines and Mineral Resources, p. 62.

Osburn, G.R., Unpublished mapping-a, Monica Saddle Quadrangle, Socorro County, New Mexico.

Osburn, G.R., Unpublished mapping-b, Oak Peak Quadrangle, Socorro County, New Mexico.

Osburn, G.R., Unpublished mapping-c, Bay Buck Peaks Quadrangle, Socorro County, New Mexico.

Phillips, E.H., Goff, Fraser, Kyle, Philip R., McIntosh, William C., Gardner, Jamie N., 2003, Collapse and resurgence of the Valles Caldera, Jemez Mountains, New Mexico: field relationships and $^{40}Ar/^{39}Ar$ ages of megabreccia blocks and constraints on the timing of resurgence, New Mexico Geological Society 2003 Annual Spring Meeting, Volume proceedings: Socorro, NM.

Reynolds, R.L., Hudson, M.R., and Hon, K., 1986, Paleomagnettic evidence for the timing of collapse and resurgence of the Lake City Caldera, San Juan Mountains, Colorado: JGR Journal of Geophysical Research B, v. 91, p. 9599-9613.

Rose, W.I., and Chesner, C.A., 1987, Dispersal of ash in the great Toba eruption, 75 ka: Geology, v. 15, p. 913-917.

Samson, S.D., and Alexander, E.C., Jr., 1987, Calibration of the interlaboratory (super 40) Ar- (super 39) Ar dating standard, MMhb-1, Sixth international conference on Geochronology, cosmochronology and isotope geology (ICOG VI) ; symposium on New developments and applications in isotope geoscience, Volume 66: Faure, Gunter, Elsevier, p. 27-34.

Smith, W.R., 1992, Geology of the southwestern margin of the Nogal Canyon Cauldron, San Mateo Mountains, Sierra and Socorro counties, New Mexico [Master's thesis]: Odessa, TX, University of Texas of the Permian Basin.

Smith, R.L., and Bailey, R.A., 1968, Resurgent cauldrons: Studies in volcanology--A

memoir in honor of Howel Williams, p. 613-662.

Spell, T.L., McDougall, I., and Doulgeris, A.P., 1996, Cerro Toledo Rhyolite, Jemez volcanic field, New Mexico; $^{40}Ar/^{39}Ar$ geochronology of eruptions between two caldera-forming events: Geological Society of America Bulletin, v. 108, p. 1549-1566.

Taylor, J.R., 1982, An Introduction to Error Analysis: The Study of Uncertainties in Physical Measurements, University Science Books, 270 p.

Tonking, W.H., 1957, Geology of Puertecito Quadrangle, Socorro County, New Mexico: Socorro, NM, New Mexico Bureau of Mines and Mineral Resources, 67 p.

Weber, R.H., 1963, Cenozoic volcanic rocks of Socorro County.

Willard, M.-E., 1957, Reconnaissance geologic map of Luera Spring thirty minute quadrangle.

Wilpolt, R.H., Bates, R.L., MacAlpin, A.J., and Vorbe, G., 1946, Geologic map and stratigraphic sections of Paleozoic rocks of Joyita Hills, Los Pinos Mountains, and northern Chupadera Mesa, Valencia, Torrance, and Socorro counties, New Mexico: Reston, VA, U. S. Geological Survey.

Winchester, D.E., 1920, Geology of Alamosa Creek valley, Socorro County, New Mexico, with special reference to the occurrence of oil and gas: U S Geological Survey Bulletin, p. 1-15.

APPENDIX A: Sample List

Sample	Unit	Location (UTM): Zone (Easting, Northing)	Geochronology	Microprobe analysis	Thin section
S025	Turkey Springs Tuff (Tts)	13N (0270193, 3728384)	X		X
S028	Rhyolite lava (Trl)	13N (0267739, 3724492)			X
S036	Rhyolite lava (Trl)	13N (0268700, 3724650)	X	X	
S038a	Vicks Peak Tuff (Tvp)	13N (0268750, 3724370)	X	X	
S047	Granite porphyry (Ti_1)	13N (0267440, 3723794)	X	X	X
S053	Rhyolite lava (Trl)	13N (0268820, 3726670)	X		
S054	Rhyolitic ignimbrite (Trlt)	13N (0269585, 3726530)	X		X
S056	Turkey Springs Tuff (Tts)	13N (0269645, 3726548)	X		X
S064	Volcaniclastic sediment (Tvc_1)	13N (0269470, 3725750)	X		X
S066	Rhyolite lava (Trl)	13N (0269568, 3728632)	X		X
S066a	Vicks Peak Tuff (Tvp)	13N (0271220, 3725622)	X		X
S067	Rhyolite intrusion (Ti_2)	13N (0269550, 3728600)	X	X	X
S067a	Granite porphyry (Ti_1)	13N (0271222, 3725620)	X	X	X
S068	Rhyolite intrusion (Ti_2)	13N (0269492, 3728620)	X	X	X
S069	Rhyolite lava (Trl)	13N (0269427, 3728849)	X	X	X
S070	Rhyolite lava (Trl)	13N (0269750, 3728895)	X	X	X
S071	Turkey Springs Tuff (Tts)	13N (0270653, 3728959)	X	X	X
S072	Rhyolite lava (Trl)	13N (0271410, 3728283)	X		X
S074	Vicks Peak Tuff (Tvp)	13N (0271219, 3728776)	X		
S075	Rhyolitic ignimbrite (Trlt)	13N (0268935, 3728460)	X	X	X
S076	Rhyolite intrusion (Ti_2)	13N (0268518, 3728871)	X	X	X
S077a	Rhyolitic ignimbrite (Trlt)	13N (0274058, 3726865)	X	X	X
S078	Rhyolite lava (Trl)	13N (0273280, 3727490)	X		
S079	Rhyolite lava (Trl)	13N (0269223, 3726845)			X
S084	Vicks Peak Tuff (Tvp)	13N (0271945, 3728234)			X
S085	Vicks Peak Tuff (Tvp)	13N (0271898, 3727800)	X	X	
S086	Rhyolite lava (Trl)	13N (0270912, 3727038)	X		
S103	Rhyolite intrusion (Ti_2)	13N (0269923, 3728311)	X		
S110	Rhyolite intrusion (Ti_2)	13N (0268525, 3729154)	X		
S111	Rhyolite intrusion (Ti_2)	13N (0268466, 3729154)	X		
S112	Rhyolite lava (Trl)	13N (0268452, 3729141)	X		
S114	Vicks Peak Tuff (Tvp)	13N (0269680, 3723370)	X		
S116	Turkey Springs Tuff (Tts)	13N (0269452, 3722681)	X		
S117	Turkey Springs Tuff (Tts)	13N (0269364, 3723250)	X		
S118	Turkey Springs Tuff (Tts)	13N (0269354, 3723574)	X		

APPENDIX B: Electron Microprobe Data from Orthoclase Standard

Oxide percentages determined from this study of the orthoclase standard:

Mineral	SiO2	Al2O3	CaO	FeO	SrO	Na2O	BaO	K2O	Rb2O	Oxy	Total
orthoclase std.	64.13	16.74	0.00	1.76	0.03	0.94	0.06	15.42			99.08
orthoclase std.	63.84	16.83	0.00	1.76	0.02	0.94	0.09	15.41			98.89
orthoclase std.	64.80	16.85	0.00	1.76	0.03	0.96	0.05	15.38			99.83
orthoclase std.	64.89	16.76	0.00	1.81	0.00	0.92	0.09	15.58			100.04
orthoclase std.	64.51	16.90	0.01	1.77	0.00	0.93	0.03	15.48			99.63
orthoclase std.	64.96	16.81	0.01	1.77	0.01	0.95	0.07	15.42			99.99
orthoclase std.	65.11	16.80	0.00	1.82	0.05	0.95	0.06	15.43			100.22
orthoclase std.	65.02	16.99	0.00	1.79	0.04	0.95	0.09	15.65			100.52
orthoclase std.	64.68	16.62	0.00	1.78	0.00	0.94	0.08	15.27			99.37
orthoclase std.	64.46	16.67	0.00	1.80	0.00	0.98	0.08	15.43			99.42
orthoclase std.	64.90	16.74	0.01	1.83	0.00	0.96	0.06	15.23			99.71
orthoclase std.	64.14	16.65	0.00	1.77	0.02	0.93	0.08	15.52			99.10
orthoclase std.	64.59	16.62	0.00	1.77	0.04	0.95	0.08	15.35			99.40
orthoclase std.	64.22	16.66	0.01	1.70	0.01	0.92	0.11	15.29			98.92
orthoclase std.	64.78	16.70	0.00	1.78	0.00	0.90	0.03	15.45			99.64
orthoclase std.	64.61	16.63	0.00	1.73	0.00	0.92	0.06	15.55			99.51
orthoclase std.	64.51	16.62	0.00	1.80	0.00	0.94	0.09	15.40			99.37
orthoclase std.	64.71	16.51	0.00	1.80	0.02	0.95	0.07	15.28			99.34
orthoclase std.	64.59	16.53	0.01	1.70	0.03	0.93	0.11	15.50			99.39
orthoclase std.	64.73	16.69	0.00	1.76	0.03	0.93	0.07	15.11			99.31
orthoclase std.	64.97	16.54	0.00	1.70	0.00	0.91	0.06	15.28			99.46
AVERAGE:	**64.63**	**16.71**	**0.00**	**1.77**	**0.01**	**0.94**	**0.07**	**15.40**			
STD. DEV. (1σ):	**0.33**	**0.12**	**0.00**	**0.04**	**0.02**	**0.02**	**0.02**	**0.13**			

Established composition of the orthoclase standard used in this study (J. Donovan, pers. comm.):

orthoclase std.	**64.79**	**16.72**		**1.88**		**0.91**	**0.05**	**15.49**	**0.03**	**0.13**	**100.00**

APPENDIX C: Electron Microprobe Data Table

Sample	Unit	SiO2	Al2O3	CaO	FeO	SrO	BaO	Na2O	K2O	Total	Or	Ab	An
S036-11	Rhyolite lava (Trl)	66.524	19.442	0.328	0.255	0.006	0	5.906	8.211	100.67	47.0	51.4	1.6
S036-3	Rhyolite lava (Trl)	66.552	19.395	0.305	0.276	0	0.007	5.621	8.805	100.96	50.0	48.5	1.4
S036-4	Rhyolite lava (Trl)	66.437	19.422	0.328	0.287	0	0	5.75	8.44	100.66	48.3	50.1	1.6
S036-9	Rhyolite lava (Trl)	66.425	19.4	0.309	0.261	0.005	0.008	5.852	8.284	100.54	47.5	51.0	1.5
	Average:	**66.485**	**19.415**	**0.318**	**0.270**	**0.003**	**0.004**	**5.782**	**8.435**		**48.2**	**50.3**	**1.5**
	Std. Dev.:	**0.063**	**0.022**	**0.012**	**0.014**	**0.003**	**0.004**	**0.125**	**0.265**		**1.3**	**0.1**	**1.3**
S038a-1	Vicks Peak Tuff (Tvp)	67.174	19.3	0.082	0.499	0.014	0	6.798	7.084	100.95	40.5	59.1	0.4
S038a-4	Vicks Peak Tuff (Tvp)	67.04	19.274	0.079	0.519	0.028	0	6.748	7.377	101.07	41.7	57.9	0.4
S038a-3	Vicks Peak Tuff (Tvp)	66.962	19.108	0.078	0.497	0.039	0	6.416	7.711	100.81	44.0	55.6	0.4
	Average:	**67.059**	**19.227**	**0.080**	**0.505**	**0.027**	**0.000**	**6.654**	**7.391**		**42.1**	**57.5**	**0.4**
	Std. Dev.:	**0.107**	**0.104**	**0.002**	**0.012**	**0.013**	**0.000**	**0.208**	**0.314**		**1.8**	**1.8**	**0.0**
S047-4	Granite porphyry (Til)	62.836	21.416	1.738	0.354	0.092	2.192	4.381	8.646	101.66	51.6	39.7	8.7
S047-5	Granite porphyry (Til)	63.096	21.341	1.9	0.284	0.033	1.758	6.124	5.915	100.45	35.2	55.3	9.5
S047-7	Granite porphyry (Til)	65.703	19.778	0.626	0.331	0.044	0.167	5.7	8.264	100.61	47.3	49.6	3.0
S047-9	Granite porphyry (Til)	63.749	20.99	1.632	0.291	0.049	1.144	6.426	5.87	100.15	34.5	57.4	8.1
	Average:	**64.726**	**20.384**	**1.129**	**0.311**	**0.047**	**0.656**	**6.063**	**7.067**		**42.2**	**50.5**	**7.3**
	Std. Dev.:	**1.382**	**0.857**	**0.711**	**0.028**	**0.004**	**0.691**	**0.513**	**1.693**		**8.6**	**7.9**	**2.9**

Sample	Unit	SiO2	Al2O3	CaO	FeO	SrO	BaO	Na2O	K2O	Total	Or	Ab	An
S067-3	Rhyolite intrusion (Ti2)	66.823	18.794	0.038	0.783	0.03	0.023	6.279	7.688	100.46	44.5	55.3	0.2
S067-4	Rhyolite intrusion (Ti2)	66.659	18.925	0.044	0.582	0.044	0.035	6.741	7.091	100.12	40.8	59.0	0.2
	Average:	**66.741**	**18.860**	**0.041**	**0.683**	**0.037**	**0.029**	**6.510**	**7.390**		**42.7**	**57.2**	**0.2**
	Std. Dev.:	**0.116**	**0.093**	**0.004**	**0.142**	**0.010**	**0.008**	**0.327**	**0.422**		**2.6**	**2.6**	**0.0**
S067a-4	Granite porphyry (Ti1)	65.957	19.421	0.477	0.36	0	0.07	5.399	8.82	100.5	50.6	47.1	2.3
S067a-7	Granite porphyry (Ti1)	67.099	20.047	0.634	0.421	0.053	0.106	6.237	7.605	102.2	43.2	53.8	3.0
	Average:	**66.528**	**19.734**	**0.556**	**0.391**	**0.027**	**0.088**	**5.818**	**8.213**		**46.9**	**50.5**	**2.7**
	Std. Dev.:	**0.808**	**0.443**	**0.111**	**0.043**	**0.037**	**0.025**	**0.593**	**0.859**		**5.2**	**4.7**	**0.5**
S068-2	Rhyolite intrusion (Ti2)	66.966	18.904	0.032	0.824	0	0.01	7.137	6.531	100.4	37.5	62.3	0.2
S068-3	Rhyolite intrusion (Ti2)	66.91	19.077	0.02	0.442	0.014	0.035	6.597	7.553	100.65	42.9	57.0	0.1
S068-4	Rhyolite intrusion (Ti2)	66.883	18.556	0.027	1.276	0.027	0.015	6.722	7.199	100.71	41.3	58.6	0.1
	Average:	**66.920**	**18.846**	**0.026**	**0.847**	**0.014**	**0.020**	**6.819**	**7.094**		**40.6**	**59.3**	**0.1**
	Std. Dev.:	**0.042**	**0.265**	**0.006**	**0.417**	**0.014**	**0.013**	**0.283**	**0.519**		**2.8**	**2.7**	**0.1**
S069-1	Rhyolite lava (Trl)	66.306	18.966	0.114	0.346	0.005	0.028	5.836	8.464	100.07	48.6	50.9	0.5
S069-2	Rhyolite lava (Trl)	66.607	19.021	0.11	0.377	0.021	0.017	5.868	8.517	100.54	48.6	50.9	.0.5
S069-3	Rhyolite lava (Trl)	66.674	18.969	0.082	0.365	0	0.013	5.971	8.391	100.47	47.9	51.7	0.4
S069-4	Rhyolite lava (Trl)	66.473	18.923	0.094	0.393	0	0	5.8	8.496	100.18	48.9	50.7	0.5
S069-5	Rhyolite lava (Trl)	66.833	18.942	0.081	0.421	0.031	0	5.957	8.549	100.81	48.4	51.2	0.4
	Average:	**66.579**	**18.964**	**0.096**	**0.380**	**0.011**	**0.012**	**5.886**	**8.483**		**48.5**	**51.1**	**0.5**
	Std. Dev.:	**0.200**	**0.037**	**0.015**	**0.028**	**0.014**	**0.012**	**0.075**	**0.060**		**0.4**	**0.4**	**0.1**
S070-1	Rhyolite lava (Trl)	66.912	18.986	0.018	0.376	0	0.043	6.368	7.966	100.67	45.1	54.8	0.1
S070-3	Rhyolite lava (Trl)	66.884	19.223	0.028	0.378	0	0.008	6.265	8.096	100.88	45.9	54.0	0.1
S070-4	Rhyolite lava (Trl)	66.558	19.232	0.009	0.421	0.028	0	6.438	7.957	100.64	44.8	55.1	0.0

Sample	Unit	SiO2	Al2O3	CaO	FeO	SrO	BaO	Na2O	K2O	Total	Or	Ab	An
S070-5	Rhyolite lava (Trl)	66.693	19.169	0.08	0.345	0.01	0	6.113	8.663	101.07	48.1	51.6	0.4
S070-6	Rhyolite lava (Trl)	67.107	19.016	0.018	0.396	0.011	0	6.327	7.961	100.84	45.3	54.7	0.1
S070-7	Rhyolite lava (Trl)	66.748	19.13	0.012	0.445	0	0.005	6.416	7.899	100.66	44.7	55.2	0.0
	Average:	**66.817**	**19.126**	**0.028**	**0.394**	**0.008**	**0.009**	**6.321**	**8.090**		**45.7**	**54.2**	**0.1**
	Std. Dev.:	**0.192**	**0.104**	**0.027**	**0.036**	**0.011**	**0.017**	**0.119**	**0.288**		**1.3**	**1.4**	**0.1**
S071-1	Turkey Springs Tuff (Tts)	66.346	19.399	0.304	0.123	0.005	0	4.862	9.689	100.73	55.9	42.6	1.5
S071-2	Turkey Springs Tuff (Tts)	66.172	19.378	0.287	0.191	0.019	0.019	4.807	9.987	100.86	57.0	41.7	1.4
S071-3	Turkey Springs Tuff (Tts)	66.033	19.465	0.347	0.151	0	0.137	4.949	9.648	100.73	55.3	43.1	1.7
S071-5	Turkey Springs Tuff (Tts)	66.036	19.474	0.397	0.186	0.009	0.075	5.05	9.424	100.65	54.1	44.0	1.9
	Average:	**66.147**	**19.429**	**0.334**	**0.163**	**0.008**	**0.058**	**4.917**	**9.687**		**55.6**	**42.9**	**1.6**
	Std. Dev.:	**0.148**	**0.048**	**0.049**	**0.032**	**0.008**	**0.062**	**0.106**	**0.231**		**1.2**	**1.0**	**0.2**
S075-1	Rhyolitic ignimbrite (Trlt)	66.92	19.046	0.124	0.395	0.051	0.014	5.902	8.377	100.83	48.0	51.4	0.6
S075-2	Rhyolitic ignimbrite (Trlt)	66.393	19.176	0.168	0.371	0.017	0.023	5.898	8.481	100.53	48.2	51.0	0.8
S075-3	Rhyolitic ignimbrite (Trlt)	66.321	19.056	0.123	0.41	0	0.016	5.876	8.528	100.33	48.5	50.9	0.6
S075-4	Rhyolitic ignimbrite (Trlt)	66.725	19.214	0.159	0.305	0.007	0.035	5.944	8.41	100.8	47.9	51.4	0.7
	Average:	**66.590**	**19.123**	**0.144**	**0.370**	**0.019**	**0.022**	**5.905**	**8.449**		**48.2**	**51.2**	**0.7**
	Std. Dev.:	**0.282**	**0.085**	**0.023**	**0.046**	**0.023**	**0.009**	**0.028**	**0.068**		**0.3**	**0.3**	**0.1**
S076-1	Rhyolite intrusion (Ti2)	67.058	19.107	0.016	0.546	0.031	0.013	6.566	7.488	100.83	42.8	57.1	0.1
S076-2	Rhyolite intrusion (Ti2)	67	18.765	0.014	0.676	0.034	0	6.68	7.44	100.61	42.3	57.7	0.1
S076-3	Rhyolite intrusion (Ti2)	66.489	18.73	0.024	0.526	0	0	6.461	7.777	100.01	44.1	55.7	0.1
S076-4	Rhyolite intrusion (Ti2)	66.476	18.948	0.013	0.354	0	0.051	6.139	8.448	100.43	47.5	52.4	0.1
	Average:	**66.756**	**18.888**	**0.017**	**0.526**	**0.016**	**0.016**	**6.462**	**7.788**		**44.2**	**55.7**	**0.1**
	Std. Dev.:	**0.316**	**0.175**	**0.005**	**0.132**	**0.019**	**0.024**	**0.233**	**0.464**		**2.3**	**2.4**	**0.0**

Sample	Unit	SiO2	Al2O3	CaO	FeO	SrO	BaO	Na2O	K2O	Total	Or	Ab	An
S077a-1	Rhyolitic ignimbrite (Trlt)	66.5	19.335	0.26	0.306	0	0.019	5.861	8.597	100.88	48.5	50.3	1.2
S077a-2	Rhyolitic ignimbrite (Trlt)	66.542	19.316	0.26	0.28	0.009	0	5.796	8.524	100.73	48.6	50.2	1.2
S077a-3	Rhyolitic ignimbrite (Trlt)	66.73	19.418	0.257	0.294	0.039	0.066	5.98	8.288	101.07	47.1	51.7	1.2
S077a-5	Rhyolitic ignimbrite (Trlt)	65.942	19.689	0.424	0.261	0.012	0.074	5.993	8.078	100.47	46.1	51.9	2.0
	Average:	**66.429**	**19.440**	**0.300**	**0.285**	**0.015**	**0.040**	**5.908**	**8.372**		**47.6**	**51.0**	**1.4**
	Std. Dev.:	**0.339**	**0.172**	**0.083**	**0.019**	**0.017**	**0.036**	**0.095**	**0.236**		**1.2**	**0.9**	**0.4**
S078-6	Rhyolite lava (Trl)	66.478	19.262	0.159	0.34	0.025	0.025	6.71	7.272	100.27	41.3	57.9	0.8
S078-7	Rhyolite lava (Trl)	66.655	19.502	0.227	0.284	0	0.015	6.931	7.057	100.67	39.7	59.2	1.1
S078-8	Rhyolite lava (Trl)	66.069	19.235	0.154	0.313	0.054	0.041	6.598	7.398	99.862	42.1	57.1	0.7
S078-9	Rhyolite lava (Trl)	66.902	19.445	0.226	0.254	0.022	0.023	6.805	7.236	100.91	40.7	58.2	1.1
	Average:	**59.121**	**17.275**	**0.232**	**0.259**	**0.021**	**0.036**	**5.646**	**6.940**		**41.1**	**57.8**	**1.1**
	Std. Dev.:	**22.045**	**6.415**	**0.098**	**0.093**	**0.016**	**0.023**	**2.126**	**2.575**		**1.7**	**1.6**	**0.2**
S085-1	Vicks Peak Tuff (Tvp)	66.039	20.042	0.944	0.379	0	0.032	6.736	6.655	100.83	37.6	57.9	4.5
S085-3	Vicks Peak Tuff (Tvp)	65.496	20.436	1.266	0.337	0.019	0.099	6.841	6.28	100.77	35.4	58.6	6.0
S085-4	Vicks Peak Tuff (Tvp)	65.543	19.975	0.758	0.341	0.026	0.041	6.183	7.276	100.14	42.0	54.3	3.7
S085-6	Vicks Peak Tuff (Tvp)	65.678	20.432	1.237	0.346	0	0.049	6.834	6.158	100.73	35.0	59.1	5.9
S085-7	Vicks Peak Tuff (Tvp)	66.01	19.577	0.631	0.385	0.014	0.007	6.076	7.681	100.38	44.0	52.9	3.0
	Average:	**65.753**	**20.092**	**0.967**	**0.358**	**0.012**	**0.046**	**6.534**	**6.810**		**38.8**	**56.6**	**4.6**
	Std. Dev.:	**0.257**	**0.359**	**0.283**	**0.023**	**0.012**	**0.034**	**0.374**	**0.653**		**4.0**	**2.8**	**1.3**

APPENDIX D: $^{40}Ar/^{39}Ar$ Data Tables

$^{40}Ar/^{39}Ar$ analytical results of samples included in Irrad.# NM-133

ID	$^{40}Ar/^{39}Ar$	$^{37}Ar/^{39}Ar$	$^{36}Ar/^{39}Ar$ (x 10^{-3})	$^{39}Ar_K$ (x 10^{-15} mol)	K/Ca	$\%^{40}Ar^*$	Age (Ma)	±2s (Ma)
S025, A1:133, single crystal sanidine, J=0.00071±0.11%, D=1.0069±0.001, NM-133, Lab#=51900								
06	19.05	0.0187	0.3322	2.31	27.4	99.5	24.12	0.10
08	19.28	0.0191	0.9818	2.81	26.8	98.5	24.16	0.10
07	19.20	0.0188	0.7146	2.19	27.1	98.9	24.17	0.10
02	19.08	0.0154	0.2754	3.09	33.2	99.6	24.18	0.10
05	19.12	0.0194	0.2634	4.22	26.3	99.6	24.23	0.09
15	19.20	0.0174	0.5108	2.47	29.4	99.2	24.24	0.09
09	19.34	0.0197	0.8886	3.00	25.9	98.7	24.27	0.10
03	19.15	0.0188	0.1422	6.25	27.1	99.8	24.32	0.08
10	19.15	0.0201	0.1313	2.64	25.4	99.8	24.32	0.10
14	19.22	0.0159	0.3557	2.98	32.2	99.5	24.32	0.10
12	19.20	0.0190	0.2287	3.47	26.9	99.7	24.34	0.09
04	19.24	0.0165	0.3258	5.25	31.0	99.5	24.36	0.09
11	19.25	0.0191	0.3289	1.12	26.7	99.5	24.37	0.16
13	19.26	0.0175	0.2590	3.91	29.1	99.6	24.41	0.08
01	19.14	0.0196	-0.1764	1.84	26.0	100.3	24.42	0.15
weighted mean:	MSWD=3.67*	n=15			28.0	±2.4	24.28	0.10 *
S036, A2:133, single crystal sanidine, J=0.0007102±0.11%, D=1.0069±0.001, NM-133, Lab#=51901								
06	22.38	0.0187	1.013	2.92	27.3	98.7	28.07	0.09
03	22.62	0.0191	1.652	1.61	26.7	97.8	28.13	0.15
15	22.33	0.0192	0.6167	1.91	26.6	99.2	28.16	0.12
02	22.26	0.0164	0.3729	2.42	31.1	99.5	28.16	0.12
07	22.48	0.0185	0.9643	2.28	27.5	98.7	28.21	0.11
05	22.38	0.0159	0.5337	3.41	32.2	99.3	28.25	0.10
12	22.17	0.0165	-0.2309	1.53	31.0	100.3	28.27	0.15
08	22.49	0.0175	0.8632	1.50	29.2	98.9	28.27	0.13
01	23.06	0.0197	2.747	3.30	26.0	96.5	28.29	0.11
14	22.40	0.0190	0.4888	1.40	26.9	99.4	28.30	0.14
13	22.53	0.0178	0.8476	2.14	28.7	98.9	28.32	0.12
04	22.49	0.0208	0.6961	1.43	24.6	99.1	28.33	0.18
09	22.50	0.0225	0.6047	3.49	22.7	99.2	28.38	0.11
11	22.56	0.0193	0.7117	1.97	26.4	99.1	28.42	0.12
10	22.43	0.0198	0.0139	1.98	25.7	100.0	28.50	0.14
weighted mean:	MSWD=3.81*	n=15			27.5	±2.6	28.26	0.13 *
S038a, A3:133, single crystal sanidine, J=0.0007104±0.11%, D=1.0069±0.001, NM-133, Lab#=51902								
10	22.59	0.0068	1.709	1.62	74.7	97.8	28.08	0.14
09	22.75	0.0051	2.229	1.62	100.7	97.1	28.09	0.14
05	22.46	0.0053	1.177	1.12	95.4	98.5	28.12	0.18
06	23.42	0.0049	4.192	1.25	103.7	94.7	28.20	0.16
03	23.33	0.0058	3.847	2.44	88.1	95.1	28.22	0.13
11	23.62	0.0050	4.740	2.52	102.4	94.1	28.26	0.14
14	22.43	0.0052	0.6337	0.995	98.9	99.2	28.29	0.19
12	23.26	0.0048	3.379	3.45	105.2	95.7	28.31	0.13
01	22.34	0.0046	0.1902	0.907	111.5	99.8	28.33	0.19
08	23.46	0.0057	3.940	1.06	89.1	95.0	28.35	0.19
07	22.54	0.0073	0.8153	2.44	69.9	98.9	28.35	0.11
02	23.58	0.0063	4.219	2.20	80.7	94.7	28.39	0.14
04	22.68	0.0045	1.124	1.35	112.4	98.5	28.41	0.16
15	22.70	0.0062	1.059	1.02	82.5	98.6	28.47	0.18
13	22.67	0.0056	0.7396	1.23	91.7	99.0	28.54	0.16

ID	$^{40}Ar/^{39}Ar$	$^{37}Ar/^{39}Ar$	$^{36}Ar/^{39}Ar$ (x 10^{-3})	$^{39}Ar_K$ (x 10^{-15} mol)	K/Ca	%^{40}Ar*	Age (Ma)	±2s (Ma)
weighted mean: MSWD=3.01*		n=15		93.8 ±12.9			28.29	0.12 *
S047, A4:133, single crystal sanidine, J=0.0007107±0.11%, D=1.0069±0.001, NM-133, Lab#=51903								
02	22.88	0.0940	2.609	6.84	5.4	96.7	28.14	0.09
05	22.85	0.1027	2.437	6.34	5.0	96.9	28.17	0.10
01&	33.19	0.0277	37.37	14.7	18.4	66.7	28.17	0.25
11	23.23	0.0958	3.677	3.33	5.3	95.4	28.18	0.13
15	23.17	0.1254	3.455	5.78	4.1	95.6	28.19	0.11
03	23.27	0.1429	3.786	6.55	3.6	95.2	28.20	0.11
04	23.16	0.1247	3.389	6.44	4.1	95.7	28.21	0.11
14	23.20	0.1139	3.359	6.18	4.5	95.8	28.26	0.12
13	23.31	0.0719	3.656	4.83	7.1	95.4	28.29	0.11
06	22.41	0.1039	0.5694	4.91	4.9	99.3	28.31	0.09
12	22.51	0.1123	0.8957	4.10	4.5	98.9	28.32	0.10
10	22.57	0.1047	1.034	2.82	4.9	98.7	28.33	0.12
08	22.62	0.1175	1.179	3.58	4.3	98.5	28.34	0.11
09	22.71	0.1149	1.436	3.28	4.4	98.2	28.36	0.10
07	22.60	0.1160	1.035	5.12	4.4	98.7	28.38	0.10
weighted mean: MSWD=2.33*		n=14			4.8 ±0.8		28.26	0.10 *
S054, A5:133, single crystal sanidine, J=0.0007112±0.11%, D=1.0069±0.001, NM-133, Lab#=51904								
11	23.14	0.0092	4.298	0.695	55.7	94.5	27.84	0.28
02	22.41	0.0112	1.803	0.481	45.7	97.6	27.86	0.31
29	23.24	0.0072	4.470	0.447	71.1	94.3	27.91	0.23
27	23.32	0.0099	4.553	0.343	51.5	94.2	27.98	0.26
04	22.81	0.0143	2.753	0.385	35.7	96.4	28.01	0.38
26	23.93	0.0158	6.535	0.519	32.3	91.9	28.01	0.22
24	22.58	0.0135	1.681	0.457	37.7	97.8	28.11	0.23
32	22.60	0.0276	1.734	0.367	18.5	97.7	28.12	0.26
34	22.60	0.0102	1.705	0.345	50.0	97.8	28.13	0.27
01	23.87	0.0115	5.957	0.950	44.4	92.6	28.15	0.22
25	22.82	0.0168	2.403	0.373	30.4	96.9	28.15	0.27
21	22.56	0.0101	1.518	0.446	50.4	98.0	28.15	0.21
28	22.40	0.0232	0.9880	0.479	22.0	98.7	28.15	0.19
07	22.47	0.0126	1.203	0.588	40.7	98.4	28.15	0.24
20	22.73	0.0062	1.993	0.448	82.7	97.4	28.19	0.23
05	24.31	0.0111	7.279	1.01	46.1	91.2	28.21	0.21
18	23.27	0.0134	3.722	0.525	38.1	95.3	28.22	0.20
35	22.67	0.0164	1.705	0.423	31.1	97.8	28.22	0.22
23	22.80	0.0174	2.126	0.637	29.3	97.3	28.23	0.16
19	23.01	0.0074	2.837	0.769	69.0	96.4	28.23	0.15
10	23.50	0.0121	4.460	0.403	42.3	94.4	28.24	0.42
16	22.86	0.0106	2.312	0.717	48.1	97.0	28.24	0.15
08	23.33	0.0143	3.818	0.506	35.7	95.2	28.27	0.26
30	23.15	0.0212	3.159	0.446	24.0	96.0	28.29	0.22
15	22.83	0.0137	1.925	0.841	37.2	97.5	28.34	0.20
33	22.51	0.0094	0.7178	0.375	54.1	99.1	28.38	0.26
14	22.73	0.0077	1.417	0.493	65.8	98.2	28.40	0.30
22	22.48	0.0115	0.5879	0.463	44.4	99.2	28.40	0.20
17	22.85	0.0098	1.786	0.532	52.0	97.7	28.41	0.18
09	22.88	0.0147	1.797	0.508	34.8	97.7	28.45	0.31
06	22.66	0.0185	0.9372	0.661	27.6	98.8	28.49	0.22
12	23.15	0.0093	2.514	0.526	55.1	96.8	28.53	0.31
31	22.53	0.0060	0.4192	0.378	84.7	99.5	28.53	0.24
13	22.52	0.0089	0.3420	0.866	57.1	99.6	28.54	0.21
03	23.09	0.0068	1.999	0.336	74.6	97.4	28.64	0.44
weighted mean: MSWD=2.25*		n=35			46.3 ±16.6		28.24	0.10 *
S056, A6:133, single crystal sanidine, J=0.0007115±0.11%, D=1.0069±0.001, NM-133, Lab#=51905								
01	19.33	0.0130	1.382	1.02	39.2	97.9	24.13	0.19
09	19.10	0.0131	0.4733	1.18	38.8	99.3	24.17	0.15
04	19.19	0.0141	0.5983	0.811	36.1	99.1	24.25	0.18
02	19.25	0.0147	0.7973	0.637	34.7	98.8	24.25	0.22
08	19.29	0.0144	0.8742	0.973	35.3	98.7	24.26	0.17
10	20.83	0.0134	6.019	1.57	38.1	91.5	24.29	0.16
15	19.32	0.0135	0.8096	1.10	37.7	98.8	24.33	0.14
13	19.54	0.0140	1.457	1.10	36.4	97.8	24.37	0.15
06	19.87	0.0136	2.396	1.20	37.6	96.4	24.43	0.16
11	19.37	0.0137	0.6137	1.39	37.4	99.1	24.47	0.14

ID	$^{40}Ar/^{39}Ar$	$^{37}Ar/^{39}Ar$	$^{36}Ar/^{39}Ar$ (x 10^{-3})	$^{39}Ar_K$ (x 10^{-15} mol)	K/Ca	%^{40}Ar*	Age (Ma)	±2s (Ma)
12	20.78	0.0125	5.284	0.958	40.7	92.5	24.50	0.21
05	19.36	0.0118	0.3563	0.908	43.3	99.5	24.54	0.19
03&	25.97	0.0145	22.72	1.15	35.3	74.2	24.55	0.25
14	20.60	0.0123	4.535	0.944	41.5	93.5	24.55	0.19
07	19.63	0.0149	1.171	0.662	34.3	98.2	24.59	0.23
weighted mean:	MSWD=2.64*		n=14		37.9	±2.6	24.36	0.11 *
S066, A7:133, single crystal sanidine, J=0.0007117±0.11%, D=1.0069±0.001, NM-133, Lab#=51906								
09#	24.74	0.0017	13.45	0.251	295.5	83.9	26.47	0.45
10#	22.73	0.0065	5.693	0.222	78.3	92.6	26.83	0.47
15#	25.67	0.0128	13.69	0.253	40.0	84.2	27.56	0.63
08#	26.16	0.0011	15.11	0.218	476.7	82.9	27.64	0.62
03#	23.91	0.0042	7.111	0.292	121.5	91.2	27.78	0.49
14#	23.76	0.0026	6.602	0.241	196.4	91.8	27.78	0.49
07	22.57	0.0071	2.539	0.455	71.8	96.7	27.80	0.27
17#	29.12	0.0251	24.49	0.129	20.3	75.2	27.89	0.80
18#	22.26	0.0010	1.107	0.245	535.4	98.5	27.94	0.41
22	24.70	0.0083	9.284	0.476	61.3	88.9	27.97	0.23
11	23.05	0.0097	3.698	0.446	52.7	95.3	27.98	0.29
04	24.78	0.0165	9.513	0.311	31.0	88.7	27.99	0.40
01	23.18	0.0020	4.068	0.681	253.9	94.8	28.00	0.23
19#	25.57	0.0045	12.08	0.242	112.8	86.0	28.03	0.43
06	23.89	0.0032	6.252	0.370	157.1	92.3	28.08	0.39
21#	23.91	0.0052	6.345	0.271	98.2	92.2	28.08	0.29
20#	22.37	0.0071	0.9134	0.209	72.0	98.8	28.15	0.37
12#	22.88	0.0007	2.168	0.225	738.9	97.2	28.33	0.49
16	27.15	0.0123	16.50	0.426	41.4	82.0	28.37	0.32
13	26.17	0.0071	12.88	0.378	71.5	85.5	28.48	0.40
02	24.40	0.0010	6.568	0.703	522.2	92.0	28.61	0.27
05	23.32	0.0023	2.776	0.331	225.2	96.5	28.66	0.39
23#	33.93	0.0410	38.63	0.091	12.4	66.4	28.68	0.93
weighted mean:	MSWD=4.09*		n=10		148.8	±153.0	28.14	0.22 *
S066a, A8:133, single crystal sanidine, J=0.0007118±0.11%, D=1.0069±0.001, NM-133, Lab#=51907								
16	28.69	0.0146	22.90	2.13	35.0	76.4	27.93	0.23
20	30.67	0.0155	29.32	1.52	32.9	71.8	28.05	0.29
03	45.99	0.0119	81.11	2.83	43.0	47.9	28.06	0.41
11	35.75	0.0106	46.45	4.09	48.1	61.6	28.07	0.28
07	39.40	0.0141	58.73	3.99	36.1	56.0	28.09	0.29
10	37.10	0.0194	50.81	1.77	26.3	59.5	28.14	0.39
18	30.37	0.0155	27.99	1.23	33.0	72.8	28.17	0.31
04	29.66	0.0136	25.43	1.39	37.4	74.7	28.22	0.25
08	26.95	0.0138	16.22	2.03	37.0	82.2	28.23	0.19
21	28.86	0.0131	22.60	1.45	38.8	76.9	28.26	0.26
09	30.25	0.0165	27.21	1.17	30.9	73.4	28.30	0.29
06	28.01	0.0140	19.60	3.72	36.4	79.3	28.31	0.18
14	33.24	0.0139	37.29	1.48	36.7	66.9	28.31	0.30
22	35.68	0.0249	45.55	1.19	20.5	62.3	28.32	0.36
12	28.32	0.0164	20.58	1.17	31.0	78.5	28.34	0.29
05	47.94	0.0208	86.86	3.59	24.5	46.5	28.38	0.40
01	26.49	0.0250	14.25	2.74	20.4	84.1	28.39	0.19
19	25.23	0.0160	9.867	1.03	31.8	88.5	28.44	0.24
13	31.55	0.0104	31.15	1.74	49.1	70.8	28.48	0.27
02	34.64	0.0128	41.36	3.05	39.9	64.7	28.56	0.28
17	26.66	0.0131	14.30	0.559	38.9	84.2	28.58	0.36
15^	54.74	0.8232	108.9	1.06	0.62	41.3	28.83	0.75
weighted mean ± Taylor err			n=21 MSWD=1.55		34.7	±7.6	28.27	0.08
S067a, A9:133, single crystal sanidine, J=0.0007118±0.11%, D=1.0069±0.001, NM-133, Lab#=51908								
07^	48.09	0.8515	90.80	0.348	0.60	44.4	27.20	0.90
08#	28.37	0.0605	22.43	0.771	8.4	76.7	27.72	0.33
15^	54.28	0.9805	109.9	0.542	0.52	40.3	27.89	0.89
09^	29.89	1.119	27.39	0.165	0.46	73.2	27.92	0.92
16^	52.55	0.9805	103.9	0.490	0.52	41.8	27.98	0.55
18^	40.26	0.9044	61.72	0.159	0.56	54.9	28.17	0.85
12#	26.08	0.0622	13.13	0.506	8.2	85.1	28.29	0.39
06	26.67	0.0542	14.96	1.27	9.4	83.4	28.35	0.24
04^	31.28	0.9222	30.85	0.259	0.55	71.1	28.36	0.68
05	24.16	0.0433	6.428	3.12	11.8	92.2	28.37	0.14

ID	$^{40}Ar/^{39}Ar$	$^{37}Ar/^{39}Ar$	$^{36}Ar/^{39}Ar$ ($\times 10^{-3}$)	$^{39}Ar_K$ ($\times 10^{-15}$ mol)	K/Ca	%^{40}Ar*	Age (Ma)	±2s (Ma)
10	28.81	0.0361	22.07	1.24	14.1	77.4	28.41	0.29
17^	28.85	1.284	22.56	0.157	0.40	77.3	28.42	0.79
13^	37.45	0.7860	51.48	0.228	0.65	59.6	28.43	0.88
01^	25.54	1.293	11.10	0.231	0.39	87.6	28.52	0.65
02	29.56	0.0380	24.23	1.89	13.4	75.8	28.55	0.28
14#	26.64	0.0199	13.47	1.20	25.6	85.1	28.87	0.23
11^	39.02	0.8384	54.33	0.220	0.61	59.0	29.36	0.85
03^	52.60	0.7804	60.56	0.333	0.65	66.1	44.13	0.87
weighted mean:	MSWD=0.52*		n=4		12.2 ±2.1		28.39	0.08 *

S068, A10:133, single crystal sanidine, J=0.0007117±0.11%, D=1.0069±0.001, NM-133, Lab#=51909

09	22.70	0.0038	2.095	1.04	135.6	97.3	28.13	0.17
05	22.16	0.0036	0.2183	4.17	142.2	99.7	28.15	0.10
03	22.22	0.0030	0.2329	1.66	172.9	99.7	28.22	0.14
01	22.24	0.0008	0.2332	4.87	658.7	99.7	28.24	0.09
04	22.25	0.0020	0.2370	4.74	253.4	99.7	28.25	0.11
10	22.27	0.0025	0.2484	3.75	200.8	99.7	28.28	0.11
02	22.30	0.0013	0.3103	5.09	398.4	99.6	28.29	0.10
13	22.30	0.0067	0.1491	2.96	75.9	99.8	28.36	0.12
11	22.35	0.0024	0.2767	2.90	216.6	99.6	28.37	0.10
14	22.32	0.0014	0.1670	4.03	354.7	99.8	28.37	0.11
08	22.32	0.0022	0.1457	3.63	228.5	99.8	28.37	0.12
07	22.35	0.0066	0.2283	2.59	76.8	99.7	28.39	0.12
12	22.42	0.0021	0.4327	2.51	237.9	99.4	28.40	0.11
15	22.43	0.0021	0.4407	3.29	242.9	99.4	28.40	0.11
06	22.35	0.0080	0.1055	2.33	64.0	99.9	28.43	0.13
weighted mean:	MSWD=2.56*		n=15		230.6 ±152.2		28.31	0.10 *

S069, A11:133, single crystal sanidine, J=0.0007114±0.11%, D=1.0069±0.001, NM-133, Lab#=51910

10	22.50	0.0052	1.068	2.07	97.8	98.6	28.26	0.13
04	22.30	0.0066	0.3154	4.00	77.1	99.6	28.28	0.10
07	22.54	0.0050	1.055	2.75	102.6	98.6	28.30	0.13
01	22.39	0.0067	0.5475	2.67	76.7	99.3	28.31	0.14
09	22.64	0.0044	1.374	2.45	114.9	98.2	28.32	0.13
08	22.47	0.0057	0.8002	3.52	88.8	99.0	28.32	0.13
15	23.48	0.0039	4.084	3.12	130.8	94.9	28.36	0.12
03	22.47	0.0058	0.6510	3.95	88.1	99.1	28.36	0.14
11	22.70	0.0064	1.336	2.04	79.2	98.3	28.40	0.13
06	22.61	0.0053	1.003	2.98	96.4	98.7	28.41	0.11
12	22.63	0.0052	1.060	3.04	97.3	98.6	28.41	0.12
14	22.52	0.0051	0.6586	3.16	99.8	99.1	28.42	0.11
05	22.54	0.0054	0.7017	2.31	93.8	99.1	28.43	0.14
02	22.79	0.0054	1.550	3.83	95.1	98.0	28.44	0.10
13	22.65	0.0065	1.011	2.74	78.8	98.7	28.46	0.11
weighted mean ± Taylor err			n=15	MSWD=1.24	94.5 ±14.7		28.37	0.07

S072, A12:133, single crystal sanidine, J=0.0007111±0.11%, D=1.0069±0.001, NM-133, Lab#=51911

07	23.04	0.0480	3.284	1.18	10.6	95.8	28.10	0.19
15	22.56	0.0404	1.386	1.46	12.6	98.2	28.21	0.14
09	22.48	0.0460	0.9425	1.76	11.1	98.8	28.26	0.15
11	22.71	0.0440	1.655	3.36	11.6	97.9	28.29	0.11
12	22.59	0.0377	1.164	1.91	13.5	98.5	28.32	0.14
05	22.51	0.0456	0.9050	2.55	11.2	98.8	28.32	0.11
10	22.82	0.0460	1.945	1.97	11.1	97.5	28.33	0.14
08	22.49	0.0392	0.7941	2.59	13.0	99.0	28.33	0.11
04	22.50	0.0431	0.8052	1.83	11.8	99.0	28.35	0.15
06	22.47	0.0488	0.6796	2.35	10.4	99.1	28.35	0.11
13	23.01	0.0466	2.359	2.32	11.0	97.0	28.40	0.12
03	22.64	0.0428	0.9589	2.56	11.9	98.8	28.46	0.11
02	22.67	0.0427	0.9564	3.86	12.0	98.8	28.50	0.11
01	22.71	0.0472	1.030	3.06	10.8	98.7	28.52	0.11
14	22.69	0.0401	0.8590	2.08	12.7	98.9	28.56	0.15
weighted mean:	MSWD=3.02*		n=15		11.7 ±0.9		28.37	0.11 *

S074, A13:133, single crystal sanidine, J=0.0007106±0.11%, D=1.0069±0.001, NM-133, Lab#=51912

07	26.18	0.0321	13.86	1.75	15.9	84.4	28.09	0.19
16	22.91	0.0113	2.750	1.68	45.2	96.5	28.11	0.13
02	23.28	0.0120	3.583	2.36	42.4	95.5	28.27	0.12
11	23.28	0.0261	3.471	1.96	19.5	95.6	28.31	0.15

ID	$^{40}Ar/^{39}Ar$	$^{37}Ar/^{39}Ar$	$^{36}Ar/^{39}Ar$ (x 10^{-3})	$^{39}Ar_K$ (x 10^{-15} mol)	K/Ca	%^{40}Ar*	Age (Ma)	±2s (Ma)
14	25.41	0.0525	10.68	1.30	9.7	87.6	28.32	0.22
22	23.43	0.0113	3.915	2.93	45.2	95.1	28.33	0.13
25	22.85	0.0245	1.957	2.33	20.9	97.5	28.33	0.13
03	23.30	0.0233	3.474	3.63	21.9	95.6	28.33	0.11
08	22.80	0.0156	1.760	1.94	32.8	97.7	28.34	0.12
04	23.57	0.0124	4.319	3.62	41.1	94.6	28.36	0.12
01	23.94	0.0175	5.557	3.10	29.2	93.1	28.36	0.13
05	22.97	0.0229	2.253	1.88	22.3	97.1	28.37	0.13
09	23.33	0.0152	3.345	2.44	33.5	95.8	28.42	0.12
06	23.80	0.0206	4.912	3.24	24.8	93.9	28.43	0.12
19	23.95	0.0287	5.421	1.67	17.8	93.3	28.44	0.17
23	24.43	0.0280	6.989	2.42	18.2	91.6	28.45	0.15
18	24.32	0.0387	6.593	1.69	13.2	92.0	28.46	0.17
17	23.23	0.0240	2.880	1.42	21.3	96.3	28.47	0.15
20	23.69	0.0166	4.413	1.99	30.7	94.5	28.47	0.15
21	28.14	0.0227	19.31	3.04	22.5	79.7	28.53	0.21
13	23.71	0.0191	4.254	2.95	26.7	94.7	28.57	0.13
10	23.25	0.0111	2.666	3.37	46.0	96.6	28.57	0.13
15	23.25	0.0243	2.672	1.87	21.0	96.6	28.57	0.13
24	25.19	0.0147	9.176	1.61	34.8	89.2	28.60	0.20
12	23.49	0.0185	3.374	2.29	27.5	95.8	28.61	0.13
weighted mean:	MSWD=3.41*	n=25			27.4	±10.5	28.40	0.12 *

S077a, A14:133, single crystal sanidine, J=0.0007103±0.11%, D=1.0069±0.001, NM-133, Lab#=51913

07	22.51	0.0130	1.103	3.18	39.3	98.6	28.21	0.10
03	22.38	0.0150	0.6553	1.94	33.9	99.1	28.22	0.12
09	22.26	0.0135	0.1618	2.39	37.8	99.8	28.25	0.10
08	22.33	0.0138	0.3574	2.63	37.0	99.5	28.26	0.11
11	22.63	0.0144	1.340	3.68	35.4	98.3	28.27	0.12
02	22.37	0.0113	0.3936	2.30	45.0	99.5	28.30	0.11
12	22.59	0.0117	1.104	1.76	43.4	98.6	28.31	0.13
13	22.40	0.0188	0.4611	3.56	27.1	99.4	28.31	0.10
01	22.48	0.0189	0.6672	3.61	27.0	99.1	28.33	0.10
14	22.71	0.0145	1.417	3.62	35.1	98.2	28.34	0.10
06	22.48	0.0160	0.6394	3.32	31.9	99.2	28.35	0.10
10	22.52	0.0131	0.6196	4.12	39.0	99.2	28.40	0.12
04	22.44	0.0095	0.2419	3.61	54.0	99.7	28.45	0.12
05	22.90	0.0118	1.781	3.05	43.2	97.7	28.45	0.12
15	22.46	0.0124	0.2484	4.07	41.2	99.7	28.47	0.11
weighted mean:	MSWD=2.21*	n=15			38.0	±7.0	28.32	0.09 *

S078, A15:133, single crystal sanidine, J=0.0007101±0.11%, D=1.0069±0.001, NM-133, Lab#=51914

06	22.61	0.0107	1.678	2.32	47.9	97.8	28.11	0.12
12	22.87	0.0132	2.352	2.16	38.6	97.0	28.19	0.14
11	22.69	0.0166	1.714	2.24	30.8	97.8	28.20	0.13
13	22.87	0.0124	2.244	2.00	41.2	97.1	28.23	0.14
02	22.46	0.0118	0.7397	4.04	43.3	99.0	28.27	0.10
09	22.55	0.0154	0.9773	3.23	33.1	98.7	28.30	0.11
04	22.76	0.0117	1.555	2.65	43.5	98.0	28.34	0.12
07	23.76	0.0136	4.846	2.76	37.5	94.0	28.38	0.16
15	22.48	0.0146	0.5173	3.05	35.0	99.3	28.39	0.11
01	22.50	0.0123	0.5345	3.90	41.5	99.3	28.40	0.12
05	22.59	0.0139	0.7865	3.31	36.8	99.0	28.42	0.11
08	22.74	0.0128	1.266	2.53	39.8	98.4	28.43	0.11
03	22.97	0.0094	1.888	2.94	54.3	97.6	28.48	0.13
14	22.81	0.0132	1.326	2.73	38.7	98.3	28.49	0.13
10	22.91	0.0104	1.667	1.85	48.8	97.9	28.49	0.12
weighted mean:	MSWD=3.68*	n=15			40.7	±6.2	28.35	0.12 *

S085, A16:133, single crystal sanidine, J=0.00071±0.11%, D=1.0069±0.001, NM-133, Lab#=51915

07	22.53	0.0159	1.187	2.25	32.1	98.4	28.19	0.13
08	22.49	0.0275	1.009	2.65	18.5	98.7	28.21	0.14
10	22.75	0.0167	1.817	2.63	30.5	97.6	28.23	0.13
09	23.06	0.0307	2.784	2.36	16.6	96.4	28.27	0.13
15	23.25	0.0709	3.391	2.02	7.2	95.7	28.28	0.14
12	22.91	0.0161	2.136	2.96	31.6	97.3	28.31	0.11
11	22.53	0.0328	0.8397	2.06	15.6	98.9	28.32	0.13
05	22.56	0.0157	0.8967	2.34	32.5	98.8	28.33	0.13
03	23.15	0.0279	2.814	2.57	18.3	96.4	28.36	0.14

ID	$^{40}Ar/^{39}Ar$	$^{37}Ar/^{39}Ar$	$^{36}Ar/^{39}Ar$ ($\times 10^{-3}$)	$^{39}Ar_K$ ($\times 10^{-15}$ mol)	K/Ca	%^{40}Ar*	Age (Ma)	±2s (Ma)
01	23.12	0.0352	2.682	3.62	14.5	96.6	28.38	0.12
06	22.69	0.0160	1.167	2.42	31.8	98.5	28.40	0.13
04	22.59	0.0431	0.7959	3.24	11.8	99.0	28.41	0.11
13	22.70	0.0245	0.9025	1.94	20.8	98.8	28.51	0.14
02	22.50	0.0334	0.2200	2.64	15.3	99.7	28.51	0.10
14	22.83	0.0170	1.147	1.15	30.0	98.5	28.58	0.18
weighted mean:	MSWD=2.90*		n=15		21.8	±8.7	28.36	0.11 *
S053, G1:133, single crystal sanidine, J=0.0006953±0.11%, D=1.0069±0.001, NM-133, Lab#=51972								
01	23.96	0.0104	4.401	3.11	48.9	94.6	28.20	0.13
07	23.06	0.0118	1.294	2.42	43.1	98.3	28.22	0.12
11	23.80	0.0131	3.734	2.60	38.8	95.4	28.25	0.13
08	24.74	0.0103	6.908	1.86	49.4	91.8	28.25	0.15
02	23.39	0.0107	2.286	3.83	47.8	97.1	28.27	0.11
09	23.62	0.0205	3.043	2.41	24.9	96.2	28.28	0.13
03	23.57	0.0083	2.863	1.95	61.3	96.4	28.29	0.15
13	24.27	0.0094	5.212	1.45	54.2	93.7	28.29	0.18
06	23.69	0.0114	3.237	2.19	44.7	96.0	28.29	0.14
12	23.78	0.0136	3.487	2.85	37.4	95.7	28.32	0.13
14	23.08	0.0201	1.010	2.06	25.3	98.7	28.35	0.13
04	23.15	0.0123	1.210	1.83	41.5	98.5	28.36	0.13
10	23.82	0.0143	3.203	1.81	35.7	96.0	28.47	0.16
05	23.29	0.0120	1.360	2.45	42.6	98.3	28.49	0.11
15	23.20	0.0166	0.6195	0.970	30.7	99.2	28.64	0.17
weighted mean:	MSWD=2.67*		n=15		41.8	±10.1	28.32	0.11 *
S064, G2:133, single crystal sanidine, J=0.0006953±0.11%, D=1.0069±0.001, NM-133, Lab#=51973								
08	22.79	0.0153	1.289	4.41	33.4	98.3	27.89	0.10
06	22.77	0.0156	1.034	2.94	32.7	98.7	27.96	0.10
31	22.60	0.0176	0.4607	3.81	29.0	99.4	27.96	0.09
01	22.66	0.0170	0.6396	3.23	30.1	99.2	27.97	0.10
45	24.57	0.0172	7.094	2.00	29.6	91.5	27.97	0.16
30	22.73	0.0157	0.8685	2.88	32.6	98.9	27.97	0.10
27	22.67	0.0177	0.4512	2.87	28.9	99.4	28.05	0.10
42	22.83	0.0152	0.9469	2.62	33.5	98.8	28.06	0.11
09	24.59	0.0161	6.939	2.92	31.6	91.7	28.06	0.12
29	22.62	0.0154	0.2343	2.76	33.0	99.7	28.07	0.12
02	22.72	0.0170	0.5572	4.39	30.0	99.3	28.08	0.10
50	22.93	0.0162	1.236	2.44	31.4	98.4	28.08	0.12
33	22.71	0.0149	0.4548	3.56	34.3	99.4	28.09	0.10
26	22.68	0.0165	0.3741	2.58	30.9	99.5	28.09	0.11
20	25.87	0.0212	11.15	2.62	24.1	87.3	28.10	0.15
05	22.70	0.0158	0.4260	4.97	32.3	99.5	28.10	0.11
12	26.13	0.0157	12.00	3.17	32.6	86.4	28.11	0.16
32	22.66	0.0156	0.2234	2.78	32.6	99.7	28.12	0.11
11	22.73	0.0156	0.4342	3.11	32.7	99.4	28.13	0.11
35	22.92	0.0165	1.038	5.09	30.8	98.7	28.14	0.12
13	22.75	0.0158	0.4608	2.05	32.3	99.4	28.15	0.13
41	22.77	0.0163	0.4951	3.62	31.2	99.4	28.15	0.09
46	22.78	0.0165	0.5103	2.93	30.9	99.3	28.16	0.10
14	23.72	0.0171	3.708	2.81	29.8	95.4	28.16	0.12
44	22.81	0.0317	0.5990	2.60	16.1	99.2	28.17	0.10
04	22.73	0.0168	0.3054	5.18	30.3	99.6	28.18	0.11
28	23.76	0.0216	3.806	2.22	23.6	95.3	28.18	0.14
34	22.83	0.0151	0.6023	2.62	33.8	99.2	28.19	0.11
19	22.87	0.0169	0.7136	2.43	30.2	99.1	28.20	0.12
24	22.75	0.0209	0.3271	3.76	24.4	99.6	28.20	0.12
15	22.77	0.0187	0.3426	3.51	27.3	99.6	28.21	0.11
36	22.91	0.0168	0.7916	3.78	30.3	99.0	28.22	0.11
21	22.90	0.0168	0.7485	2.52	30.3	99.0	28.22	0.12
43	23.05	0.0244	1.220	3.33	20.9	98.4	28.23	0.10
22	22.98	0.0165	0.9786	3.06	31.0	98.7	28.24	0.10
23	22.86	0.0173	0.5521	3.88	29.4	99.3	28.24	0.11
40	22.75	0.0168	0.1802	2.22	30.4	99.8	28.25	0.13
38	22.89	0.0189	0.6466	2.70	27.1	99.2	28.25	0.11
10	24.60	0.0221	6.456	3.85	23.0	92.3	28.25	0.12
39	22.84	0.0201	0.4348	3.47	25.4	99.4	28.26	0.11
03	23.14	0.0183	1.475	4.22	27.8	98.1	28.26	0.09
25	22.89	0.0163	0.6125	2.33	31.4	99.2	28.26	0.13

ID	$^{40}Ar/^{39}Ar$	$^{37}Ar/^{39}Ar$	$^{36}Ar/^{39}Ar$ (x 10^{-3})	$^{39}Ar_K$ (x 10^{-15} mol)	K/Ca		%^{40}Ar*	Age (Ma)	±2s (Ma)	
07	22.89	0.0165	0.6067	4.46	30.9		99.2	28.26	0.12	
48	22.90	0.0146	0.6008	2.43	34.9		99.2	28.27	0.14	
17	23.05	0.0160	1.090	2.82	32.0		98.6	28.28	0.12	
16	22.82	0.0178	0.2999	2.94	28.6		99.6	28.29	0.10	
49	22.79	0.0180	0.1700	3.79	28.4		99.8	28.29	0.10	
18	22.84	0.0162	0.3138	2.53	31.5		99.6	28.31	0.11	
37	24.45	0.0159	5.707	2.46	32.1		93.1	28.33	0.15	
47	23.15	0.0158	0.6945	2.04	32.4		99.1	28.55	0.13	
weighted mean:		MSWD=4.52*	n=50		29.9	±3.6		28.16	0.12	*
S067, G6:133, single crystal sanidine, J=0.0006937±0.11%, D=1.0069±0.001, NM-133, Lab#=51977										
10	22.75	0.0015	0.5797	2.58	335.2		99.2	28.04	0.11	
01	22.86	0.0060	0.8932	4.33	85.1		98.8	28.06	0.09	
11	22.76	0.0033	0.3752	2.78	155.9		99.5	28.12	0.11	
07	22.85	0.0101	0.6824	3.77	50.4		99.1	28.12	0.09	
04	23.02	0.0021	1.251	4.47	247.6		98.4	28.13	0.10	
05	23.09	0.0018	1.367	5.59	287.9		98.3	28.17	0.10	
02	23.19	0.0017	1.706	6.85	307.1		97.8	28.17	0.09	
06	23.12	0.0021	1.466	5.61	247.8		98.1	28.17	0.11	
08	22.82	0.0074	0.3694	5.32	68.9		99.5	28.20	0.08	
03	22.90	0.0022	0.5764	6.58	228.4		99.3	28.22	0.09	
13	22.97	0.0028	0.6079	3.16	180.3		99.2	28.29	0.11	
15	22.97	0.0015	0.5545	2.92	332.9		99.3	28.31	0.11	
09	23.83	0.0017	3.460	4.96	296.8		95.7	28.32	0.11	
12	23.01	0.0025	0.6996	2.51	206.3		99.1	28.32	0.12	
14	22.94	0.0034	0.4337	3.91	152.3		99.4	28.32	0.12	
weighted mean:		MSWD=3.23*	n=15		212.2	±94.5		28.19	0.11	*
S070, G10:133, single crystal sanidine, J=0.0006928±0.11%, D=1.0069±0.001, NM-133, Lab#=51981										
04	22.93	0.0054	0.8858	8.27	94.0		98.9	28.11	0.11	
06	22.86	0.0061	0.4975	8.01	83.5		99.4	28.17	0.11	
12	23.11	0.0058	1.301	5.55	87.6		98.3	28.19	0.11	
02	22.84	0.0063	0.3233	6.53	81.4		99.6	28.20	0.09	
11	22.96	0.0068	0.7093	5.09	75.0		99.1	28.21	0.10	
03	23.05	0.0083	1.017	11.3	61.5		98.7	28.21	0.14	
14	23.06	0.0069	0.9819	5.67	74.4		98.7	28.24	0.11	
09	23.11	0.0049	1.099	4.65	104.1		98.6	28.25	0.11	
08	23.88	0.0058	3.714	8.10	88.1		95.4	28.26	0.14	
07	23.15	0.0049	1.223	8.49	103.7		98.4	28.26	0.11	
15	23.05	0.0061	0.8353	7.21	84.0		98.9	28.28	0.10	
05	22.91	0.0054	0.3309	9.74	94.3		99.6	28.29	0.10	
10	23.30	0.0058	1.563	5.78	88.6		98.0	28.33	0.11	
13	23.21	0.0051	1.146	5.93	99.2		98.5	28.36	0.10	
01	23.08	0.0061	0.6282	6.49	83.7		99.2	28.40	0.10	
weighted mean:		MSWD=2.07*	n=15		86.9	±11.5		28.26	0.09	*
S071, G13:133, single crystal sanidine, J=0.000694±0.11%, D=1.0069±0.001, NM-133, Lab#=51984										
13	19.83	0.0193	1.461	3.93	26.4		97.8	24.12	0.10	
10	19.73	0.0210	0.8642	2.89	24.3		98.7	24.22	0.09	
08	19.62	0.0181	0.4527	3.24	28.3		99.3	24.24	0.09	
15	19.68	0.0166	0.6191	2.06	30.7		99.1	24.25	0.12	
11	19.70	0.0186	0.6588	2.54	27.5		99.0	24.26	0.11	
14	19.93	0.0205	1.325	4.09	24.9		98.0	24.30	0.11	
07	19.83	0.0207	0.7602	1.21	24.6		98.9	24.38	0.14	
12	20.04	0.0198	1.475	3.23	25.8		97.8	24.39	0.10	
01	19.70	0.0166	0.3053	3.84	30.8		99.5	24.39	0.08	
04	19.72	0.0151	0.3585	3.77	33.8		99.5	24.39	0.08	
05	19.78	0.0233	0.5011	1.77	21.9		99.3	24.42	0.11	
09	19.90	0.0166	0.8210	3.09	30.7		98.8	24.44	0.10	
06	19.88	0.0182	0.7096	3.27	28.1		99.0	24.47	0.11	
03	20.21	0.0171	1.675	4.22	29.8		97.6	24.52	0.10	
02	19.96	0.0186	0.7047	3.79	27.4		99.0	24.57	0.11	
weighted mean:		MSWD=5.96*	n=15		27.7	±3.1		24.35	0.13	*
S075, G14:133, single crystal sanidine, J=0.0006944±0.11%, D=1.0069±0.001, NM-133, Lab#=51985										
15	22.73	0.0069	0.4480	2.64	73.9		99.4	28.09	0.11	
04	22.73	0.0064	0.3770	3.86	80.1		99.5	28.12	0.09	
01	22.90	0.0090	0.7437	2.59	56.9		99.0	28.19	0.11	
12	23.03	0.0079	1.174	3.05	64.7		98.5	28.19	0.12	

ID	$^{40}Ar/^{39}Ar$	$^{37}Ar/^{39}Ar$	$^{36}Ar/^{39}Ar$ (x 10^{-3})	$^{39}Ar_K$ (x 10^{-15} mol)	K/Ca	$\%^{40}Ar^*$	Age (Ma)	±2s (Ma)
08	22.77	0.0057	0.2572	2.54	89.9	99.7	28.21	0.12
06	22.81	0.0073	0.3518	3.41	70.0	99.5	28.22	0.11
03	23.43	0.0059	2.423	4.25	87.0	96.9	28.24	0.10
14	23.03	0.0082	0.8803	2.71	62.2	98.9	28.30	0.11
13	22.90	0.0092	0.4263	3.76	55.7	99.5	28.31	0.11
10	22.87	0.0073	0.1666	2.77	69.7	99.8	28.36	0.11
11	22.82	0.0066	0.0153	2.81	77.3	100.0	28.36	0.12
05	23.04	0.0057	0.7422	2.51	89.3	99.1	28.36	0.11
02	22.87	0.0065	0.1571	2.39	78.8	99.8	28.37	0.11
09	24.35	0.0055	5.117	2.38	93.3	93.8	28.39	0.12
07	23.01	0.0062	0.5717	1.76	82.6	99.3	28.40	0.14
weighted mean:	MSWD=3.27*	n=15			75.4	±12.0	28.26	0.11 *

S086, G15:133, single crystal sanidine, J=0.0006948±0.11%, D=1.0069±0.001, NM-133, Lab#=51986

18	22.88	0.0354	1.420	0.416	14.4	98.2	27.94	0.24
19	23.33	0.0300	2.742	0.537	17.0	96.5	28.01	0.21
01	22.99	0.0232	0.9514	0.731	22.0	98.8	28.24	0.23
16	22.96	0.0227	0.6969	0.288	22.5	99.1	28.30	0.26
14	23.02	0.0358	0.8656	0.630	14.3	98.9	28.31	0.15
15	23.02	0.0300	0.8811	0.372	17.0	98.9	28.32	0.22
07	22.71	0.0288	-0.1906	0.448	17.7	100.3	28.32	0.28
12	22.65	0.0330	-0.5082	0.424	15.4	100.7	28.36	0.24
03	22.95	0.0320	0.0478	0.505	15.9	100.0	28.53	0.28
17	22.90	0.0302	-0.1913	0.388	16.9	100.3	28.55	0.20
02	23.04	0.0336	0.1237	0.561	15.2	99.9	28.61	0.25
13	22.90	0.0287	-0.6235	0.597	17.8	100.8	28.71	0.18
10	23.16	0.0329	0.2003	0.526	15.5	99.8	28.73	0.20
04	23.07	0.0322	-0.1254	0.586	15.8	100.2	28.73	0.26
08	23.06	0.0273	-0.2223	0.376	18.7	100.3	28.76	0.30
11	22.89	0.0321	-0.8021	0.420	15.9	101.0	28.77	0.23
09	23.32	0.0277	0.5955	0.603	18.4	99.3	28.79	0.24
05	22.89	0.0288	-0.9053	0.555	17.7	101.2	28.80	0.26
06	23.30	0.0301	-0.6452	0.459	17.0	100.8	29.21	0.27
weighted mean:	MSWD=6.86*	n=19			17.1	±2.2	28.50	0.20 *

S076, J4:133, single crystal sanidine, J=0.0006852±0.11%, D=1.0069±0.001, NM-133, Lab#=51995

09	22.83	0.0054	0.0878	3.10	94.4	99.9	27.97	0.10
04	22.85	0.0048	0.1100	1.93	106.6	99.9	27.99	0.12
05	22.88	0.0012	0.0562	2.83	429.4	99.9	28.04	0.11
01	22.94	0.0060	0.0682	4.48	85.1	99.9	28.11	0.11
07	22.99	0.0020	0.2035	4.69	251.1	99.7	28.12	0.09
08	22.98	0.0027	0.1452	3.86	191.0	99.8	28.13	0.09
13	23.69	0.0015	2.469	2.25	342.3	96.9	28.16	0.13
15	23.01	0.0123	0.0666	3.86	41.5	99.9	28.20	0.12
14	23.10	0.0015	0.3067	1.61	339.5	99.6	28.23	0.14
06	23.07	0.0035	0.1279	3.08	145.7	99.8	28.24	0.13
03	23.13	0.0010	0.2976	3.81	497.0	99.6	28.26	0.10
11	23.10	0.0036	0.1419	2.53	140.7	99.8	28.28	0.11
12	23.09	0.0020	0.0839	3.60	261.5	99.9	28.29	0.10
02	23.07	0.0084	-0.0633	2.88	60.8	100.1	28.31	0.12
10@	23.28	0.0062	0.0777	1.87	82.5	99.9	28.52	0.14
weighted mean:	MSWD=4.26*	n=14			213.3	±143.7	28.16	0.13 *

* MSWD outside 95% confidence interval
^ = Plagioclase, & = low yield, # = small signal, @ = xenocryst, $ = alteration, ! = anomalously young
Isotopic ratios corrected for blank, radioactive decay, and mass discrimination, not corrected for interferring reactions.
Individual analyses show analytical error only; mean age errors also include error in J and irradiation parameters.
Discrimination = 1.00690±0.00100 a.m.u.
Correction factors:
$(^{39}Ar/^{37}Ar)_{Ca}$ = 0.00070±0.00002
$(^{36}Ar/^{37}Ar)_{Ca}$ = 0.00028±0.00001
$(^{38}Ar/^{39}Ar)_K$ = 0.0108
$(^{40}Ar/^{39}Ar)_K$ = 0.0002±0.0003

$^{40}Ar/^{39}Ar$ analytical results of samples included in Irrad.# NM-144

ID	$^{40}Ar/^{39}Ar$	$^{37}Ar/^{39}Ar$	$^{36}Ar/^{39}Ar$ (x 10^{-3})	$^{39}Ar_K$ (x 10^{-15} mol)	K/Ca	%^{40}Ar*	Age (Ma)	±2s (Ma)
S103, D1:144, single crystal sanidine, J=0.0007719±0.10%, D=1.0056±0.00118, NM-144, Lab#=52678								
14!	21.02	0.0068	2.761	2.59	75.2	96.1	27.92	0.64
10	20.66	0.0023	0.4904	2.22	220.9	99.3	28.35	0.13
08	20.65	0.0070	0.3499	4.20	73.3	99.5	28.39	0.12
13	20.83	0.0067	0.7957	1.19	76.7	98.9	28.45	0.18
02	20.87	0.0077	0.9255	1.96	66.1	98.7	28.46	0.13
09	20.95	0.0025	1.064	2.82	205.1	98.5	28.52	0.13
05	20.94	0.0028	0.8777	1.48	180.6	98.8	28.57	0.16
01	20.81	0.0057	0.2852	2.99	89.0	99.6	28.64	0.12
12	21.06	0.0098	0.7945	1.51	52.2	98.9	28.77	0.16
06	21.21	0.0116	1.188	2.30	43.9	98.3	28.81	0.19
07	21.50	0.0035	2.026	2.77	144.1	97.2	28.88	0.15
04@	21.47	0.0074	1.106	1.78	68.8	98.5	29.20	0.14
03@	21.54	0.0166	1.310	1.97	30.7	98.2	29.22	0.15
11@	21.41	0.0065	0.5560	2.38	78.4	99.2	29.34	0.11
15@	21.50	0.0067	0.6693	2.69	75.7	99.1	29.43	0.15
weighted mean:	MSWD=5.93*		n=10		115.2	±66.5	28.56	0.18 *
S110, D2:144, single crystal sanidine, J=0.0007717±0.10%, D=1.0056±0.00118, NM-144, Lab#=52679								
07&	442.5	0.0924	1467.6	0.010	5.5	2.0	12.31	19.16
03	20.96	0.0066	1.839	3.78	76.9	97.4	28.20	0.23
04	20.79	0.0073	1.154	2.79	69.4	98.4	28.25	0.12
05	20.73	0.0075	0.8852	2.50	68.2	98.7	28.28	0.12
15	20.64	0.0076	0.5316	2.77	67.0	99.2	28.29	0.11
01	20.72	0.0063	0.7753	3.58	81.4	98.9	28.31	0.11
13	20.73	0.0058	0.6183	2.44	87.9	99.1	28.38	0.12
02	20.76	0.0037	0.6410	2.96	137.5	99.1	28.41	0.13
06	20.67	0.0025	0.2609	2.34	201.2	99.6	28.44	0.12
12	20.83	0.0036	0.7601	2.65	142.2	98.9	28.46	0.12
14	20.83	0.0058	0.7682	2.78	87.7	98.9	28.46	0.12
08	20.95	0.0072	1.123	3.49	71.1	98.4	28.48	0.10
10	20.75	0.0099	0.3655	2.09	51.3	99.5	28.51	0.13
11@	20.93	0.0138	0.4199	1.99	37.1	99.4	28.73	0.14
09@	20.97	0.0060	0.5171	2.28	85.7	99.3	28.75	0.13
weighted mean:	MSWD=2.45*		n=12		95.2	±43.2	28.38	0.10 *
S111, D3:144, single crystal sanidine, J=0.0007713±0.10%, D=1.0056±0.00118, NM-144, Lab#=52680								
04	23.08	0.0018	9.374	3.17	278.0	88.0	28.04	0.16
02	21.96	0.0013	5.356	2.96	404.3	92.8	28.14	0.16
12	21.41	0.0044	3.215	1.43	116.2	95.6	28.24	0.17
10	21.55	0.0030	3.549	3.60	171.7	95.1	28.30	0.13
15	22.69	0.0014	7.332	3.25	365.5	90.5	28.34	0.15
01	22.98	0.0016	8.288	3.26	322.0	89.3	28.34	0.15
05	21.97	0.0019	4.759	2.72	270.7	93.6	28.39	0.13
06	22.96	0.0021	8.083	2.69	248.6	89.6	28.40	0.18
08	20.90	0.0057	1.027	4.03	89.2	98.6	28.43	0.11
11	22.14	0.0018	5.154	0.666	289.3	93.1	28.46	0.28
14	21.63	0.0013	3.363	2.89	407.3	95.4	28.48	0.12
03	20.89	0.0071	0.7951	2.53	71.7	98.9	28.52	0.13
13	21.15	0.0017	1.507	1.56	308.6	97.9	28.58	0.14
09#	25.45	0.0028	15.65	0.158	183.4	81.8	28.74	0.79
07@	21.83	0.0072	3.364	3.94	71.3	95.4	28.76	0.11
weighted mean:	MSWD=4.07*		n=13		257.2	±113.4	28.37	0.14 *
S112, D4:144, single crystal sanidine, J=0.0007707±0.10%, D=1.0056±0.00118, NM-144, Lab#=52681								
05!	24.56	0.0051	14.07	5.00	99.9	83.1	28.14	0.16
15	21.39	0.0050	2.843	3.95	101.7	96.1	28.35	0.12
07	21.54	0.0056	3.332	9.39	91.1	95.4	28.35	0.11
14	21.34	0.0090	2.641	4.07	56.8	96.3	28.36	0.10
06	21.28	0.0063	2.405	4.84	81.5	96.7	28.37	0.12
13	23.74	0.0092	10.72	3.64	55.3	86.7	28.38	0.16
01	20.85	0.0055	0.8011	2.64	92.7	98.9	28.44	0.11
09	21.25	0.0056	2.122	5.21	91.4	97.1	28.45	0.11
02	22.47	0.0068	6.170	3.98	75.3	91.9	28.48	0.14
11	22.50	0.0055	6.292	2.66	92.7	91.7	28.48	0.15
03	20.97	0.0045	1.058	4.65	113.7	98.5	28.49	0.10

ID	$^{40}Ar/^{39}Ar$	$^{37}Ar/^{39}Ar$	$^{36}Ar/^{39}Ar$ (x 10^{-3})	$^{39}Ar_K$ (x 10^{-15} mol)	K/Ca	%^{40}Ar*	Age (Ma)	±2s (Ma)
08	21.12	0.0053	1.525	5.16	95.9	97.9	28.52	0.13
04	20.94	0.0056	0.8660	4.19	91.3	98.8	28.53	0.10
12	22.53	0.0051	6.243	3.79	100.5	91.8	28.54	0.14
10	21.65	0.0071	3.264	2.54	72.0	95.5	28.54	0.14
weighted mean ± Taylor err			n=14 MSWD=1.49		86.6 ±16.7		28.45	0.06
S114, D6:144, single crystal sanidine, J=0.0007689±0.10%, D=1.0056±0.00118, NM-144, Lab#=52683								
10!	22.50	0.4395	7.194	1.58	1.2	90.7	28.10	0.28
15!	23.28	0.1920	9.634	1.85	2.7	87.8	28.15	0.18
13	25.02	0.5022	14.99	1.63	1.0	82.5	28.41	0.23
05	21.63	0.4076	3.421	1.66	1.3	95.5	28.43	0.17
09	22.64	0.2980	6.806	1.84	1.7	91.2	28.43	0.17
14	21.45	0.4432	2.762	1.45	1.2	96.4	28.46	0.18
01	22.91	0.3668	7.605	2.50	1.4	90.3	28.48	0.15
12	23.21	0.0999	8.527	1.96	5.1	89.2	28.48	0.16
02	23.11	0.3426	8.278	2.52	1.5	89.5	28.49	0.17
06	22.86	0.0810	7.283	3.16	6.3	90.6	28.50	0.14
08	22.80	0.1065	7.030	1.80	4.8	90.9	28.53	0.17
04	23.06	0.0846	7.781	2.79	6.0	90.1	28.58	0.16
03	21.67	0.4248	3.066	2.65	1.2	96.0	28.63	0.12
07	23.06	0.1038	7.661	1.54	4.9	90.2	28.63	0.20
11	22.31	0.0860	5.066	3.03	5.9	93.3	28.65	0.14
weighted mean ± Taylor err			n=13 MSWD=1.08		3.3 ±2.2		28.53	0.07
S116, D7:144, single crystal sanidine, J=0.0007683±0.10%, D=1.0056±0.00118, NM-144, Lab#=52684								
15	18.08	0.0152	1.443	2.24	33.6	97.6	24.31	0.12
04	17.89	0.0148	0.7276	3.01	34.5	98.8	24.33	0.10
08	17.81	0.0181	0.4200	4.01	28.3	99.3	24.35	0.09
11	17.87	0.0150	0.5873	2.60	34.0	99.0	24.36	0.10
05	18.01	0.0143	1.048	3.12	35.7	98.3	24.37	0.11
06	18.07	0.0153	1.223	1.94	33.3	98.0	24.38	0.13
07	17.93	0.0174	0.7462	2.88	29.3	98.8	24.39	0.11
10	17.88	0.0170	0.5158	2.93	30.1	99.2	24.41	0.11
01	18.05	0.0216	1.061	4.45	23.6	98.3	24.42	0.09
09	18.03	0.0144	0.9924	2.22	35.5	98.4	24.42	0.11
02	18.39	0.0145	2.153	4.97	35.2	96.5	24.45	0.10
12	17.97	0.0151	0.7088	1.41	33.8	98.8	24.45	0.13
14	17.94	0.0180	0.6090	2.22	28.3	99.0	24.46	0.12
13	17.92	0.0161	0.3832	2.26	31.8	99.4	24.51	0.12
03	18.28	0.0169	1.433	2.61	30.1	97.7	24.58	0.11
weighted mean ± Taylor err			n=15 MSWD=1.65		31.8 ±3.5		24.41	0.06
S117, D8:144 single crystal sanidine, J=0.0007679±0.10%, D=1.0056±0.00118, NM-144, Lab#=52685								
01!	17.75	0.0130	0.6788	1.74	39.4	98.9	24.15	0.13
11	17.77	0.0136	0.4650	4.09	37.6	99.2	24.26	0.13
04	17.66	0.0137	0.0519	2.90	37.2	99.9	24.27	0.09
03	18.62	0.0125	3.296	4.95	40.8	94.8	24.29	0.10
12	17.74	0.0148	0.2134	3.37	34.4	99.7	24.32	0.10
09	17.77	0.0139	0.2605	2.79	36.7	99.6	24.35	0.11
13	17.79	0.0124	0.2886	2.64	41.3	99.5	24.37	0.10
15	17.83	0.0145	0.3962	2.88	35.1	99.4	24.37	0.11
08	17.81	0.0139	0.3320	1.99	36.7	99.5	24.38	0.12
02	17.84	0.0141	0.4050	3.18	36.3	99.3	24.38	0.09
10	18.03	0.0146	0.9050	3.40	34.8	98.5	24.45	0.10
14	17.82	0.0141	0.1510	2.78	36.1	99.8	24.47	0.10
05	17.94	0.0131	0.4687	2.52	38.9	99.2	24.50	0.10
06	17.85	0.0139	0.0934	2.53	36.6	99.9	24.52	0.11
07	17.88	0.0135	-0.0173	2.38	37.9	100.0	24.61	0.11
weighted mean: MSWD=3.60*			n=14		37.2 ±2.0		24.39	0.11 *
S118, D9:144, single crystal sanidine, J=0.0007677±0.10%, D=1.0056±0.00118, NM-144, Lab#=52686								
03	17.78	0.0130	0.3275	2.69	39.3	99.5	24.32	0.10
08	17.76	0.0145	0.2551	3.65	35.3	99.6	24.33	0.10
14	17.82	0.0129	0.4397	2.93	39.7	99.3	24.34	0.10
05	19.19	0.0137	5.073	4.11	37.2	92.2	24.35	0.12
10	17.76	0.0144	0.1778	2.69	35.5	99.7	24.36	0.10
02	17.82	0.0125	0.3269	4.22	40.9	99.5	24.39	0.10
04	17.79	0.0118	0.1898	4.20	43.1	99.7	24.40	0.08
11	17.87	0.0127	0.4409	3.89	40.2	99.3	24.40	0.09

ID	$^{40}Ar/^{39}Ar$	$^{37}Ar/^{39}Ar$	$^{36}Ar/^{39}Ar$ (x 10^{-3})	$^{39}Ar_K$ (x 10^{-15} mol)	K/Ca	$\%^{40}Ar^*$	Age (Ma)	±2s (Ma)
07	17.77	0.0142	0.0990	2.87	35.9	99.8	24.41	0.10
01	17.88	0.0105	0.4125	2.49	48.8	99.3	24.43	0.11
09	17.93	0.0133	0.5878	3.60	38.4	99.0	24.43	0.08
13	18.64	0.0134	2.977	3.22	38.0	95.3	24.43	0.14
12	17.94	0.0122	0.6006	4.08	42.0	99.0	24.44	0.09
06	17.92	0.0138	0.5144	3.49	37.0	99.2	24.45	0.10
15	17.90	0.0124	0.3602	1.93	41.3	99.4	24.47	0.13
weighted mean ± Taylor err			n=15	MSWD=0.78	39.5	±3.5	24.40	0.06

* MSWD outside 95% confidence interval
^ = Plagioclase, & = low yield, # = small signal, @ = xenocryst, $ = alteration, ! = anomalously young
Isotopic ratios corrected for blank, radioactive decay, and mass discrimination, not corrected for interferring reactions.
Individual analyses show analytical error only; mean age errors also include error in J and irradiation parameters.
Discrimination = 1.00560±0.00118 a.m.u.
Correction factors:
$(^{39}Ar/^{37}Ar)_{Ca}$ = 0.00070±0.00002
$(^{36}Ar/^{37}Ar)_{Ca}$ = 0.00028±0.00001
$(^{38}Ar/^{39}Ar)_K$ = 0.0108
$(^{40}Ar/^{39}Ar)_K$ = 0.0002±0.0003

APPENDIX E: Comparison of K/Ca Data from Electron Microprobe and $^{40}Ar/^{39}Ar$ Geochronology

Table of Average K/Ca

Sample	Unit	K/Ca (Microprobe)	±1σ	K/Ca ($^{40}Ar/^{39}Ar$ Geoc.)	±1σ
S071	Turkey Springs Tuff (Tts)	34.3	5.6	27.7	1.6
S067	Rhyolite intrusion (Ti2)	211.1	33.8	212.2	47.3
S068	Rhyolite intrusion (Ti2)	328.5	102.1	230.6	76.1
S076	Rhyolite intrusion (Ti2)	498.4	124.1	213.3	71.9
S075	Rhyolitic ignimbrite (Trlt)	69.8	11.3	75.4	6.0
S077a	Rhyolitic ignimbrite (Trlt)	34.0	7.9	38.0	3.5
S036	Rhyolite lava (Trl)	30.9	1.9	27.5	1.3
S069	Rhyolite lava (Trl)	104.5	16.4	94.5	7.4
S070	Rhyolite lava (Trl)	372.4	184.6	86.9	5.8
S078	Rhyolite lava (Trl)	45.6	10.4	40.7	3.1
S047	Granite porphyry (Ti1)	7.2	5.5	4.8	0.4
S067a	Granite porphyry (Ti1)	17.7	5.3	12.2	1.1
S038a	Vicks Peak Tuff (Tvp)	107.9	7.3	93.8	6.5
S085	Vicks Peak Tuff (Tvp)	9.0	3.6	21.8	4.4